PURIFICATION OF PLASMID DNA FOR USE IN HUMAN GENE THERAPY

John Mark Woodgate

Doctor of Philosophy

The University of Aston in Birmingham

January 2001

PURIFICATION OF PLASMID DNA FOR USE IN HUMAN GENE THERAPY

John Mark Woodgate

Doctor of Philosophy

2001

THESIS SUMMARY

Two key issues defined the focus of this research in manufacturing plasmid DNA for use in human gene therapy. First, the processing of E.coli bacterial cells to effect the separation of therapeutic plasmid DNA from cellular debris and adventitious material. Second, the affinity purification of the plasmid DNA in a simple one-stage process. The need arises when considering the concerns that have been recently voiced by the FDA concerning the scalability and reproducibility of the current manufacturing processes in meeting the quality criteria of purity, potency, efficacy, and safety for a recombinant drug substance for use in humans.

To develop a preliminary purification procedure, an EFD cross-flow micro-filtration module was assessed for its ability to effect the 20-fold concentration, 6-time diafiltration, and final clarification of the plasmid DNA from the subsequent cell lysate that is derived from a 1 liter E.coli bacterial cell culture. Historically, the employment of cross-flow filtration modules within procedures for harvesting cells from bacterial cultures have failed to reach the required standards dictated by existing continuous centrifuge technologies, frequently resulting in the rapid blinding of the membrane with bacterial cells that substantially reduces the permeate flux.

By challenging the EFD module, containing six helical wound tubular membranes promoting centrifugal instabilities known as Dean vortices, with distilled water between the Dean numbers of 187_{Dn} and 818_{Dn}, and the transmembrane pressures (TMP) of 0 to 5 psi. The data demonstrated that the fluid dynamics significantly influenced the permeation rate, displaying a maximum at 227_{Dn} (312 lmh) and minimum at 818_{Dn} (130 lmh) for a transmembrane pressure of 1 psi. Numerical studies indicated that the initial increase and subsequent decrease resulted from a competition between the centrifugal and viscous forces that create the Dean vortices. At Dean numbers between 187_{Dn} and 227_{Dn}, the forces combine constructively to increase the apparent strength and influence of the Dean vortices. However, as the Dean number in increases above 227_{Dn} the centrifugal force dominates the viscous forces, compressing the Dean vortices into the membrane walls and reducing their influence on the radial transmembrane pressure i.e. the permeate flux reduced.

When investigating the action of the Dean vortices in controlling the fouling rate of E.coli bacterial cells, it was demonstrated that the optimum cross-flow rate at which to effect the concentration of a bacterial cell culture was 579_{Dn} and 3 psi TMP, processing in excess of 400 lmh for 20 minutes (i.e. concentrating a 1L culture to 50 ml in 10 minutes at an average of 450 lmh). The data demonstrated that there was a conflict between the Dean number at which the shear rate could control the cell fouling, and the Dean number at which the optimum flux enhancement was found. Hence, the internal geometry of the EFD module was shown to sub-optimal for this application. At 579_{Dn} and 3 psi TMP, the 6-fold diafiltration was shown to occupy 3.6 minutes of process time, processing at an average flux of 400 lmh. Again, at 579_{Dn} and 3 psi TMP the clarification of the plasmid from the resulting freeze-thaw cell lysate was achieved at 120 lmh, passing 83% (2.5 mg) of the plasmid DNA (8.3 ng μl^{-1}), 10.8 mg of genomic DNA (~23,00 0bp, 36 ng μl^{-1}), and 7.2 mg of cellular proteins (5-100 kDa, 21.4 ng μl^{-1}) into the post-EFD process stream. Hence the EFD module was shown to be effective, achieving the desired objectives in approximately 25 minutes.

On the basis of its ability to intercalate into low molecular weight dsDNA present in dilute cell lysates, and be electrophoresed through agarose, the fluorophore PicoGreen was selected for the development of a suitable dsDNA assay. It was assessed for its accuracy, and reliability, in determining the concentration and identity of DNA present in samples that were electrophoresed through agarose gels. The signal emitted by intercalated PicoGreen was shown to be constant and linear, and that the mobility of the PicoGreen-DNA complex was not affected by the intercalation.

Concerning the secondary purification procedure, various anion-exchange membranes were assessed for their ability to capture plasmid DNA from the post-EFD process stream. For a commercially available Sartorius Sartobind Q15 membrane, the reduction in the equilibrium binding capacity for ctDNA in buffer of increasing ionic demonstrated that DNA was being adsorbed by electrostatic interactions only. However, the problems associated with fluid distribution across the membrane demonstrated that the membrane housing was the predominant cause of the erratic breakthrough curves. Consequently, this would need to be rectified before such a membrane could be integrated into the current system, or indeed be scaled beyond laboratory scale. However, when challenged with the process material, the data showed that considerable quantities of protein (1150 µg) were adsorbed preferentially to the plasmid DNA (44 µg). This was also shown for derived Pall Gelman UltraBind US450 membranes that had been functionalised by varying molecular weight poly-L-lysine and polyethyleneimine ligands. Hence the anion-exchange membranes were shown to be ineffective in capturing plasmid DNA from the process stream.

Finally, work was performed to integrate a sequence-specific DNA-binding protein into a single-stage DNA chromatography, isolating plasmid DNA from *E.coli* cells whilst minimising the contamination from genomic DNA and cellular protein. Preliminary work demonstrated that the fusion protein was capable of isolating pUC19 DNA into which the recognition sequence for the fusion-protein had been inserted (pTS DNA) when in the presence of the conditioned process material. Although the pTS recognition sequence differs from native pUC19 sequences by only 2 bp, the fusion protein was shown to act as a highly selective affinity ligand for pTS DNA alone. Subsequently, the scale of the process was scaled 25-fold and positioned directly following the EFD system.

In conclusion, the integration of the EFD micro-filtration system and zinc-finger affinity purification technique resulted in the capture of approximately 1 mg of plasmid DNA was purified from 1L of *E.coli* culture in a simple two stage process, resulting in the complete removal of genomic DNA and 96.7% of cellular protein in less than 1 hour of process time.

ACKNOWLEDGEMENTS

ABBREVIATIONS

ADA	Adenosine deaminase
amp	Amplicillin
AMPs	Ammonium persulphate
bp	Base pair
BSA	Bovine serum albumin
C/C_0	Dimensionless effluent output
CNDB	1-chloro-2, 4-dintrobenzene
ctDNA	Calf thymus DNA
D	Ratio of the Dean number to the initiation Dean number
Dn	Dean number
DNA	Deoxyribonucleic acid
dsDNA	Double stranded DNA
ssDNA	Single stranded DNA
DMSO	Dimethyl sulfoxide
EDTA	Ethlene-diamine-tetra acetic acid
f	Friction factor
f.Re	Friction
FDA	Food and Drug Administration (USA)
GT	Gene therapy
Gn	Germano number
GSH	Glutathione
rGSH	Reduced glutathione
GST	Glutathione S-transferase
HIV	Human immuno-deficiency virus
kDa	Kilo Dalton
LB	Lurium broth
lmh	Litres per metre squared per hour
MLV	Murine leukemia vector
MWCO	Molecular weight cut off
OD	Optical density
PAGE	Polyacrylamide gel electrophoresis
PBS	Phosphate buffered saline
PCR	Polymerase Chain Reaction
P_D	Power consumption
PEG	Polytheyleneglycol
PEI	Polytheyleneimine
Psi	Pounds per square inch
rpm	Revolutions per minute
RNA	Ribonucleic Acid
RNase	Ribonucelase
SCID	Severe combined immunodeficiency syndrome
SDS	Sodium dodecyl sulphate
SGT	Somatic cell therapy
TBS	Tris buffered saline
TE	Tris(hydroxymethyl)methlamine, Ethlene-diamine-tetra acetic acid
TEMED	N, N, N', N'-tetramethylethylenediamine
TF	Transcription factor
TMP	Trans-membrane pressure
Tris	Tris(hydroxymethyl)methlamine
VEGF	Vascular endothelial growth factor
VGT	Vaccination gene therapy
WHO	World Health Organisation
γ	Gamma number

TABLE OF CONTENTS

LIST OF TABLES

LIST OF FIGURES

1. INTRODUCTION

1.1. Human gene therapy

Gene therapy as a way of transferring genes into human cells to induce a corrected phenotype was first proposed nearly thirty years ago. It concluded that an explosion in cancer, virology and bacterial genetic research in the late 1960's, that demonstrated how the manipulation of human cells at the molecular level in order to cure rare genetic diseases was possible (Friedman & Roblin, 1972). However, it was nearly twenty years later that the first clinical study involving human gene therapy was initiated, where in 1990 a patient with severe combined immunodeficiency syndrome (SCID) underwent *ex vivo* transduction of peripheral T lymphocyte with a murine leukemia vector (MLV) carrying the adenosine deaminase (ADA) gene. Tests conducted four years later showed that more than 30% of circulating T cells of the patient contained the transduced gene resulting in a significant improvement in their immune system (Blaese *et al.*, 1995). Since that landmark study, approximately 300 clinical protocols involving gene therapy have been approved, mostly in the USA, where more than 3500 patients have been administered with experimental gene therapies (Mountain, 2000). Until recently the majority of these clinical tests have been small Phase I/II studies where the main objectives was demonstrating safety, gene transfer, and obtaining relevant information to guide dose selection for Phase II and III efficacy studies.

Of the 300 clinical gene therapy protocols that have been approved since 1990, the majority have been directed at life threatening diseases, for which currently available therapies are not highly effective e.g. HIV infection and certain cancers. It is only within the last few years that the clinical benefit for gene therapy has been realised for the first time (Baumgartner, 1998). In this series of studies, naked DNA encoding the angiogenic protein vascular endothelial growth factor (VEGF) was injected into the skeletal muscles of patients with critical limb ischchaemia resulting from an inadequate blood supply. The results indicated a dramatic and long lasting benefit in a large proportion of the patients, including those who would otherwise have faced amputation. In addition, injection of the same therapy into the heart muscle of patients with ishchaemic heart disease is now also giving encouraging efficacy data.

As a consequence of this study, and the recent publication of the sequence of human chromosome 22 (Dunham, 1999), increasing the data of the genetic components involved in disease causation, it is reasonable to expect that gene-based therapies can transfer from efficacy and safety studies to providing effective treatments that offer real, tangible, and long term benefits to patients suffering from a number of major diseases. Of the 300 gene therapy protocols that have currently been approved, of which two thirds are directed at cancer, and most of the remainder at inherited monogenic disorders like cystic fibrosis and infectious diseases such as HIV, none have transferred into the therapeutic market.

However, the recent patient fatalities which have been reported in gene therapy clinical studies, including the death of an 18 year old patient receiving high dose adenoviral gene-therapy for an inherited deficiency in ornithine transcarbamylase (an enzyme involved in the urea cycle and ammonia metabolism), and the reporting of 691 patients, (at the time of writing), experiencing serious adverse events including deaths in gene therapy trials, highlight the intrinsic problems associated with gene therapy and the absolute requirements for comprehensive regulatory guidelines and stringent review

procedures for clinical protocols (Dyer *et al.,* 2000). As such, the FDA stepped in to halt all eight gene therapy trials at the institute in question where the 18 year old patient died, questioning the:

- Specificity and efficiency of gene transfer,

- Specificity, magnitude and duration of expression,

- Immunogenicity,

- And manufacturing of the therapeutic.

Consequently, the FDA stated that additional information should be fully documented and proved before Phase I human clinical trials are initiated. Information including:

- ·Details of source materials, including the origins of cloned species.

- The steps involved in vector construction, information about the sources and functions of components including regulatory sequences and encoding proteins.

- Characterisation of constructs, including the nucleotide sequence, the restriction enzyme map, and analysis of the expressed gene product.

- Description of the targeted host cell for in vivo therapy and/or the producer cell system.

- Characterisation and quality control of master and working cell banks as well as master and working virus stocks.

- Details of manufacturing and purification steps.

- Method of quality control of bulk vectors are other biological products.

- Quality control method for the final product.

- The stability potency, and activity of the product (determined and standardised).

- Full description of the pre-clinical pharmacology and toxicology studies.

- Efficacy of therapy of atherosclerotic vascular disease in appropriate animal models, defined as the ability to suppress atherogenesis quantitatively.

It is under these guidelines governing human gene therapy clinical trials, that a scaleable manufacturing process, which reproducibly meets the quality criteria of purity, potency, efficacy, and safety for a recombinant drug substance, needs to be developed in such a way that it reduces the astronomical costs associated with the purchase of such therapies. Thus, availability will not be limited to only the wealthiest countries in the developed world.

1.2.   Plasmid DNA for use in human gene therapy

The employment of plasmid DNA within current clinical studies can be distinguished between three separate strategies.

1.2.1. Gene therapy (GT)

Defined as the *ex vivo* or *in vivo* medical intervention to modify genetic material in living cells. In GT, the deleterious gene expression is to be suppressed or modified by genetic manipulation. For example, the generation of a deleterious protein product of a mutated gene can be negated either by the introduction of antisense oligonucleotides or antibodies into vulnerable cells. Antisense oligonucleotides might inactivate the relevant complimentary mRNA, while intracellularly produced antibodies might negate the effect of the deleterious proteins. Another example of GT is the upregulation of the expression of a gene that is analogous to a mutant gene, whose protein product is missing. For example, it has been hypothesised that upregulation utophin gene expression in Duchenne muscular dystrophy (DMD) might have therapeutic benefits. In this scenario, utrophin would take the place of the missing dystrophin and thus spare muscle fibres from necrosis.

1.2.2. Somatic cell therapy (SGT)

Defined as the administration to humans of autoglomas, allogenic, or xenogenic living cells that have been manipulated or processed *ex vivo*. Manufacture of products for somatic cell therapy includes the *ex vivo* propagation, expansion, selection, or pharmacological treatment of cells, or other alterations of their biological characteristics. Such cellular products might be used for diagnostic, therapeutic, or preventative purposes.

1.2.3. Vaccinations (VGT)

The use of naked plasmid DNA as a preventative vaccine. Naked DNA manufactured in bacteria does not provoke specific immune responses, but it contains dinucleotide sequences comprising of cytosine followed by guanine (CpG sequences); these sequences are unmethylated when produced in bacteria and elicit immune stimulatory and inflammatory cytokines in animals. This is an advantage for vaccine applications (indeed, these CpG sequences are now regarded as the most powerful adjuvant known (Krieg, 1999) but a disadvantage for chronic-disease therapy.

Plasmid DNA may also be used for the creation of a stable gene reservoir to express therapeutically useful molecules in non-monogenetic diseases. Examples of this include degenerative diseases of the central nervous system such as Parkinsons disease or Altzheimers disease where neurotrophic factors may enhance neuronal survival. Plasmid DNA may also be used in the treatment of malignant melanomas by various strategies including the transfer of genes that code apoptotic molecules and molecules that convert non-toxic prodrugs to cytotoxic agent (i.e. 'suicide genes'). Finally plasmid DNA may also find application in the prevention of infectious diseases by introducing genes encoding vaccine-like molecules by injecting naked DNA directly into the blood stream (i.e. hepatitis B antigens).

1.3. Production of plasmid DNA

In consideration of the FDA guidelines, much research has been conducted to ascertain the correct vector and delivery vehicle. However, considerable effort has also been applied to develop methods that could enable the efficient production and purification of plasmid DNA for human clinical trials. Plasmid DNA can be manufactured simply and cheaply in bacteria (Horn *et al.*, 1995), an advantage that is magnified in strategies that require the co-delivery of several genes, and should serve to lower the final cost of treatments. However, clinical trials that incorporate direct *in vivo* gene therapies require the development of scaleable manufacturing processes that reproducibly meet the quality

criteria of purity, potency, efficacy, and safety for a recombinant drug substance as described by the FDA guidelines. As such the existing manufacturing processes relying upon DNA extraction with toxic organic solvents, ethidium bromide, caesium chloride gradient centrifugation, and the use of animal derived enzymes such as lysozyme, proteinase K, and RNase, pose considerable challenge to process validation and raise many regulatory concerns about residual material within the final product. (Hoeg,1998). Therefore, any manufacturing process that is to be developed has to be done so in compliance with the regulations and guidelines that apply to the manufacture of recombinant pharmaceuticals (Code of Federal regulations 21, 1994, 1995, 1998), i.e. the elimination of the animal derived enzymes, toxic organic extractions, and free of host-derived contaminants such as protein, lipids, carbohydrates, endotoxin, DNA and RNA.

However, the type of information that is required to ensure adequate safety of the recombinant DNA product depends, in part, on the nature of the clinical trial i.e. the final dosages, delivery, and intended patients. Assuming that the construct of the vector intended for the clinical trial has been subjected to the sequencing tests, and that the vector/host cell system has been pre-approved by the FDA, the manufacturing process is subject to the following guidelines (Guidance for Industry, Guidance for Human Somatic Cell Therapy and Gene Therapy. 1998):

1.3.1. Cell Culture Procedures

The fermentation of bacterial cells must be carefully managed, ensuring the quality of materials, manufacturing controls, and the validation of the processing equipment.

1.3.2. Cell culture media

That all the media components, including any additives and growth factors, must be validated as free from adventitious agents. That medium components that can potentially cause sensitisation, for example certain animal sera, selected proteins etc, should be avoided. Concerning additional growth factors, the identity, purity, and potency should be established in order to assure reproducibility of cell culture characteristics, a prerequisite of FDA approval. Therefore, certain chemicals such as DMSO should not be used within the manufacturing process. The specification for medium components and other additive that are added to cell cultures can be seen in 'Points to Consider in the Characterisation of Cell Lines Used to Produce Biologicals (1993)" and the "Points to Consider in the Collection, Processing, and Testing of Ex-Vivo-activated Mononuclear Leukocytes for Administration to Humans (1989).'

1.3.3. Adventitious agents in cell cultures

The FDA states that the laboratory procedures where cells are handled should be designed and operated under conditions that minimise the contamination with adventitious agents. That testing should demonstrate that the cell cultures are free of other bacteria, mycoplasma, and adventitious viruses etc. Again, this is discussed in more detail within "Points to Consider in the Characterisation of Cell Lines Used to Produce Biologicals" (1993). These regulations also apply for any downstream processing of the therapeutic product, including harvesting, lysis and the subsequent purification stages. With emphasis placed on demonstrated reproducibility, intrinsic safety, and the minimisation of contact with adventitious material during the process.

1.3.4. Tests of recombinant DNA (bulk product not necessarily in final formulation)

Under the current guidelines, the FDA states that any of the standard assays for the material listed below can be used if they are quantitative. However, any assay employed must clearly demonstrate specificity and sensitivity before validation of the assay protocol. The tests that are currently accepted by the FDA are detailed below:

1.3.4.1. Purity

Test for total DNA or RNA content, e.g. A260/A280. Test for homogeneity of size and structure, supercoiled vs. linear, e.g. agarose gel electrophoresis. Test for contamination with RNA or with host DNA, e.g. gel electrophoresis. Test for proteins if present as a contaminant, e.g. silver stained gel. Test for non-infectious virus in cases in which that would be a contaminant, such as empty capsids. Tests for toxic materials involved in production, e.g. endotoxin.

1.3.4.2. Identity

Test for the plasmid identity by procedures such as PCR to distinguish between product and contamination.

1.3.4.3. Adventitious agents

Test for adventitious material in the product with, sterility tests for aerobic and anaerobic bacteria and fungi. Mycoplasma testing, (Points to Consider in the Characterisation of Cell Lines Used to Produce Biologicals, 1993). Testing for adventitious source materials or cell lines used in vector production introduce the risk of contamination. (Points to Consider in the Characterisation of Cell Lines Used to Produce Biologicals, 1993).

Therefore, it can be stated that the purification of pharmaceutical grade plasmid DNA requires the development of highly reproducible, scaleable, and validated processing method that meets the required regulatory standards. Although the actual level of contamination in the final dosage form is determined by the type of clinical trials that have been applied for, other workers have quoted, where the trials involve *in vivo* injection of naked plasmid DNA into established tumours of HLA-B7 negative patients, that contaminating *E.coli* DNA levels kept below 1%, endotoxin less than 0.03% units μg^{-1}, and residual protein being undetectable. (Horn *et al.*, 1995). However, the devised manufacturing process by Horn *et al.*, whilst meeting the purity criteria, only yielded 50% of the plasmid DNA from the cell culture.

1.4. Project objectives

The research detailed in this thesis is concerned with the development of a generic, and scaleable, lab-scale process for the manufacture of plasmid DNA specifically for human gene therapy. As such, the project divides equally into two distinct sections:

- The harvesting, diafiltration, and clarification of plasmid DNA from adventitious material present within the culture medium and subsequent cell lysate.

- The purification of the therapeutic plasmid DNA from the subsequent lysate.

In consideration of the FDA guidelines concerning the design and operation of the manufacturing equipment in minimising the risk of contamination of adventitious material into the process stream, the number of stages within the production train, as afar as possible, were designed to be kept at a minimum.

The first piece of work employed an experimental EFD micro-filtration module (Millipore, UK) for the harvesting, washing, lysis, and final partitioning of the plasmid DNA from the culture media and cellular debris. In response to the FDA guidelines stated above, the partitioning of the cells from the growth medium must be achieved because the FDA states that the media components, including additives, growth serum and adventitious agents, must be removed. (As will be detailed later in this section, this partitioning of media components and reducing the risks of contamination from adventitious material is critical as the final manufacturing process employs sequence-specific DNA binding proteins that are expressed within the host cell, i.e. requiring the use of freeze-thaw cell lysis rather than alkaline lysis for cell disruption). Therefore, proof that this technology can perform such a role must be demonstrated. The EFD micro-filtration module offers such an opportunity to demonstrate the initial partitioning of medium components, and the final plasmid clarification from the cellular debris, theoretically allowing passage of liquids and sufficiently small material through 0.65 μm pores within the membrane. However, the ability of the EFD to harvests cells, wash cells, and finally partition plasmid DNA from the cellular debris has never been demonstrated considering that it is a prototype module. Furthermore, the ability to do so under process conditions where the membrane is previously fouled with the harvested cells has also not been demonstrated (i.e. an integrated process where the risks of contamination are minimised by refraining to clean fouled material between separate operations). Although previous studies indicate that similar such technologies are able to achieve the design remit, it is this lack of integrated characterisation that needs to be demonstrated.

The second piece of work entailed the demonstration of the EFD to achieve the design remit quoted by the manufacturers. The promotion of centrifugal instabilities to effect the de-polarisation and the re-entrainment of fouled material whilst creating flux enhancements over existing linear membrane modules (i.e. demonstrate that the EFD is competitive with existing technologies for this application). At the inception of this project, the action of these centrifugal instabilities as promoted by the EFD module were not sufficiently characterised, whether experimentally or numerically. Therefore, the second piece of work addressed the need to characterise the fluid dynamics occurring within the EFD module in order to demonstrate the performance, and subsequent optimisation, when employed within the required tasks.

The third piece of work was devised to address the current employment of numerous non-specific purification stages that have previously required the addition of organic solvents, ethidium bromide, caesium chloride, and animal derived products, such as RNase and protease etc. (i.e. invoking further validation to comply with the FDA guidelines). Although the more recent procedures have ameliorated the problem of animal derived enzymes and toxic chemicals, they still require five stages (and vessels) involving 2-propanol, ammonium acetate, PEG-8000, anion-exchange chromatography and final precipitation with ethanol, to effect the purification of plasmid DNA from alkaline lysis material (Horn *et al.*, 1995). Therefore, the third piece of work addresses the ability of standard anion-exchange membrane chromatography to effect the partitioning of plasmid DNA from the crude *E. coli* cell lysis material.

As a consequence of the third piece of work, a method by which the identity and quantity of DNA can be efficiently, and reproducibly, determined in the process material and final product had to be produced to demonstrate compliance with the FDA guidelines. Poly-acrlyamide gel electrophoresis and Coomassie blue, coupled with Bio-Rad protein assay reagent was deemed appropriate for the purpose of protein identification and quantification.

The final piece of work is concerned with the integration of sequence-specific zinc-finger DNA-binding proteins to effect the capture of genetically modified plasmid DNA (i.e. carrying a recognition sequence) from the crude *E.coli* cell lysate. Considering that such DNA-binding proteins have never previously been integrated into such a purification strategy, proof that they can perform such a role must be demonstrated. However, issues relating to final polishing and formulation of the plasmid DNA into a therapeutic dose were not tackled, but discussed within the 'Future work' section.

1.5.   Genomic DNA as a contaminant in the manufacture of therapeutic plasmid DNA

The importance of removing host-cell genomic DNA within the therapeutic preparation is clearly demonstrated when considering that the residual DNA may include active oncogenes that could transfect cells and cause cancer when administered to a patient. However, the actual quantity of residual DNA within a therapeutic dose depends upon the type of gene therapy that has been applied for. Whether the DNA is to be injection *in vivo* into muscle and skin tissues, injection onto the blood stream for the vaccination against infections diseases, or whether the DNA is to be combined with a delivery vehicle for direct *in vivo* transfection into human cells. In fact, it was reported that the FDA would consider each case as it was presented to them but would generally expect DNA to be reduced to 100 picogram per dose (Charlton, 1999). This value arose from studies indicating that naked DNA gave virtually no transfection into cells *ex vivo*, Again, this has been demonstrated by Dortant *et al.*, (1997) where 250 µg of hybridoma DNA from tumourigenic cell lines were injected into mice and rats with no elevation in risk of tumour development was observed. (Dortant *et al.*, 1997). However, naked DNA gives surprisingly efficient gene transfer into several tissues following local injection *in vivo*, notably in muscle and skin (Mountain. 2000). In order to indicate the context, it should be noted that a single blood transfusion contains DNA in microgram quantities such that a single transfusion could contain 450 µg of DNA over 800 bp (Charlton, 1999). However, depending upon the efficiency of the gene delivery system, such as cationic condensation polymers that are taken up by the cells by enodocytosis, or transfection of naked DNA, the regulation concerning residual DNA content will vary accordingly. However, it should be noted that the future stance of the FDA, dependant upon current research, would probably reduce the residual levels to minimum values as delivery vehicles move more towards 'smart-weapons' in their targeting and ultimate transfection efficiency.

1.5.1.   Removal of genomic DNA from therapeutic plasmid DNA

The removal of residual genomic or non-therapeutic DNA from plasmid DNA has been demonstrated by the employment of numerous downstream non-specific operations, differentiating on the basis of size with molecular weight cut-off membranes, and insolubility within various organic solvents. The most notable study (Horn *et al.*, 1995) demonstrated clearance by a series of precipitation techniques, 2-propanol, re-suspension in ammonium acetate, precipitation with PEG-8000, Sepharcryl S-100 anion-exchange chromatography and final ethanol precipitation, presumably to concentrate the sample prior to formulation. However, Baumann and Bloomfield (Baumann *et al.*, 1995) favoured ammonium acetate precipitation, enzymatic digestion of RNA, protein removal by phenol ectraction

under dialysis, a procedure that raises many safety concerns. As a consequence of the numerous downstream operation, Horn et al., (1995) demonstrated that only a 53% yield of the plasmid DNA challenged was possible. However, considering the recent advances in targeting the cells in need of therapeutic treatment, it seem reasonable to suggest that new manufacturing techniques will have to employ affinity techniques to effect the complete removal of residual DNA, techniques of similar affinity to those currently employed within therapeutic protein manufacturing techniques.

1.5.2. Quantification and identification of DNA

The accurate quantification and identification of DNA is both important and of general interest within Biotechnology and a wide range of biological sciences. It has been the subject of intense work over recent years, and numerous methods of DNA determination are now available. For the purposes of this work there is a requirement for an assay for DNA that will accurately report the quantity and identity of DNA passing through the initial stages of plasmid DNA purification. The following serves as a review of the methods that are often used for determination of DNA under various circumstances, and an analysis of their suitability for application to this work. A brief description of the structure of DNA is provided in Appendix 1 that may be used to embellish the following descriptions.

1.5.2.1. Spectrophotometry

Spectrophotometry is unrivalled in its simplicity for simultaneous confirmation of purity and quantification of DNA. Calculation of the ratio of absorbencies at 260 nm and 280 nm gives an indication of the purity of the sample. A ratio of 1.7 to 2.0 indicates that the DNA is clean (i.e. free of RNA and protein) whereas a ratio of below 1.7 indicates the presence of protein, and above 2.0 the presence of RNA is implied. Its successful application requires relatively high levels of DNA, typically in the microgram range. Single oligonucleotide, proteins and aromatic molecules can interfere with accurate determination of DNA (Sambrook et al., 1989). Spectrophotometry cannot be used for direct determination of DNA for work detailed in this thesis because samples are protein rich and interference would certainly prohibit use.

1.5.2.2. Fluorescence based assay for DNA

Although fluorescence based assays for the quantification of DNA have been available since 1966 where Le Pecq first applied ethidium bromide for this application, Sharp et al., (1973) was the first to integrate the dye into the electrophoretic techniques that are still employed today to identify and quantify DNA. However, many compounds have been developed recently, named fluorochromes, and demonstrated to improve the selectivity, safety and fluorescence enhancements over ethidium bromide (i.e. ethidium bromide is carcinogenic).

Fluorochromes bind DNA within the major or minor groove, where the quaternary amines are placed in close contact with the phosphate anions within the bases on a given chain in the double helix. As the conformation of the ligand deforms upon binding the DNA groove, the excitement of the molecule at a specific wavelength will case the intercalated molecules to fluoresce whilst the non-deformed molecules will not. Consequently, the detected fluorescence is proportional to the quantity of DNA base pairs that have been intercalated with the probe (i.e. quantification can be achieved by calibration as long as the probes:DNA base pair ratio remains constant and independent on the source organism). Such fluorochromes typically intercalate into dsDNA at a ratio of one molecule to 4-

5 base pair, where, according to the sensitivity of the detection equipment, relatively short DNA molecules can be detected.

1.5.2.3. Ethidium bromide

Ethidium bromide was the first fluorochrome to be applied to the quantification and identification of nucleic acids (Le-Pecq and Paoletti, 1966) where the optimum dye-base pair ratio for more accurate determinations was published by Dutton *et al.*, 1995. The fluorescent enhancement of ethidium bromide has been cited as 80:1 when excited at 365 nm (Sambrook *et al.*, 1989) where 50 ng DNA ml^{-1} can be readily visualised (Stryer, Biochemistry 3rd Ed, 1988). However, due to the relatively high background fluorescence within agarose electrophoresis gels and non-specific fluorescence with RNA and ssDNA, and the lack of sensitivity, ethidium bromide cannot effectively quantify dsDNA within agarose electrophoresis gels.

1.5.2.4. PO-PRO-3

PO-PRO-3 is a fluorochrome synthesised by Molecular Probes (Molecular Probes, Inc., Eugene, OR) where the probe is excited at 540 nm and the resulting emission visualised at 575 nm. The probe, upon binding dsDNA, exhibits a 35-fold fluorescence enhancement that is independent of base pair compositions (Sherwood *et al.*, 1995). The di-quaternary amine structure of PO-PRO-3 in which the linear distance between quaternerised nitrogen's of PO-PRO-3 is ca. 14.4A (i.e. the bond length summation equals 17.02A) which, allowing for the deformation of the ligand upon binding to the major groove, should place the quaternary amines in close contact with the phosphate anions associated with the n and n+2 base pairs on a given chain in the double helix.

PO-PRO-3 has been used to quantify samples of DNA or various origin where the fluorescent signal was shown to linear dependence on the concentration of dsDNA present (0.9 ng in 60µl). This sub-nanogram detection limit compares favourably with similar assays based on other major-groove binding fluorophores, such as Hoechst 33258 (Spink *et al.*, 1994). However, it was shown that the effect of ionic strength was to substantially reduce the fluorescent emissions as salt was increased passed 140 mM (i.e. that of cell culture and PBS/TBS process buffers). In addition, a significant fluorescent enhancement was observed as protein concentration was increased (>1%). PO-PRO-3 was tested in a dilute solution where linear DNA binding was shown to be indistinguishable to binding super-coiled plasmid DNA. Therefore, it is considered that PO-PRO-3 does not possess that ability to fulfil its pre-defined role under the test conditions that would be experienced when challenged with crude cell lysate.

1.5.2.5. PicoGreen

Although the structure of PicoGreen (Molecular Probes) has not been published it will presumably have similarities with the previously defined PO-PRO-3 (Molecular Probes), where the enhancement in fluorescent signal upon intercalation into the major groove of dsDNA is dependant upon the shortening of the distance between quaternerised nitrogen's.

PicoGreen has been shown to quantify dsDNA in relatively pure samples of various complexities, whether super-coiled, linear or histone bound (Ahn *et al.*, 1996). In addition, it has also bee shown to quantify DNA present within a dilute cell lysate and unused culture broth's where the samples contain various concentrations of nutrients, nutrients, salt (Singer *et al.*, 1997) and protein (Charlton, 1999). It

was demonstrated that none of these parameters had a significant impact on the fluorescent signal emitted by the PicoGreen, quantifying dsDNA to nominal levels of 25 pg dsDNA ml^{-1} where the resulting calibrations curves were shown to be linear when in the presence of all the contaminating species. However, whereas Enger, (1996) demonstrated that PicoGreen could be used for the determination of PCR products within an agarose electrophoresis gel, it has yet to be shown that it can accurately and reproducibly quantify and identify dsDNA within an assay where the sample is a dilute cell lysate. However, in consideration of the reported studies, PicoGreen remains the most suitable candidate for the quantification and identification of dsDNA in bacterial cell cultures and lysate.

1.5.3.   Cellular proteins as contaminants in the manufacture of therapeutic plasmid DNA

As with genomic DNA, the importance of removing cellular proteins from the final therapeutic product is clearly demonstrated when considering potential inflammatory, immune, or auto-immune responses induced by adventitious material such as cellular proteins. Consequently, the FDA states that ' These components should be clearly identified and a qualification program with set specifications should be established for each component (i.e. proteins) to determine its acceptability for use during the manufacturing process', in order to limit possible toxicity. In addition, the host immune responses against a therapeutic dose containing residual proteins will limit the number of administrations and therefore the usefulness of the therapy within the clinic (i.e. they should be avoided).

1.5.3.1. Removal of cellular proteins from therapeutic plasmid DNA

Cellular proteins, and their enzymatic activity, are normally denatured when alkaline lysis techniques are employed to release the plasmid DNA from bacterial cells. The denatured material is then separated from the plasmid DNA by the series of precipitation and re-suspension stages employed previously to differentiate between the genomic DNA and plasmid DNA (Horn et al., 1995). However, for this thesis these techniques have had to be rethought as the DNA-binding protein employed as an affinity ligand is to be expressed within the plasmid host cell. Therefore the cells are to be disrupted by freeze-thaw lysis rather than alkaline lysis.

1.5.3.2. Quantification and identification of cellular proteins

For the accurate identification and quantification of cellular proteins, polyacrylamide gel electrophoresis techniques are normally employed. The protein bands are normally visualised by the stain Coomassie blue where the quantitative detection limit is between 0.2 and 20 µg. However, for greater sensitivity of quantities between nanogram and fentogram, or when using higher resolution techniques such as 2-D electrophoresis, silver staining can be employed. Depending upon the protocol chosen, silver-staining techniques can be between 5 and 200-times more sensitive than Coomassie blue. This methods involves a fixation step where silver nitrite is exposed to the protein and the silver ions thought to react with basic and thiol groups in proteins leading to a deposition of silver in the protein bands. Although silver staining has clear benefits in terms of sensitivity, the staining can be non-specific, since DNA and polysaccharides may stain on the same gel as proteins. Alternative methods for detecting electrophoretically separated components include autoradiography, fluorescence, and Periodic acid-Schiff (PAS) stain using dansyl hydrazine for glycoproteins. However, the choice of detection methods for this thesis was limited to Coomassie blue by dedicated instrument being able to determine the absorbance at 560-575nm and quantify single components (i.e. Coomassie blue absorbance).

1.6. EFD cross-flow micro-filtration

The application of filtration techniques, such as dead-end filtration, sedimentation, and centrifugation, that have been used to harvest cells from culture broth in continuous pharmaceutical applications poses many practical difficulties, mainly because of the hydrated and viscous nature of low density bacterial cells. Consequently, much effort has been employed in developing alternative methods involving the use of cross-flow membrane filtration in which the permeate passes through a membrane by virtue of a pressure differential (i.e. the transmembrane pressure, TMP). In cross-flow micro-filtration, the product to be filtered is passed over a porous surface where the flow rate of the process stream theoretically controls the thickness of the deposited cell layer (Bhattacharjee et al., 1999, Jiao et al., 1994, Lu et al., 1995), maintaining a permeation rate closer to the original. As such, cross-flow filtration is pressure-driven process that is profoundly influenced by the applied pressure differential between the retentate and permeate.

However, whilst cross-flow filtration is a significant improvement over dead-end filtration, permeate fluxes still decrease with time, even when the feed concentration is kept constant (Mondor et al., 1999). Typically fluxes of 50 lmh to 72 lmh have been observed where fluxes between 150 lmh and 400 lmh have been quoted as necessary for cross-flow micro-filtration to compete with established technologies such as continuous centrifuges (Caridis et al., 1997).

A serious limitation in using pressure driven membrane processes for filtration is the deposition and build-up of bacterial cells onto the membrane surface. To reduce this concentration polarisation and fouling, some researchers have considered various approaches for lowering the concentration gradient between the bulk phase and the membrane surface and for re-entraining the cells deposited on the membrane surface. These include chemical modification to the membrane surface, physical methods such as scouring with sponge balls, and hydrodynamic methods such as the use of eddies during turbulent flow (Belfort et al., 1989). One of the more successful depolarisation methods was demonstrated when well-ordered Taylor vortices were established within rotating annular filter modules (Belfort et al., 1989). Consequently, rotating annular filters have been successfully employed to harvest bacterial cells, cell debris, and even diagnose fouling characteristics (Belfort et al., 1993). However, such rotating equipment suffers from design problems concerning sealing difficulties that do not make the technology particularly amenable to scale-up. However, alternative methods for establishing centrifugal vortices, known as Dean vortices, have been investigated by Mallubhotla et al., (1995) where vortices are formed from the onset of unstable flow in spiral wound membrane ducts (Chung et al., 1993, Crowder et al., 1997, Kakuvi et al., 2000, Manno et al., 1998). As such, Dean vortex flow displays similar advantages to Taylor vortex flow but with the additional feature of being scaleable, not being expected to consume unreasonable amounts of energy, and not have the sealing difficulties stated previously.

Whereas at sufficiently low flows rates the velocity in a curved channel is approximately parabolic, the centrifugal instabilities known as Dean vortices are formed as the velocity increases (i.e. Dean number increases) above a critical value (Belfort et al., 1993). The vortices that are produced twist and spiral in the streamwise direction (Dean, 1928) with there rotational speed and size being directly related to the cross-flow rate, radius of curvature and torsion (i.e. Dean number). According to the theory, it is these vortices that can be used to lower the concentration gradient between the bulk phase and the membrane surface, and for re-entraining the cells deposited on the membrane surface back into the bulk phase (Manno et al., 1998). As such, well-defined Dean centrifugal instabilities have been shown

to promote a beneficial effect on the membrane performance in micro-filtration, improving the flux by up to 43% over identical linear modules (Mallubhotla *et al.*, 1995). It was shown that the flux enhancements due to the Dean vortices increased with flow-rate and transmembrane pressure, but decreased with increasing concentration of suspended matter.

However, such Dean vortex modules have only been shown to effect the depolarisation of solute and build up and fouling, not the re-entrainment of fouled material into the bulk phase. Manno *et al.*, (1998) demonstrated that membrane fouling and concentration polarisation in cross-flow filtration can be reduced by the use of Dean vortices and whilst processing bakers yeast, flux enhancements of up to 5-fold were observed as compared with conventional straight modules. Moulin *et al.*, (1999) also demonstrated that Dean vortices cause an increase in permeate flux for a given transmembrane pressure. However, the real effects of Dean vortices are noted when the concentration of the feed suspension is high, and when the technology needs to be scaleable.

The cross-flow micro-filtration modules are generally used under one of two modes: constant pressure whereby the membrane fouls and the flux reduces, or constant flow rate where as the cells accumulate on the membrane there is an increase in transmembrane pressure. Understanding the critical pressure experienced by *E. coli* bacterial cells (Tanny *et al.*, 1980, Reismeier *et al.*, 1987, Forman *et al.*, 1990) and their apparent irreversible fouling nature (Caridis *et al.*, 1997), this project employed the EFD modules at constant transmembrane pressure that could be used to provide the driving force to feed sufficient process material through successive purification stages within the purification train. Since the system should be designed where there is no storage of material between the harvesting and purification strategies, the holding-volume of the EFD system is minimised at 50 ml.

1.7. Purification of plasmid DNA from the post-EFD process material

1.7.1. Anion-exchange membranes

Membrane chromatography was developed as an integrative technology for the purification of biological substrates. The main feature of such chromatographic separation based on membranes is the absence of pore diffusion, which is the main transport resistance in conventional column chromatography using porous particles. As film diffusion is usually orders of magnitude faster than pore diffusion, mass transport limitations are drastically reduced in membrane chromatography, shifting the limitation of the process more to the properties of the adsorbent-adsorbate interactions. The result is that the whole separation process is essentially speeded up and will be characterised by short loading, washing and eluting time cycles.

The purification of biological substrates is achieved by attaching active ligands to the inner surface of the through-pores of the membrane, the position where mass transfer takes place mainly by convective flow and thus reducing the transport limitations from pore to film diffusion. In combination with characteristic low-pressure drop across the membrane and large surface areas, high volumetric flows are possible in a membrane purification step, controlled by the association kinetics between the adsorbates and adsorbents, thus reducing the time penalty incurred by other chromatographic procedures. The procedure is characterised by fast processing, at preserved or even increased resolution, rates compared to standard chromatographic particulate materials (Thommes *et al.*, 1995).

The first applications of membrane process were reported favourably using well-documented proteins when compared to the various column matrixes (Briefs and Kula, 1992), and that membrane

processes could elicit fractionation of amino acids (Garem *et al.*, 1997). However it was reported that the problem of uniform flow distribution from a relatively thin pipe to a large area had to be solved, as well as the problem of recollecting the eluate at the other end of the module with minimal back-mixing and distortion zones (Thommes *et al.*, 1995).

Although anion-exchange membranes have not been applied in the plasmid DNA purification stages, they were investigated for their potential to selectively capture plasmid DNA from crude *E.coli* lysis material that had been disrupted by freeze-thaw cycles. As such, various membranes were employed for this purpose, all containing positively charged polymeric ligands where their potential was investigated as compared with each other.

1.7.2. Sequence-specific DNA-affinity chromatography

Currently, the affinity-based purification of plasmid DNA from *E.coli* has relied upon short triplex-forming oligonucleotides as affinity-ligands (Wils *et al.*, 1997). However, whilst exhibiting high specificity for the target DNA sequence, they lack the necessary tight DNA-binding properties that are exhibited by DNA-binding proteins to immobilise the plasmid onto a solid support. However, effective techniques have been demonstrated where immobilised DNA affinity-ligands have been successfully employed to selectively purify sequence-specific DNA-binding proteins and restriction endonucleases from a clarified cell lysate (Pierrou *et al.*, 1995; Pozidis *et al.*, 1993). Therefore, using immobilised DNA-binding proteins within a solid matrix could potentially provide an effective DNA chromatography to target a recognition sequence within plasmid DNA with sufficient specificity and affinity to discriminate against genomic DNA and cellular protein present in a crude *E.coli* cell lysate. However, the reverse has not been demonstrated where sequence-specific DNA-binding proteins have been employed to effect the capture of plasmid DNA form a crude *E.coli* lysate. A permutation of the mouse transcription factor Zif268, fused to the protein glutathione S-transferase (GST), has been employed within this study.

1.7.2.1. Zinc-finger DNA-binding proteins

1.7.2.2. Historical perspective

From the moment Biologists first demonstrated that the primary method of regulating gene expression was through protein transcription factors (TF's) (Derman, 1981), a whole host of sequence-specific DNA-binding proteins that could hypothetically be integrated into a DNA chromatographic technique were discovered. Protein transcription factors are a group of proteins that recognise specific 'regulatory' DNA sequences that are predominantly located within the control region of a gene, and as such are present in very small quantities in cells. However, researchers found one eukaryotic transcription factor (TFIIIA) that was present at very high levels in immature oocytes of the frog *Xenopus laevis*, and employed as a storage particle complexed with 5S RNA (Klug *et al.*, 1995). It was found that the 30 amino acids were folded around a central zinc ion with a tetrahedral arrangement of cysteine and histidine metal ligands, an arrangement that formed a DNA-binding domain. Consequently, TFIIIA was named a zinc-finger protein and subsequently shown to contain a ubiquitous structural motif for the recognition of specific nucleic acid sequences. Indeed it has been estimated that between 300 and 700 human genes encode zinc-finger proteins, representing approximately 1% of the entire human genome (Hoovers *et al.*, 1992). Consequently, it was shown that the repeated nature of this motif is a feature common to all proteins containing zinc-fingers. After

the discovery of the zinc-finger motif in TFIIIA, other similar but distinct zinc-binding motifs were identified in several other families of proteins. Of these, the family utilising Cis_2His_2 zinc-fingers are the largest and most widespread (Berg 1993).

1.7.2.3. Structure of Cis_2His_2 zinc-fingers motifs and the protein Zif268

However, it was not until the structure of a single zinc finger for the *Xenopus* protein Xfn (Lee *et al.*, 1989) was solved using NMR spectroscopic techniques. Lee *et al.*, (1989) work presented direct evidence revealing that the 30-residue motif in Xfn folded to form an independent domain with a single zinc ion tetrahedrally co-ordinated between irregular, anti-parallel, two stranded β-sheet and a short α-helix. In addition, Miller *et al.*, (1985) demonstrated that the Cis_2His_2 zinc-finger family predominantly consists of 28-30 amino acids and contain a single zinc atom that co-ordinates and stabilises the protein structure of the DNA-binding domain (Miller *et al.*, 1985). The structure shown by Miller *et al.*, (1985) can be seen in Figure 1-1. Finally, the identity of the zinc-fingers and residues α, β and γ that are responsible for contacting the DNA bases was predicted by mutagenesis studies (Nardelli *et al.*, 1992) and confirmed by X-ray crystal structure analysis (Pavletich *et al.*, 1991). The resulting structure of the three zinc-fingers of Zif268 bound to the DNA can be seen in Figures 1-2, where the Cys_2His_2 zinc finger is folded into its three dimensional structure by the cysteine residues that are located within the β-sheet (Figure 1-3). The β-sheet extends towards the tip of the finger. The other side of the finger forms an α-helix that contain the DNA contacting residues α, β, and γ and the zinc co-ordinating histidine residues.

The X-ray crystallographic structures (Figure 1-2) reported by Pavletich *et al.*, (1991) demonstrated by that each zinc finger normally recognises three bases in DNA. Showing that when the zinc fingers bind to the DNA, the amino terminus of the α-helix angles downwards to fit into the major groove (Figure 1-2 shows the zinc-finger bound to DNA), the helix then aligns itself within the major groove so that the residues α, β and γ line up with the three target bases (Figure 1-4). It is these residues are responsible for the specificity of the DNA binding. The β-sheet is located behind the helix, away from the major groove so as not to interfere. The arrays of fingers can then arrange themselves around the major groove in a C-shape binding the three base sub-site of DNA as discrete modules. It is the amino acids at three key positions on the surface of the α-helix (13, 16, or 19 relative to the amino terminus of the helix) play the dominant role in base recognition. It was stated that an important contact between the first of the two histidine zinc ligands and the phosphate backbone of the DNA contributed to fixing the orientation of the recognition helix.

The Zif268:DNA complex that can be seen in Figure 1-2 has been stabilised by a series of hydrogen bonds with the DNA backbone. These are non-specific with respect to the target sequence. In total, seven hydrogen bonds are made between Zif268 and the phosphate backbone of DNA, stabilising the protein-DNA structure. In total, nine contacts are made between amino acid residues and the DNA bases. Six are responsible for specificity and the remaining three, which are asparagine residues, bind to base at the 3' end of the preceding sub-site located on the opposite DNA strand. Zif268 also contains a number of water contacts (Elrod-Erickson *et al.*, 1996) that may be of importance where no hydrogen bond is present. It has been shown that these are important in the overall affinity of the DNA for the DNA sequence (Schwabe *et al.*, 1997).

1.7.2.4. The zinc finger-glutathione S-transferase fusion protein

The zinc finger protein employed within this thesis is a permutation of Zif268 and was constructed initially by Berg in 1993. It was initially constructed to determine whether zinc-fingers could be designed with pre-determined specificity for a given target sequence. A strategy that could be applied for providing 'tailor made' gene suppressers in patient specific oncogenesis studies. Berg et al., (1993) demonstrated that zinc-finger could be employed as building blocks, linking fingers (three base recognition) by the linker sequences.

Berg et al., (1993) altered Zif268 to contain Arg^{13}, His^{16} and Arg^{19} for finger 1, Arg^{13}, Glu^{16}, Arg^{19} for finger 2 and Gln^{13}, Asp^{16}, Arg^{19} for finger 3 (Figure 1-5). This protein is termed QDR-RER-RHR. The orientation of recognition residues in each finger is anti-parallel to the 5'-3' orientation of bases, so that residue 19 recognises the first base of the triplet on the G rich strand. Consequently, the permutation of Zif268 was designed with specificity for the sequence 5'-GGG-GCG-GCT-3'. Berg et al., (1993) demonstrated that this zinc finger protein bound the predicted binding site with a dissociation constant of 2 nM (Figure 1-6). Furthermore, selection experiments demonstrated that this is the optimal binding site.

1.7.2.5. Fusion of the zinc finger to Glutathione S-transferase (GST)

Although the affinity and specificity of the zinc finger protein created by Berg et al., (1993) for its recognition sequence has been demonstrated, for its successful employment as an affinity ligand in chromatographic processes, a secondary affinity site must first be engineered into the protein. This secondary affinity site that will not adversely affect the affinity or specificity whilst allowing the capture of the protein-DNA complex from the process material. Consequently, Hine and co-workers fused the zinc-finger protein to glutathione S-transferase (GST), a protein that has affinity for immobilised glutathione (GSH).

Although such a zinc finger fusion protein has not been employed within the affinity stage of plasmid DNA purification, such a technique, if demonstrated to be sequence specific, can theoretically remove the need for numerous stages by capturing the protein-DNA complex from the crude *E.coli* cell lysate. Therefore, the zinc finger fusion protein was investigated for the potential to purify plasmid DNA sequence specifically from a post-EFD crude *E.coli* cell lysate as compared to other anion-exchange chromatographic stages.

2. MATERIALS AND METHODS

2.1. Chemicals, Kits and Dyes

Amersham Pharmacia Biotech. Bucks., UK. Sequenase kit, Thermosequenase kit, [α-33P] Terminators, Kadak Biomax MR film, Kodak X-Omat AR film, GST fusion vector (pGEX-2TK), GST bulk purification modules, GST detection modules (CNDB assay and anti-GST antibody).

Amincon Ltd, Gloucs., UK. Microcon concentrators.

Bio-Rad Laboratories, Detroit, USA. Bio-Rad protein assay, Nitrocellulose membrane, Ethidium bromide.

Difco Laboratories, Detroit, USA. Yeast extract, Tryptone.

Fisher Scientific UK. Ltd., Loughborough, UK. Sodium chloride, Sodium hydroxide, Glycerol, Visking dialysis tubing MWCO: 12,000-14,000.

Fisons laboratory supplies, Loughborough, UK. Glacial acetic acid, Methanol, Sulphuric acid, Analytical grade urea.

FMC Bio products, Rockland, USA. Sea plaque GTG agarose.

Gibco BRL Life Technologies, Paisley, Scotland, UK. Electrophoresis grade agarose, Super-competent *E. coli* DH5α cells.

MBI fermentas Ltd., Sunderland, UK. T4 polynucleotide kinase, T4 DNA ligase.

Molecular Probes, Leiden, Netherlands. PicoGreen.

New England Biolabs, Herts, UK. DNA polymerase 1, large (Klenow) fragment.

OXOID, Hampshire, UK. Agar technical.

Millipore, Hertfordshire, UK. EFD cross-flow micro-filtration modules,, Pro-Stak cross-flow filtration cassette, 13mm Stainless steel housing, 150mm Stainless steel housing.

MWG-Biotech, UK. Oligonucleotides.

Perkin Elmer ltd, Cheshire, UK. Taq polymerase, dNTP's.

Promega UK, Hampshire, UK. Wizard Plus Maxi prep kit, Wizard Plus Mini prep kit.

Severn Biotech ltd, Worcestershire, UK. 30% Acrylamide / Bisacrlyamide ration 29:1, 6% Acrylamide sequencing solution.

Sigma, Dorest, UK. Calf thymus DNA, Bovine Serum Albumin (BSA) Poly-L-lysine, Polyetheyleneimine.

2.2. Recipes

2.2.1 Buffers

1.	1x TAE:	400 mM pH8 Tris-HCl, 1 mM EDTA, 1.142% Glacial acetic acid
2.	1x TBE:	87 mM pH8 Tris-HCl, 2 mM EDTA, 87 mM Boric acid
3.	1x sequencing:	87 mM pH8 Tris-HCl , 2 mM EDTA, 3.6% Taurine
4.	10x SDS-PAGE:	250 mM Tris, 1 mM EDTA
5.	TE:	10 mM pH7.4 Tris-HCl, 1 mM EDTA
6.	TBS:	10 mM pH7.4 Tris-HCl, 140 mM NaCl
7.	PBS:	4 mM NaH_2PO_4, 16 mM Na_2HPO_4, 150 mM NaCl
8.	Glucose:	25 mM pH8 Tris-HCl, 10 mM EDTA, 50 mM glucose

All buffers were made up using DI water from a Millipore MilliQ Plus Ultra Pure Water System.

2.2.2. Electrophoresis gel loading buffers

1.	Agarose:	0.025% Xylene cyanol, 0.025% Bromophenol blue, 15% Ficaoll-400
2.	Agarose:	50% sucrose
3.	SDS-PAGE:	0.0125% Xylene cyanol, 6.25% SDS
4.	Sequencing:	Sequencing: 0.05% Xylene cyanol, 0.05% Bromophenol blue, 95% Formamide, 20 mM Na_2EDTA pH8

All buffers were made up using DI water from a Millipore MilliQ Plus Ultra Pure Water System.

2.2.3. Growth media

LB Medium: Tryptone (Difco) (1%), 0.5% yeast extract (Difco) and 1% NaCl dissolved in de-ionised water and adjusted to pH7.0 with NaOH. The medium was sterilised by autoclaving at 121°C, 15 psi for 15 minutes and ampicillin added to 50 μg ml^{-1} when the material had cooled below 60°C.

LB-agar: 1.6% agar (Oxoid) added to the LB medium, sterilised by autoclaving at 121°C, 15 psi for 15 minutes. For LB-agar-amp, ampicillin (50 μg ml^{-1}) was added after the autoclaved materials temperature reduced below 60°C.

Minimal Medium: Sterile water or water-agar (containing 1.5% agar with respect to the final volume) was combined with M9 salts (20%), 10 glycerol (2.5%), 200 mM $MgSO_4$, 10mM $CaCl_2$ (1%) and Thiamine (0.1%).

32

2.3. Bacterial strains

E. coli DH5α: φ80d*lacZ*ΔM15, *recA1*, *endA1*, *gyrA96*, *thi-1*, *hsdR17*($r_K^-m_K^+$), *supE44*, *relA1*, *deoR*, Δ(*lacZYA-argF*)U169

E. coli BL21 (DE3): F⁻, *ompT*, *hsdS_B*, (r_B^-, m_B^-), *dcm*, *gal*, λ(DE3)

Symbol	Description	Effect
dcm	Cytosine methylase mutation	Blocks methylation of cytosine in the sequence 5'...C^{m}CAGG...3' or 5'... C^{m}CTGG ...3'
deoR	Regulatory gene allowing constitutive expression of gene for deoxyribose synthesis	Allows uptake of large plasmids
endA1	Endonuclease mutation	Blocks catabolism of galactose
HsdR17 ($r_K^-m_K^+$)	Restriction minus, modification positive	Allows cloning without cleavage of transformed DNA by endogenous restriction endonucleases. DNA prepared from this strain can be used to transform r_K^+ E.coli strains
λ(DE3)	Bacteriophage carrying the gene for T7 RNA polymerase is integrated in the host genome	
F'	Host contains an F' episome with the stated features	
lacZΔM15	Partial deletion of β-D-galactosidase gene	Allows complementation of β-galactosidase activity by α-complementation sequence pGEM-Z vectors. Allows blue/white selection for recombinant colonies when plated on X-Gal
relA	Relaxed phenotype; mutation eliminating stringent factor	Allows RNA synthesis in the absence of protein synthesis
recA1	Mutation in recombination	Prevents recombination of introduced DNA with host DNA, ensuring stability of inserts.
supE	Suppressor mutation	Suppress ochre (UAA) and amber (UAG) mutation
thi-1	Mutation in thiamine metabolism	Thiamine required for growth in minimal media

References: Promega: Protocols and applications guide, Third Edition (1996).

2.4.   Electrophoresis

2.4.1.   Agarose gel electrophoresis

Agarose gel electrophoresis facilitates the separation of nucleic acids on the basis of their size and mobility. Electrophoresis gels were made from ultra-pure grade agarose (0.8-4% agarose, Gibco BRL), 1x TAE and 1 μg ml^{-1} ethidium bromide where PicoGreen was not used. The DNA sample was mixed with 1/5th volume agarose loading buffer and loaded into the well. The gels were run within 1x TAE running buffer at 10V cm^{-1} of gel for approximately 1 hour. Where ethidium bromide was used, gels were viewed on a transilluminator and images captured using a UVP system. Elsewhere, the dye PicoGreen was viewed on a TUNDRA™ digital imaging device where the probe was excited at 495nm and the resulting fluorescent signal detected at 535 nm.

2.4.2.   Sequencing gels

Sequencing plates (Bio-Rad Sequi-Gen sequencing cell) are cleaned with detergent, rinsed thoroughly in DI water and wiped with ethanol. The spacers were glued to the bottom plate that was supported horizontally. Glycerol tolerant gels (50 ml) containing 6% acrylamide (Severn Biotech Ltd), 21g Urea and 1x glycerol tolerant buffer were mixed where TEMED (25 μl) and 250 μl 10% AMPS solutions was added. The gel was pored within the two plates, secured and allowed to set for 30 minutes. The buffer 1x TBE or 1x glycerol tolerant buffer was pre-warmed to 60°C, added to the assembled sequencing cell where the entire equipment was allowed to warm up for 20 minutes (i.e. approximately 2000V).

2.4.3.   Polyacrylamide gels for protein analysis

Plates (Bio-Rad mini protean II) were cleaned with ethanol and assembled according to the manufacturers instructions. The resolving gel (14.25 ml) was made containing acrylamide diluted to the appropriate concentration for a 30% stock (Severn Biotech Ltd), 1.88 ml 3M Tris-HCl pH 8.8 and 0.15 ml 10% SDS (for a non-denaturing gel the SDS was left out of the mixture). Prior to pouring the gel, 7.5 μl of TEMED and 75 μl 10% AMPS was added, subsequently poured and overlaid with DI water for 30 minutes. The stacking gel was made containing 625 μl 30% acrylamide, 1.25 ml 0.5M Tris-HCl pH 6.8 and 50 μl 10% SDS (again, leave out SDS if necessary). After removing the overlaid water completely, 3.75 μl of TEMED and 35 μl 19% AMPS was added and poured on top of the resolving gel, the appropriate comb inserted finally and allowed to set for 30 minutes.

Where the protein was to be denatured, the samples were suspended in 1/10th v/v SDS-PAGE and heated to 95°C for 5 minutes immediately before loading. In addition, the appropriate markers were also denatured. Electrophoresis was performed in 1x SDS running buffer (without SDS if non-denaturing) at 100V for 2 hours. The gel could then be removed and stained with Coomassie blue (70°C) for 20 minutes.

2.4.5.   Coomassie blue staining

Gels were stained at 70°C within a 50% methanol, 7.5% acetic acid and 0.12% Coomassie blue solution for 20 minutes. The visualised the resulting protein bands, the unbound Coomassie was removed by incubating the gel in 5% methanol and 0.75% acetic acid overnight. Images of the protein bands were captured using a UVP system.

2.4.6. Gel retardation assay

The electrophoresis plates were cleaned and assembled according to the manufacturers recommendations. A non-denaturing gel was made (without SDS) where 29 ml of the resolving gel was prepared as previously. Immediately after the addition on TEMED and AMP into the mixture, the gel was poured in the plates, sealed with an appropriate comb and allowed to set for 30 minutes. The protein and DNA-Cye3 sample combined with a sucrose loading buffer (1/5th). Depending on sizes of the DNA and protein samples and their apparent mobility at 100V, the less mobile sample was loaded into the wells and run into the gel (~20 minutes) and then the other directly afterwards (~1 hour). The DNA-Cye3 was visualised in a TUNDRA™ digital imaging device. The protein bands are stained with camas blue.

2.4.7. PicoGreen

The fluorochrome PicoGreen was used according to the manufactures instructions, where 0.5 µl of the stock solution was added to the sample, incubated for 2 minutes and reading the fluorescence by excitation at 495 nm, emission at 535 nm in a TUNDRA™ digital imaging device. Depending on whether a plate or agarose electrophoresis gel is to be used, a calibration sample was assayed with either one well/lane left blank to determine the baseline fluorescence. The average baseline was subtracted from the fluorescence of the other samples.

2.5. Cell culture and molecular biology techniques

2.5.1 Preparation and transformation of competent cells

A single colony of *E.coli*, either DH5α of BL21 (DE3), was used to inoculate into sterile LB media and incubated overnight (37°C) where the resulting OD was determined by absorbance at 600nm of 1/10th culture diluted into PBS pH 7.4. Subsequently 300 µl of the overnight culture was inoculated into 30ml sterile LB and grown until the absorbance was between 0.4 and 0.6. At this point the cells were harvested in a fixed rotor centrifuge (Beckman J2-21, JA20 rotor) at 6,000 rpm for 5 minutes at 4°C. After discarding the culture media, the cells were re-suspending in ice-cold 10 mM $CaCl_2$ (6 ml) for 5 minutes. The cells were harvested, placed on ice, harvested and finally re-suspended in 1.2 ml ice-cold 50 mM $CaCl_2$ and incubated for a further 20 minutes. To transform the plasmid into the cells, 100 µl of the cell mixture was incubated with the DNA (300 ng) for 30 minutes, heat-shocked for 30 seconds at 37°C and returned to the ice for a further 2 minutes. Finally, the cells were incubated with 500 µl of LB-media at 37°C for 40 minutes. To select single transformed cells the transformants are plated out onto LB-agar-amp plates and incubated at 37°C overnight. The *E.coli* strain was checked for ampicillin resistance by plating out 100ml of untransformed cells onto the LB-agar-amp plates and subsequent incubation at 37°C.

2.5.2. Annealing oligonucleotides

Complimentary single stranded oligonucleotides (1 pmol µl^{-1}) were incubated at 95°C in a thermocycler (Hybaid OmniGene) for 5 minutes. The resulting mixture was allowed to cool slowly to room temperature by placing in a beaker of water at 95°C for 2 hours.

2.5.3. DNA preparation

Plasmid DNA was extracted from whole cells by Wizard (Promega) plasmid DNA purification kits according to the manufacturers instructions. 500 ml of the bacterial cell culture is pelletted at 5000g for 10 minutes and resuspended in 15 ml Promega 'cell resuspension solution'. 15 ml of Promega 'cell lysis solution' is added and stirred by inversion for 20 minutes. Finally 15 ml of Promega 'neutralisation solution' is added. The solution is centrifuged at 14,000g for 15 minutes and the resulting supernatant filtered through filter paper. 0.5 volume of room temperature isopropanol is added and the solution mixed by inversion. The solution is centrifuged at 14,000g for 15 minutes at room temperature. The DNA pellet is resuspended in 2 ml DI water.

Add the solution to 10 ml of Promega 'DNA purification resin' and pull through using a vacuum pump. Wash the resin with 25 ml of Promega 'column wash' and finally rinse the resin with 5 ml of 80% ethanol. Allow the vacuum pump to pull for an additional 1 minute. Insert the Promega 'maxicolumn' into a 50ml centrifuge tube and centrifuge at 2,500 rpm for 5 minutes. Add 1.5 ml of 70°C DI water to the resin and centrifuge the maxicolumn at 2,500 rpm for 5 minutes. Finally, filter the solution using a 0.2 μm sterilising grade filter and store at –20°C.

2.5.6. Ethanol precipitation of DNA

A 1/10 volume of 3M tri-sodium acetate pH5.5 and 2 volumes of ice-cold ethanol are mixed with the DNA by vortex. After incubating the mixture at –20°C for 20 minutes, the precipitated DNA was pelletted at 13,000 rpm in a micro-centrifuge for 15 minutes where the supernatant was removed by an aspirator. The resulting pellet was dried at room temperature for 10 minutes.

2.5.7. Polymerase chain reaction (PCR)

PCR's were performed within 1x PCR buffer (Perkin Elmer) with 10 μl dNTP's (Perkin Elmer) and 1 μM oligonucleotide primer where the final volume for each reaction was 20 μl. When PCR was used to screen bacterial colonies directly, a small amount of cells were transferred to the reaction tube using a pipette tip. The reactions were overlaid with 20-30 μl of mineral oil (molecular biology grade, Sigma). Tubes were placed in a thermo-cycler (Hybaid OmniGene) and the following programme executed. Denaturing at 95°C for 30 seconds, annealing at 50°C for 30 seconds and finally elongation at 72°C for 1 minute. The cycle was repeated 30 times after which the PCR products were examined by 2% agarose gel electrophoresis.

2.5.8. 'Fill in' and 'Blunt ending' reactions

Annealed products (40 μl) are 'filled-in' and 'blunt-ended' with dNTP's (deoxynucleotide triphosphate; 100mM) and ATP's (adenosine triphosphate; 1.6mM) by the enzymes polynucleotide kinase (0.5 units; PNK) and Klenow DNA polymerase (0.5 units; KLE) in 60μl 1xPCR buffered reactions. The enzyme PNK catalyses the transfer of the γ-phosphate from ATP to the 5' terminus of the polynucleotide whilst KLE fills the 5'-protuding ends with dNTP's. The reaction was incubated at room temperature for 10 minutes and terminated by heating the mixture to 75°C for a further 10 minutes.

Products (40 μl) from PCR reactions are incubated with 20 mM ATP (6 μl), 10units T4 polynucleotide kinase (1 μl), 10 units DNA polymerase I (1 μl), PCR buffer (1 μl) and sterile DI water (1 μl). The mixture was incubated at 37°C for 30 minutes after which time the enzymes were deactivated by raising the temperature to 95°C.

2.5.9. Ligation

Ligations were performed in 1x ligase buffer (MBI Fermentas) with 1 mM ATP, 5 units of T4 DNA ligase, approximately 20 ng of pre-phosphatased plasmid DNA and a 10 molar excess of the insert. The ligation is performed in 20 µl volumes overnight at 16°C.

2.5.10. Zinc-finger fusion protein expression

From transforming the competent *E. coli* BL21 (DE3) cells with the appropriate plasmid, a single colony is inoculated into pre-warmed 200 ml LB media containing 50 µg ml^{-1} ampicillin and 0.2% w/v sterile filtered glucose and grown overnight. The resulting culture was inoculated into 1800 ml pre-warmed LB-amp media and incubated at 37°C until an OD of ~0.5 is reached. The resulting culture is harvested in a fixed bucket centrifuge at 5,000 rpm for 10 minutes, re-suspended in 2L sterile LB-amp media containing 0.2 mM IPTG and incubated overnight at 30°C. Finally the cells are harvested as above and re-suspended in 80 ml volume 1x PBS pH 7.4.

2.5.11. Zinc-finger fusion protein purification

The Glutathione Sepharose 4B affinity matrix (2.66 ml) is prepared by centrifuging the slurry at 2,000 rpm for 5 minutes in a bench-top swinging bucket centrifuge. The supernatant is discarded and the matrix re-suspending in 20 ml 1x PBS pH7.4. This procedure is repeated twice and finally re-suspended in 2 ml PBS pH7.4 and stored on ice. PMSF is added to the cells containing the expressed fusion-protein to resulting in a final concentration of 1 mM. The cells are lysed by 6 cycles of freeze-thaw lysis i.e. liquid nitrogen and 37°C water bath. The resulting lysate is centrifuged (10,000 rpm, 10 min, 4°C) and the supernatant incubated with the matrix (4 ml) prepared previously. The fusion-protein and slurry are incubated on a roller at room temperature for 10 minutes. The slurry is subsequently centrifuged (2,000 rpm, 5 min, 4°C) and re-suspended in PBS pH 7.4 (20 ml) twice where finally the slurry is centrifuged and re-suspended in reduced glutathione elution buffer (3ml) on ice (2min). Centrifuge the slurry, retain the supernatant and repeat the previous step to yield approximately 6ml of fusion-protein. The eluate is dialysed against PBS pH 7.4 (1L, 4°C, 3hr), 20% glycerol 80% PBS pH 7.4 (1L, 4°C, 3 hr), and finally 50% glycerol 50% PBS pH 7.4 (1L, 4°C, 24hr) and stored at –20°C.

2.5.12. Dialysis

Visking (MWCO: 12,000-14,000) dialysis tubing (Fisher Scientific) was boiled for 10 minutes in de-ionised water, rinsed and stored at 4°C in de-ionised water. After clipping one end of the tubing, protein was loaded into the other and sealed. The tubing was then stirred in the appropriate buffer at 4°C.

2.5.13. Protein assay

For determination of protein in samples a Bio-Rad protein assay reagent was employed. For calibration purposes, samples of BSA (800µl) containing 25 µg ml^{-1}, 20 µg ml^{-1}, 15 µg ml^{-1}, 10 µg ml^{-1}, 5 µg ml^{-1}, 2.5 µg ml^{-1} and 1 µg ml^{-1} were created by diluting a pure 2mg ml^{-1} stock (Sigma) in DI water. After the addition of reagent (200µl) the resulting adsorbance is measured at 595nm using DI water as a reference. The concentration of fusion-protein can then be determined from the resulting calibration curve.

2.5.14. DNA assay

The concentration of DNA in a sample was established by measuring its absorbance at 260nm against a DI water blank in a Shimadzu UV-1201 Spectrophotometer (Tokyo, Japan) using a 1 ml quartz cuvette.

2.5.15. Viscosity

Cell culture viscosity was determined using a programmable rheometer fitted with an ultra-low viscosity adapter. A calibration curve was generated by determining the viscosity of cells varying between OD 2.5 to OD 100.

2.5.16. Optical density

The optical density of a cell culture was established by measuring its absorbance at 600nm against a LB-media blank in a Shimadzu UV-1201 Spectrophotometer (Tokyo, Japan) using a 1 ml quartz cuvette.

2.5.17. Freeze-thaw cell lysis

Freeze-thaw lysis is a technique that is able to disrupt cells without denaturing the cellular proteins within. To ensure complete disruption, the samples follow six cycles of freezing (liquid nitrogen, -70°C) and thawing (water bath, 37°C).

2.6. EFD cross-flow micro-filtration system

2.6.1. Preparation of EFD micro-filtration modules

The EFD micro-filtration modules were held within the system seen in Figure 3-1, chemically cleaned with 300 ml of NaOCl (60°C) diluted into DI water (400 ppm) for 20 minutes under 3 psi transmembrane pressure (TMP), and finally expelled from the system. Prior to introducing the challenge material, the remaining NaOCl was flushed from the system with 5L DI water (60°C), 5L DI water (25°C) and the resulting water permeability measured.

2.6.2. Operation of the EFD system

Depending on the process material that is being studied, the EFD module was equilibrated with either DI water or sterile LB-amp media (1L), determining the appropriate valve positions for the desired test conditions and finally the initial permeability. The TMP at which the permeability was determine in one of two ways, either by simply restricting the exit retentate flow (i.e. exit pressure) resulting in an average axial TMP, or by restricting the exit retentate flow and pumping the permeate co-currently within the shell to equilibrate the axial TMP (See Chapter 3). The challenge material was introduced slowly into the EFD module, the retentate re-circulated back into the feed tank (i.e. this was done without permeation, TMP=0) and the flow rate slowly increased to the desired cross-flow conditions.

2.7. Affinity membranes

2.7.1. Preparation of membranes

The membranes were held in 25 mm (Sartorius SartoBind Q15), 13 mm or 150 mm stainless steel housings (Millipore), and flushed with 300 ml or 1000 ml respectively. The UltraBind US450 membrane was housed in the 150mm Millipore stainless steel membrane holder, flushed with 50ml water where a bleed valve was employed to expel the water and air from the housing and introduce the challenge solution containing the DNA. For determination of breakthrough curves or the equilibrium binding capacity, 1 ml fractions of the effluent was collected at the exit of the filter, and their DNA content was assayed using UV adsorption at 260 nm as calibrated against known calf thymus DNA quantities.

2.7.2. Challenge material for membranes

Test solutions of calf thymus DNA were prepared by dissolving 10 mM Tris and 1 mM EDTA (TE) in water and titrating with HCl until the desired pH values (7.4) were reached. NaCl was then added to the concentration required and the pH value of the resultant solution confirmed. Calf thymus DNA was added to the solution, after reserving 100 ml as a blank, where 1 ml was retained to determine the pre-membrane DNA concentration. Process samples were taken from the post-EFD process stream where a 1L of *E. coli* DH5α culture transformed with the plasmid pTS had been concentrated, diafiltered and finally lysed (freeze-thaw), passing through 300 ml of the clarified plasmid DNA, genomic DNA, cellular protein and unknown concentrations of endotoxin and RNA.

3. DEAN VORTEX MICRO FILTRATION

3.1. Overview

As discussed previously, cross-flow micro-filtration (CFMF) was described as a relatively new technology attempting to provide an economical but realistic alternative to the continuous centrifuges that are currently employed to harvest cultured bacterial cells within the Biotechnology industry. Historically, CFMF has been unable to compete as typical permeation rates ranged between 40 and 60 lmh (ProStak, Millipore) rather than the 150-400 lmh achieved by continuous centrifuges (Caridis *et al.*, 1997). This was largely due to the inherent problems associated with deposition of fouling material onto the membrane that resulted in a fouled layer of low permeability (Mondor *et al.*, 1999). However, the employment of CFMF remains economically advantageous due to low capital, and operating costs, when compared to other technologies. Consequently, workers within the Biotechnology field have attempted to develop CFMF to the point where the intrinsic problems discussed are minimised. Therefore, current research has focused on exploiting the specific fluid characteristics that are derived from the module geometry and the cross-flow rate (Crowder *et al.*, 1997, Moulin *et al.*, 1999, Mallubhotla *et al.*, 1995, 1997, 1998). The EFD (Millipore, UK) is one of these CFMF modules, incorporating tubular membranes that are wound in a helix to promote centrifugal instabilities within the flow channel. Within the literature, these centrifugal instabilities are known as secondary flows or Dean vortices. However, it should be noted that previous studies have only shown that such Dean vortices can produce flux enhancement over linear membranes (Kluge *et al.*, 1999, Kakuvi *et al.*, 2000, Manno *et al.*, 1998). At the time of writing, the ability of these Dean vortices to control the deposition of fouling material had not been effectively demonstrated. Therefore, this chapter describes the work performed to ascertain the potential of the EFD system within three, normally distinct, sections of the plasmid DNA purification process. These three stages are:

- Harvesting *E.coli* bacterial cells from the culture media at a rate between 150-400 lmh,

- Diafiltration of the harvested cells into a suitable lysis buffer,

- Clarification of the target plasmid DNA from the cellular debris resulting from freeze-thaw cell lysis.

Note, a freeze-thaw lysis technique was employed to maintain the highest integrity of the zinc-finger affinity ligand discussed within Chapter 5. Experiments were designed with a two-fold objective, to demonstrate the intrinsic ability of the EFD module to perform each of the three tasks detailed above, and to determine the nature and influence of the primary flow and Dean vortices on the observed performance. Therefore, this chapter includes the work performed to develop a numerical understanding of the helical flow system employed by the EFD system. The information gathered from this study was the used to interpret the experimental observations whilst flowing pure de-ionised (DI) water through the EFD system at various cross-flow rates. The system was operated at zero transmembrane pressure (TMP) (i.e. without permeation) to determine the effect of the fluid dynamics at a particular cross-flow rate on the friction factor (f), friction (f.Re), power dissipation (P_D) and axial pressure drop (ΔP_x). Consequently, a positive TMP was applied to the EFD system and the influence of cross-flow on the permeation rate was determined. Finally, the EFD system was challenged with a fouling solution containing *E.coli* bacterial cells in order to determine the ability of the Dean vortices to control the fouling rates that have previously restricted the use of similar CFMF systems.

3.2. The EFD system

Figure 3-1 shows the schematic of the EFD system, consisting of a single EFD module, three peristaltic pumps (Cole Palmer), six peristaltic heads (Cole Palmer), four stainless steel pressure gauges (Cole Palmer, -15 to 30 psi) and one restriction valve (Fisher). Silicon (Masterflex^{TM}, Size 16) tubing was used throughout the system and connected by plastic fittings (Fisher). Within the EFD module, six individual hollow fibre membranes (poly-ether-sulfone) are wound in a helix around a central steel rod, and placed within a clear cylindrical housing. The design specifications and operating characteristics as recommended by the manufacturer are detailed below within Table 3.1.

Property	Symbol	Value
Active surface area (cm^2)	a_t	125
Inside diameter of fibre (mm)	d_I	1.25
Outside diameter of fibre (mm)	d_o	1.95
Diameter of central rod (mm)	d_{rod}	6.35
Active fibre length (mm)	l	302
Number of fibres	m	6
Pitch (mm)	p	1.86
Radius of curvature (mm)	r_c	7.33
Torsion (mm^{-1})	τ	0.09
Curvature (mm^{-1})	κ	0.2
Operating temperature range (°C)	T	0-60
Operating pH range	pH	3-13
Critical Dean number	Dn_{CRIT}	13

Table 3.1: Design specifications and operating characteristics of the helical EFD (Millipore UK) cross-flow micro-filtration modules.

Consequently, the system was able to measure seven individual parameters including the inlet ($p_{r,in}$) and outlet ($p_{r,out}$) retentate pressures, inlet ($p_{p,in}$) and outlet ($p_{p,out}$) permeate pressures, the inlet retentate flow-rate ($Q_{R,IN}$), the permeate ($Q_{r,in}$) flow-rates and the permeate flux (lmh). The peristaltic pumps were equipped with twin heads off-set to 90°C to dampen the characteristic flow and pressure pulses. Although there is no explicit evidence to suggest so, oscillations in the pressure and cross-flow rate are thought to significantly effect the initiation and propagation of Dean vortices that would be characteristic of a particular cross-flow. The single restriction valve (RV1, Cole Palmer), located at the retentate outlet, is used to vary the retentate inlet, the retentate outlet pressure and consequently the transmembrane pressure (TMP). The permeate recycle rate ($Q_{P,IN}$) is used to control the permeate inlet ($p_{P,IN}$) and outlet ($p_{P,OUT}$) pressures, so adjusting the axial TMP within the module.

3.3. Preliminary studies

Prior to elucidating the governing fluid dynamics that were induced by the cross-flow within the EFD module, experiments were devised to demonstrate the intrinsic ability of the EFD to process *E. coli* bacterial cell cultures and the subsequent lysate. Initially, a procedure (Method 2.6.2) suggested by previous researchers (Kluge *et al.*, 1999) was used to operate the EFD system (Figure 3-1a).

3.3.1. Cleaning

The flow system was cleaned before, and after each experiment, until the initial pure water permeability for the processing conditions was returned. Firstly, a solution of 400 ppm NaOCl (60°C) was pumped (400 ml min^{-1}) through the system for approximately 20 minutes under the influence of 3 psi TMP i.e. the permeate valve was open and recycling back into the feed tank. Secondly the system was flushed with 5L of pure distilled water (60°C) and flushed again with 5L of pure distilled water (25°C) and the water permeability measured. This step was repeated when necessary.

3.3.2. Flow system

Depending on the type of material to be processed, either DI water or sterile lurium broth media (LB-amp), containing 50 μg ml^{-1} of the antibiotic ampicillin (LB-amp), was pumped through the system under identical conditions of pressure and flow-rate as would be employed during experiments. This was done to ascertain the correct valve positions required for the experiment and to expel any trapped air from the system. The challenge material was introduced to the system without permeation (TMP=0), allowed to equilibrate (1 min) at the desired cross-flow and permeation slowly induced until the desired condition was reached. A stop-watch was started at the appearance of permeate, and the permeation rate was measured with time. The permeate and retentate was re-circulated to the feed tank to maintain constant viscosity and density throughout the experiments. After completing the experiments, the membrane was cleaned, as described above, and the water permeability measured, and compared to the initial value. For the purposes of this experiment, the mean TMP was defined by:

$$TMP = \left(\frac{p_{r,in} + p_{r,out}}{2} \right) - p_{p,out} \tag{3.1}$$

3.3.3. Experimental

Figure 3-9a ('Old') shows the resulting flux-time graph where the high fouling rates caused the initial permeate flux (420 lmh) to reduce (230 lmh) after 10 minutes whilst apparently achieving a pseudo-steady state after 30 minutes. In a rather crude sense, this preliminary result indicated that the current EFD system was apparently able to compete with the existing technologies but only for a short time period. However, during the experiment, the actual axial TMP experienced within the EFD module was seen to differ considerably with that defined by the mean TMP (Eq 3.1), decreasing sharply from the inlet (6 psi) to the outlet (0 psi) of the module. It is known that permeation is solely a pressure driven phenomenon (Kluge *et al.*, 1999), as described by Darcy's law, where permeate flux is dependant upon the TMP experienced at a particular axial position. Therefore, it was valid to assume that the permeation rate would mimic the axial TMP (6 psi – 0 psi), initially decreasing sharply from 840 lmh flux at the inlet and 0 lmh flux at the outlet i.e. an average of 420 lmh.

Understanding (Kluge *et al.*, 1999) that excessive permeation imposes a significant de-stabilising influence on the fluid dynamics, this observation also indicated that the loss in stability was seen in the fouling rate. In addition, it was known that *E. coli* cells experience a critical TMP within similar micro-filtration modules, at which *E. coli* cells irreversibly foul and compress onto the membrane surface at pressures exceeding 4-5 psi (Caridis *et al.*, 1997) i.e. lower than the observed inlet TMP. Therefore, the combined influence suggests that the observed fouling rate was directly related to the stability of the system and that any experiments devised would be unable to observe the occurrence of a specific fluid dynamic within the EFD system. The experimental procedure was, therefore, modified to equalise the axial TMP within the EFD module, recycling the permeate co-currently within the shell of the EFD module, whilst simultaneously altering the retentate outlet pressures until the desired axial TMP was achieved. Consequently, the axial TMP was re-defined as:

$$TMP = \left(p_{r,in} - p_{p,in} \right) = \left(p_{r,out} - p_{p,out} \right)$$

(3.2)

whilst Darcy's law, equating the axial TMP to the flux was defined as:

(3.3)

$$Q_p = \frac{TMP}{\mu \cdot R}$$

Figure 3-9a ('New') shows the flux-time plot under the exact conditions, previously employed, where the equalisation in axial TMP resulted in a significant reduction in fouling rate. After 10 minutes, the revised procedure maintained a flux of approximately 400 lmh, 170 lmh greater than seen previously. Therefore, all further experiments employed this procedure, to introduce stability into the system, whilst promoting an accurate representation of the action of the underlying fluid dynamics within the experimental data.

3.4. Characterisation of the EFD system

Although other workers (Belfort *et al.*, 1993) demonstrated experimentally the existence of primary flows and Dean vortices within similar helical tubes when employing MRI imaging techniques, the physical action of these flows, and their implication for processing bacterial cell cultures, had not been determined. Considering that MRI techniques could not be employed within this study, numerical techniques were used to determine the influence of the primary flows and Dean vortices on the experimental behaviour of the EFD system. The observed experimental manifestations of the primary flows and Dean vortices were detailed as follows:

- Permeation rate (flux),

- Axial pressure drop (ΔP_x),

- Power consumption (P_d),

- Friction factor (f),

- Friction (f.Re),

- Fouling rate.

A numerical study was initially employed to evidence, as far as possible, the influence of each of the above and finally to determine the nature of the primary flows and Dean vortices that resulted in the observed experimental data.

3.4.1. Numerical studies

Numerical studies of laminar flows within toroidal pipes (a helical pipe with zero pitch) have received extensive treatment within the published literature as initiated by Dean in 1927 (Dean, 1927, 1928). However, the numerical solution to laminar flows, within helical pipes of finite pitch, was only accomplished recently. Truesdell and Adler (1970) were the first to replace toroidal flow with simplifying helical approximations for geometry's with a small pitch, until Germano (1982, 1988) introduced an orthogonal co-ordinate system (Appendix 3) which subsequently lead to the first complete solution to the Navier-Stokes equations being published. It was with this co-ordinate system that the current workers published their work, (Liu *et al.*, 1993, Bara *et al.*, 1992, Chen *et al.*, 1992, Finlay *et al.*, 1988, Huttl *et al.*, 1999, Ito, 1969) and developed our understanding of the specific fluid dynamics occurring within helical tubes under the combined influence of torsion and pitch. Liu *et al.*, (1993) formulated the numerical problem by transforming the continuity, momentum, and energy equations into orthogonal co-ordinates. This can be seen within Appendix 3. However, that formulation was based on simplifying assumptions concerning a solid domain boundary (membrane), a Newtonian incompressible flow that was fully developed (steady state) and displaying 'no-slip' of the fluid elements at the wall. In addition, a loose-coiling analysis was also introduced to further simplify the equations (Appendix 3) into a solvable format. However, this numerical solution was studied to demonstrate numerically how the 'observable' experimental parameters could be influenced by the underlying flow equations. It was observed that the movement of fluid elements, within a helical pipe, was subject to three dimensionless parameters. Those being the curvature ratio (λ), torsion (η) and Reynolds number (Re). As such they were all able to influence the momentum, continuity and energy equations. The curvature was defined as:

$$\kappa = \left(\frac{r}{r^2 + p^2} \right) \qquad\qquad (3.4)$$

Whilst torsion was defined as:

$$\tau = \left(\frac{p}{r^2 + p^2} \right) \qquad\qquad (3.5)$$

The corresponding dimensionless quantities used by Kao (1987) were then:

$$\varepsilon = \kappa a = \left(\frac{r}{r^2 + p^2} \right) a \qquad\qquad (3.6)$$

$$\lambda = \tau a = \left(\frac{p}{r^2 + p^2} \right) a \qquad\qquad (3.8)$$

Where p is the pitch and r_c the radius of curvature i.e. the radius of curvature of the tube coiled in a single plane:

$$r_c = \frac{r^2 + p^2}{r} \tag{3.7}$$

Whilst the pitch (p) was given by:

$$p = \frac{m}{2\pi} d_o \tag{3.8}$$

Where d_o is the outer diameter of the tube, m is the number of tubes lying next to each other and r the radius of curvature within a single plane. Reynolds (Re) was defined as:

$$Re = \frac{2aV_m\rho}{\mu} \tag{3.9}$$

Where V_m is the mean azimuthal velocity, ρ the density, μ the viscosity and a the inner radius of the tube. Within the adopted formulation, Liu *et al.*, (1993) neglected any axial variations in flow so as to equate the Reynolds number (Re) to a normalised (within orthogonal co-ordinate system) axial pressure gradient. The introduction of that assumption was able to simplify the equations further:

$$f.Re = -4\frac{\partial p}{\partial x} \tag{3.10}$$

Where the friction factor (f) is defined by Keulega *et al.*, (1937) as:

$$f = \frac{2}{\rho}\frac{d}{l}\frac{\Delta P_x}{V_m^2} \tag{3.11}$$

Where d is the inside diameter, ΔP_x the axial pressure drop and l the length of the tube. From this analysis, two dominant flow groups were seen to emerge, $Re\eta$ and $Re^2\lambda$, imposing the greatest control over the governing equations.

3.4.1. Germano number (Gn)

The first group was defined as the Germano number (Gn) (Germano 1988) and was identified as contributing 'twisting' forces to the fluid elements within the helical pipe.

$$Gn = Rea\tau = Re\left(\frac{p}{r^2 + p^2}\right)a \tag{3.12}$$

It is stated that these forces cause the fluid elements to 'twist' or 'swirl' within the flow field, as they are proportional to $\rho\eta U^2$. However, the counteracting viscous forces are proportional to μU. Therefore, the Germano number (Gn) directly measured the ratio of 'twisting' forces to 'viscous' forces i.e. the Germano number measures the effect of torsion.

3.4.2. Dean number (Dn)

The second dominant group was identified as a generalised Dean number (Dn).

$$Dn = Re\left(\frac{a}{r_c}\right)^{0.5} \tag{3.13}$$

The flow group Dn is sometimes referred to as the helical number, or a modified Dean number within the literature, modified in the sense that it has changed from that initially defined by Dean (1927). The inertial force was proportional to ρU^2, centrifugal forces to $\rho\lambda U^2$ and the viscous forces to μU. Therefore, the square of the Dean number directly measured the product of the ratio of centrifugal to viscous forces and the ratio of inertial to viscous forces. Centrifugal forces are known to cause fluid elements to move towards the outer-wall whilst viscous forces bring the fluid elements back towards the inner-wall. Hence, the Dean number is a direct measure of the competing centrifugal and viscous flows that are finally seen as Dean vortices. From this, the Dean ratio (D) was defined as the ratio of Dn to the critical Dn (point of initiation of Dean vortices), thus allowing the direct comparison between different systems.

$$(3.14)$$

$$D = \frac{Dn}{Dn_{Crit}}$$

3.4.3. Gamma number (γ)

From Gn and Dn, a new group emerged indicating the importance of the Germano number for any given Dean. The group was known as Gamma (γ) and is related to Gn and Dn by:

$$\gamma = \frac{Gn}{Dn^{1.5}}$$
$$(3.15)$$

The group emerged after substitution of the relationship $f.Re\alpha Dn^{0.5}$ into the governing equations (this assumption was shown to be valid for the EFD). Therefore, for the Germano number to impose a noticeable influence on the helical flow field, $GnDn^{-0.5}$ had to be be large (Appendix 3). For large Dean flows in relation to Gn, it was expected that γ should characterise the transition from a torus-like flow into a swirling flow. When γ was small, the secondary flow pattern was torus-like (twin vortex in the 'up' and 'down' positions (Figure 3-2b), while for a large γ, the secondary profile was 'swirl' like (single rotating vortex). Similar transitions in the flows were predicted numerically elsewhere within the literature (Wang *et al.*, 1981, Tuttle *et al.*, 1990, Yamamoto *et al.*, 1998). Therefore, the meaning of γ can be understood as a measure of swirl strength, due to twisting forces (μru_1), and swirl strength due to the centrifugal forces (u_3).

The physical implication of γ suggests that when γ is large, the centrifugal forces becomes less significant. Consequently, helical flow fields are expected to be related to γ rather than η or Gn when under the influence of torsion. Liu *et al.*, (1993) demonstrated that torsion could be neglected when $\gamma < 0.1$ for moderate Dn values only. Theoretically, the critical value for which secondary flows change from twin vortices to single is $\gamma > 0.2$ for Dn>20 (Kluge *et al.*, 1999). As Dn increases towards high values, γ indicates the orientation of the secondary flows, inclining towards the upper and lower walls. Therefore, to devise relevant experiments which demonstrate the implications these numerical prediction will have on the experimentally determine data, certain facets should be discussed.

3.4.5. Cross-plane pressure gradient

Liu *et al.*, (1993) and Huttl *et al.*, (1999) showed that by increasing Dn, the centrifugal and viscous combined to influence the cross-plane pressure gradient, i.e from the inside to outside of the flow plane. The magnitude of this effect can be seen within Table 3-2 where the maximum (p_{max}) and minimum (p_{min}) pressures were 20.11 and −9.07 for 100_{Dn}, and 94.39 and −35.54 for 500_{Dn} (Huttl *et al.*, 1999) respectively. Note, these values are scalar function of the pressure experienced at the centre of the cross plane. Consequently, it was demonstrated by Huttl *et al.*, (1999) that increases in the Dean number result in an increase in the cross-plane pressure gradient, and so force the Dean vortices across the flow-plane and towards the outer wall. Huttl *et al.*, (1999) also demonstrated that the translocation of the Dean vortices resulted in their compression i.e. reducing their influence over the fluid elements within the flow-plane. It was thought that the practical effect would be a reduction in the average radial TMP, i.e. reducing the observed friction factor and permeate flux.

3.4.6. Power consumption (P_d)

It was discussed that decreases in γ cause the centrifugal forces to dominate the viscous forces. An effect that relocates the Dean vortices towards the outside of the flow-plane, i.e. more fluid elements moving towards the outer, rather than the inner wall. Therefore, the distorted fluid profiles being more energy intensive were thought to increase the power consumption (P_D) and therefore infer when additional complexity had been introduced into the flow regime. Accordingly, the power dissipated (P_D) was defined as:

$$P_D = \left(Q \cdot \Delta P_x + Q_P \Delta P_{TMP}\right)$$

(3.16)

Where Q is the feed flow rate and Q_P is the permeate rate (Manno *et al.*, 1998).

3.4.7. Friction factor (f)

Friction factor (f) was stated as the direct ratio of the force exerted by the fluid over a specific area of membrane surface and the kinetic energy possessed by that fluid element per unit volume. For laminar flow within long tubes (l/d>>1) the friction factor was defined as (Transport Phenomena, R. Bird *et al*, 1960):

(3.17)

$$f = \frac{16}{Re}$$

Whilst for coiled pipes:

$$f = \frac{1}{4}\left(\frac{d}{l}\right)\left(\frac{\Delta P_x}{1/2\rho V_m^2}\right)$$

(3.18)

Therefore, the influence that increasing the Dn had on the friction factor would describe the average radial TMP experienced within the EFD. Liu *et al.*, (1993) demonstrated that an increase in the friction factor corresponded to an increase in the apparent Dean vortex strength, whilst a decrease suggested the opposite i.e. increases in the Dean vortex strength can increase in the radial TMP and therefore increase the permeation rate. However, it should be noted that the average radial pressure can be reduced if the cross-plane pressure gradient increases to such a level as to leave areas experiencing lower pressure than the that of the initiation pressure i.e. <-0.25 psi, back-flow.

3.4.8. Development of a series of experiments to determine EFD fluid dynamics

In consideration of that described above, a series of experiments were developed to determine how the three flow group (Dn, Gn and γ) influenced the power dissipation (P_d), friction (f.Re), fiction factor (f), permeate flux and finally the fouling rate. Accordingly, the experiments were planned within three distinct areas of operation:

- Non fouling fluid without permeation,

- Non-fouling fluid with permeation,

- Fouling fluid with permeation.

The experiments were designed to demonstrate, as far as possible, compliance with the simplifying assumptions imposed onto the numerical studies.

3.5. Non-fouling fluid without permeation

3.5.1. Experimental

Initially, the experiments were designed to confirm that the numerical assumptions stated by Liu *et al.*, (1993) were also valid for the EFD system. Therefore, the system was operated without permeation (solid wall boundary), at constant pressure, temperature, and cross-flow rate. After cleaning (see Section 3.3.1), the cross-flow rate was set and the axial TMP reduced to zero. It was seen that for all Dean numbers, permeation occurred only once a TMP of +/- 0.25 psi was induced i.e. the initiation TMP resulted from a membrane resistance (R_m) of $4.0x10^{12}$ s^{-1}. However, it should be noted that by simply closing the permeate valve without equilibrating the axial TMP, the shell and tube side pressure drops suggested that the EFD was experiencing re-circulation effects i.e. the solid wall assumption was invalid. This was not the case when recirculating the permeate co-currently within the shell side. Finally, the simplifying relationship introduced by Liu *et al.*, (1993), (f.Re $\alpha Dn^{0.5}$) was shown to be true for the EFD system (data not shown).

Whilst the accuracy and reliability of the numerical studies had been demonstrated, it was assumed that the EFD system would exhibit increased levels of friction over the equivalent numerical study. This suggested that any numerical correlation from the literature would not accurately describe the EFD system. Consequently, the validity of using such numerically determined correlation's was uncertain. In addition, due to the manufacturing processes and the inherent nature of permeable hollow fibres, a 'smooth wall' assumption could not be presupposed valid. Therefore, it is suggested that the data collected, concerning the friction (f.Re), friction factor (f) and power dissipation (P_D), could only be used to infer the behaviour of the fluid within the EFD system rather than equating the results to actual numerical solutions.

3.5.2. Results

The experimental results can be seen within Figures 3-5 and 3-6 (0 psi data), where the axial pressure drop (ΔP_x), friction (f.Re) friction factor (f) and power-loss (P_D) is presented as a function of the flow groups γ and Dn. Included in the plots are the numerical correlation's presented by Ito *et al.*, (1969) Gnielinsky *et al.*, (1986) and Liu *et al* (1993), all of which have only demonstrated accuracy whilst the influence of torsion was assumed negligible. The correlation given by Liu *et al.*, (1993) had been shown by the author to be valid for Dn<5000 and γ<0.1:

$$f \cdot Re = \left[16 + \left(0.378 \cdot Dn \cdot \lambda^{0.25} + 12.1\right) \cdot Dn^{0.5} \cdot \lambda^{0.5} \gamma^2\right] \times \left[1 + \frac{\left(0.0908 + 0.0233 \cdot \lambda^{0.5}\right) \cdot Dn^{0.5} - 0.132 \cdot \lambda - 0.2}{1 + 49/Dn}\right]$$

The deviation was quoted as less than +/- 2% (Liu *et al.*, 1993). Ito *et al.*, (1969) presented a boundary layer approximation to predict energy losses due to Dean vortices within coiled tubes. An assumption that resulted in the following correlation:

(3.20)

$$\frac{f_c}{f_s} = 0.1008 \cdot Dn^{0.5}\left[\left(1 + \frac{1.729}{Dn}\right)^{0.5} - \frac{1.315}{Dn^{0.5}}\right]^{-3}$$

The friction factor for either a straight or curved pipe was defined as (Bird *et al.*, 1960):

(3.21)

$$\Delta p_x = f \cdot \frac{l}{2 \cdot d} \rho V_m^2$$

Finally, Gnielinski *et al.*, (1986) recommended an experimental correlation for laminar flow of fluid within an helical pipe:

(3.22)

$$\frac{f_h}{f_s} = 1 + 0.033 \left(\log_{10} De\right)^{4.0}$$

As predicted, Figures 3-5 and 3-6 demonstrate that the EFD system experienced increased levels of friction over that approximated by the numerical/experimental correlation's. In part, this demonstrates that effect of torsion cannot be considered negligible. i.e. assumed negligible for the purposes of the correlation's. However, it should be appreciated that the EFD is a manufactured membrane. There appeared to be convergence between the experimental and correlated data whilst Dn remained small i.e. an increased γ suggests negligible torsion effects. This indicated that the elevated friction experienced experimentally was due to the effect of torsion rather than the membrane surface. In addition, the subsequent increases in power dissipation (P_d) above that of friction (f.Re), as seen in Figure 3-6, indicated that the system energy is being dissipated by the complexity of the fluid elements rather than solely by friction. As opposed to the previous statements, this now suggested that the effect of torsion of on the fluid was not negligible within the EFD system. Numerically this was supported by the definition of Gn (Section 3.4.1). Consequently, the numerical correlations could be used to describe the experimental system.

However, Liu *et al.*, (1993) and Huttl *et al.*, (1999) described a numerical system which was very similar to that of the EFD without assuming the effect of torsion to be negligible. They demonstrated numerically that such increases in the Gn caused Dean vortices to be unidirectional through the body-centred azimuthal velocity ($\xi = w - \eta r u / h_1$). When λ (experimentally 0.2) and Dn were large in the governing equations, Gnλ and Gnλ^2 ($\lambda \eta Re$ and $\lambda^2 \eta Re$) became significant and influenced the source terms within the Dean vortex momentum equations (Appendix 1). As such, the torsion caused the Dean vortices and primary flow to become increasingly more complicated i.e. γ became small. Therefore, it is hypothesised that the observation discussed above were caused by these complications that in turn caused the experimental f.Re, f and P_D to increase.

In explanation of the torsion effect, increases in Gn (γ decreases), cause the centrifugal components of the fluid to dominate the flow plane, compressing the position of the Dean vortices (Figure 3-2 and 3-3) into the outside walls, so increasing their energy usage. This registers experimentally by the

increases in P_D and f.Re. However, such a distortion in the flow pattern also causes the shear profile within the cross-plane to change considerably, creating a localised maximum towards the outside of the helical turn (Figures 3-2c and 3-3). It should be noted that such a shear profile would have large ramifications concerning the ability of the EFD system to control the deposition rate of a fouling mixture.

In agreement with the series-expansion method presented by Kao *et al.*, (1987) (Appendix 4), full numerical studies (Liu *et al.*, 1993, Huttl *et al.*, 1999) located the positions of the Dean vortices within 'up' and 'down' positions when Dean is of moderate values ($10-120_{Dn}$). However, Liu *et al.*, (1993) suggested that torsion only distorted the primary flow profile once the limit of the series solution had been exceeded i.e. $>120_{Dn}$.

Accordingly, the strength of the Dean vortices appeared to reduce as Dn increased above 500_{Dn}. Liu *et al.*, (1993), demonstrating that a centrifugal plane had been created within the centre of the cross-plane at 500_{Dn}, and directed from the inside to the outside of the helical turn. As Dn was further increased, this plane expanded to form a 'large' centrifugal plateau. It was shown that it was this plateaux that had compressed the secondary flows into the walls whilst increasing the cross-plane pressure gradient sharply (Figure 3-4). This effect can be seen within Table 3.2 where increases in the Dn number increased the cross-plane pressure distribution by 345% and reduced both the central ($x=0$, $y=0$) axial velocity ($u_{0,0}$) and the maximum axial velocity (u_{max}).

Dn	λ	η	Gn	γ	f.Re	$u_{0,0}$	u_{max}	p_{max}	$-p_{min}$
100_{NUM}	0.2	0.1	22.36	0.0224	25.36	0.6374	0.8120	20.11	9.07
500_{NUM}	0.2	0.1	111.8	0.01	46.6	0.5739	0.7748	94.39	35.54
500_{EXP}	0.2	0.09	129.99	0.0114	122.2	"	"	"	"

Table 3.2: Comparing numerical (Liu et al., 1993) and experimental data characterising the flow within a helical pipe under the effect of torsion. The data indicates how the Dean number (Dn) influences the cross-plane pressure gradient and axial velocity profile for a numerical system closely relating the helical EFD micro-filtration module studied experimentally. Consequently, numerical observations were employed to understand particular fluid dynamics manifesting within the experimental data. Where $u_{0,0}$ is the axial velocity at the centre of the flow plane and u_{max} the maximum axial velocity.

In conclusion, it was hypothesised that the experimental increase in friction (f.Re) and power dissipation (P_d) indicated that the system was directly influenced by torsion as Dn was increased beyond 187_{Dn}. Practically this was seen within Figures 3-5 and 3-6 where the friction factor was plotted as a function of the Dean number i.e. the average radial TMP. Whilst Dn is small (high γ) the friction factor is seen to increase by 60%. This increase is followed immediately by a small decrease between 227 and 408_{Dn}, and finally a gradual 20% decrease as Dn is increased to 818_{Dn}. This suggests that the action of the primary and secondary flow profiles within the EFD system are influencing the average radial pressure. Accordingly this effect would be seen whilst an axial TMP was imposed onto the system.

3.6. Non-fouling fluids with permeation

Permeation is known to be a solely pressure driven process (Darcy, 1931). As described previously, increases in the system Dean number influence the friction factor (f) which is related to the average radial TMP. This was in accordance with previous studies performed by Mullhubolta *et al.*, (1997) where secondary flows were shown experimentally to affect the permeation rate at constant TMP. However, the system studied by Mullhubolta operated between a D of 1 and 18_D (see Equation 3.14).

As stated previously, flux is solely a pressure driven phenomena (Darcy, 1931), therefore, for Dean vortices and primary flows to influence they must be capable of changing the average radial TMP. Therefore, friction factor is thought to mirror these changes in average radial TMP, and manifest itself whilst the EFD membrane is permitted to permeate i.e. TMP >0.25 psi. Furthermore, previous studies (Mallhubholta *et al.*, 1997) demonstrated that Dean vortices could increase the observed permeation rates at low D numbers ($1-18_D$). Note, the EFD system was operated between 14.4 and 63_D.

3.6.1 Experimental

In accordance with the protocol detailed previously, the axial TMP was equilibrated within the EFD by recirculating the permeate co-currently within the shell of the module. All experiments were performed with DI water (25°C). After allowing the system to equilibrate for 1 minute, TMP was slowly induced to the desired value over a 0.5 minute time period. The steady-state permeation rate was determined by measuring the volume collected over a 1-minute period. The resulting data can be seen within Table 3-3 and Figures 3-5 and 3-6 where the range of 1-5 psi TMP and $187-818_{Dn}$ was studied.

	TMP = 1psi	TMP = 2psi	TMP = 3psi	TMP = 4psi	TMP = 5psi
Dn_{in}	lmh (Dn_{out})	lmh (Dn_{out})	lmh (Dn_{out})	lmh (Dn_{out})	lmh (Dn_{out})
182	278 (146)	494 (119)	715 (91)	Full (0)	Full (0)
227	312 (187)	557 (156)	894 (114)	Full (0)	Full (0)
273	288 (236)	523 (206)	787 (173)	1073 (136)	Full (0)
318	267 (284)	518 (252)	730 (225)	988 (192)	1251 (159)
363	278 (328)	500 (300)	715 (273)	979 (239)	1276 (201)
409	235 (379)	500 (345)	86 (305)	1104 (269)	1402 (231)
454	240 (424)	436 (399)	734 (361)	1017 (325)	1272 (293)
500	202 (474)	413 (447)	700 (411)	955 (378)	1190 (348)
545	192 (521)	427 (491)	634 (465)	874 (434)	1152 (399)
590	173 (567)	403 (539)	576 (517)	864 (481)	1070 (454)
656	173 (614)	370 (589)	571 (563)	826 (531)	1070 (500)
681	163 (660)	365 (634)	595 (605)	806 (578)	998 (554)
727	172 (704)	374 (679)	576 (653)	806 (624)	998 (599)
772	163 (751)	345 (728)	576 (698)	777 (673)	998 (646)
818	130 (801)	346 (773)	542 (748	744 (723)	979 (693)

Table 3-3: Pure water flux through a helical EFD cross-flow micro-filtration module under the influence of Dean number (Dn) and axial trans-membrane pressure (TMP). Distilled water was used at 25°C within the scheme (Figure 3.1.a) where the system was allowed to equilibrate for 1 minute (0 psi axial TMP) prior to pressure induced permeation (Method 2.6.2). The equilibration time allowed fluid dynamics to develop within the module to promote the observation of single effects seen in the experimental data. Using pure water, no fouling was observed suggesting that only resistance to permeation was the membrane. 'Full' defines the situation where all the retentate was passed through the EFD module.

Considering the experiment is designed to observe the influence of the Dn on the permeate flux (average radial TMP), Table 3-3 included both the inlet and outlet Dn number. It was considered that if the difference between these values increased too much, the system would no longer reflect the desired situation. This can be seen within Figures 3-5a and 3.6a whereas at low TMP's the friction factor (f) and permeate flux follow identical profiles. As the TMP was increased, the two parameters deviated until no conformity can be seen i.e. a TMP of 5 psi. It was considered that this deviation is related to the net effect of a variable axial Dn and the resulting instability caused. In addition, it was known that excessive permeation had a destabilising influence on the fluid dynamics (Manno *et al.*, 1998). Therefore, data representing an axial variation in Dn of more than 20% was considered invalid when comparisons were drawn between numerical and experimental data i.e. representing more than 1% volume loss of fluid per cm travelled.

3.6.2 Results

The results can be seen within Table 3-3 and Figures 3-5 and 3-6. In accordance with Mullhobolta *et al.*, (1997), the permeate flux increased with friction factor while D was between 14 and 17.5_D. This suggested that the combination of primary flow Dean vortices had increased the average radial TMP and therefore the permeate flux. Between these D values, the friction factor (41%), friction (75%), power dissipation (106%) and centrifugal forces (46%) increase with a 25% increase in Dn. This resulted in a 12% increase in the permeate flux. However, as Dn increased, the friction factor reduced by 10%, and the permeate flux by 4.4%. This decrease happened as Dn (80%), friction (64%), power dissipation (322%) and centrifugal force (224%) all increased. Considering that the data within Figures 3-5 and 3-6 bore close resemblance, it was suggested that this uniformity in friction factor could be used to compare the numerical studies presented by Liu *et al.*, (1993) to that seen experimentally. Therefore, as seen within Table 3-2 and discussed previously, increasing the Dn from 100 to 500_{Dn} created a centrifugal plateau within the cross-plane that decreases the influence of the Dean vortices. The decrease was seen experimentally in the reduction in friction factor (average radial TMP) and the resulting permeate flux.

TMP	Dn	D	$LMH_{@\ 1psi}$	Gn	Re	γ	f	P_D (W)	f.Re
1psi	181.7	14	278	46.2	513.1	0.0189	0.252	0.015	129.3
1psi	227.1	17.5	312	57.7	641.4	0.0169	0.355	0.031	227.5
1psi	409	31.5	235.0	103.9	1154.4	0.0126	0.324	0.131	373.5
2psi	409	31.5	500.5	103.9	1154.4	0.0126	0.299	0.140	433.7
1psi	818	63	129.6	207.8	2309	0.0089	0.284	0.761	655.0
2psi	818	63	345.6	207.8	2309	0.0089	0.274	0.737	632.0

Table 3.4: The pure water flux showing the influence of the Dean vortices and primary flows on the permeation rate. The results are shown in relation to the Dean number (Dn), Germano number (Gn), γ, friction factor (f), friction (f.Re) and power dissipation (P_D).

Again, the above trend was observed as the Dn number increased to 818_{Dn}. For 1 and 2 psi TMP data the friction factor (14%, 8.4%) and permeate flux (45%, 31%) were seen to decrease whilst the friction (75%, 44%), power dissipation (480%, 426%) and centrifugal force (300%) all increased. Consequently, the situation described by Liu *et al.*, (1993) was thought to dominate the flow field with the Dean vortices exhibiting little influence over the radial TMP. It was assumed that the cross-plane pressure gradient would also increase with Dn. However, this was a scenario that suggests that the shear profiles seen within Figure 3-2 would be further distorted and therefore raise further concerns concerning the ability of the EFD to support a high permeation rate, whilst minimising the deposition rate of a fouling material. It should be noted that these hypotheses were inconclusive as no numerical work had yet been published for the EFD system when incorporating a permeable boundary.

3.3.6. Summary

It was shown that the trend in friction factor (average radial TMP) accurately reflected the permeation flux when operating at relatively low axial TMP's i.e. less than a 1% fluid loss to permeation per axial centimetre. Consequently, a numerical study of a near identical system (Liu et al., 1993) was used to determine the internal fluid dynamics occurring as a function of the Dn. It was observed that an initial increase in the friction factor (45%) and permeate flux (12%), was followed by a slow decrease, as the fluid dynamics became more complicated i.e. elevated levels of power dissipation. It was thought that the initial increase was due to the Dean vortices increasing in strength as with the data published by Mullhubolta et al., (1997). However, due to the increases in the Dn and centrifugal forces, these Dean vortices slowly compressed so reducing their influence over the average radial TMP i.e. friction factor. This hypothesis was in accordance with the work presented by Liu et al., (1993) that described the emergence of a centrifugal plateau as Dn is increased through 500_{Dn}. Consequently, the permeation rate showed a maximum at 227_{Dn} and a minimum at 818_{Dn}. However, when considering the cross-plane pressure distribution and shear profile within the flow plane, it was thought that the ability of the EFD module to control the deposition rate of a fouling material would be critical rather than the maximum permeation rate.

3.7. Fouling fluid permeation: Low OD bacterial cell cultures.

3.7.1. *E. coli* bacterial cells

The bacterial strain *E. coli* DH5α, a fast growing gram negative prokaryote capable of supporting a high copy number plasmid, was selected as the most suitable host for the plasmid pTS. The *E. coli* bacterial cell exists as a rod approximately 2 μm in length and 0.7 μm in diameter possessing a net negative charge at pH 7.4, the optimum pH for cell culture. The outermost layer of the bacteria is known as the envelope and consists of an outer membrane, a peptidoglocan layer that increases the rigidity to the envelope, a periplasmic region, and an inner membrane. Two types of appendages can be found attached to the outer membrane of *E. coli.*

- Flagella: responsible for cell mobility. Each cells normally containing between 0 and 100, each about 20 μm long and 20 nm in diameter (the actual quantity of flagella, which mediate the swimming mobility, is unknown for the DH5α strain).

- Common pili: These are smaller than the flagella (about 1 μm x 10 nm) and can exist in large quantities.

It has been shown that, in spite of their lack of nervous system, *E. coli* are able to swim towards more favourable locations, including those with a better supply of nutrients, and away from unfavourable locations where high mechanical stresses or toxins are present. Therefore, *E. coli* does not exhibit Brownian motion used to describe most cross-flow micro-filtration systems. It has been shown that bacteria, characteristically walking or tumbling (Genetic element in *Escherichia coli*. P. Smith-Keary, 1988) when moving within a liquid medium in contact with a solid surface, can modify their characteristic swimming behaviour to suit their environment. Electrostatic, ionic and hydrodynamic interactions have also been found to influence bacterial motion in the presence of a solid surface. In relation to micro-filtration modules, several studies have indicated that bacterial cells such as *E. coli* adhered irreversibly to membranes or existing cell cakes, suggesting that de-polarisation effects will not easily re-entrain fouled material back into the bulk flow. Reismeirer et al., (1987) demonstrated

that rinsing membranes, fouled with *E. coli* cells, frequently led to only a small increase in permeate flux, indicating that bacteria tends to adhere strongly to membrane surfaces during micro-filtration processes. Also, this was demonstrated for the EFD modules during the preliminary studies where the fouled flux increased only by 10% after taking of the TMP. Also, Forman *et al.,* (1990) showed that *E. coli* forms a compressible cake when experiencing more that 3.6 psi TMP for a membrane with pore sizes between 0.45 and 0.65 μm.

3.7.2. Experimental

From the previous studies, the ability of the EFD system to control the deposition rate of a fouling material was examined. The *E.coli* bacterial cells were transformed (Method 2.5.1) with the plasmid pTS and grown overnight (37°C) on LB-amp plates (Method 2.2.3). A single colony was inoculated into 50 ml LB-amp media and grown to an OD of 0.3_{OD} and subsequently inoculated into 950 ml of LB-amp media and culture overnight (37°C) to produce 1L of bacterial cell culture. The EFD system was operated as before, but with the additional check of measuring the pure water flux prior to processing the bacterial cell culture. This was done to demonstrate that the membrane was clean and free from contaminating material. Considering that viscosity and optical density are inextricably linked to the Dean number, a calibration was formulated. The relationship between viscosity and optical density was found to be:

$$\mu = 8.037e^{-6}(OD) + \mu_w \tag{3.23}$$

$$\rho = 0.998(OD) + \rho_w \tag{3.24}$$

Initially experiments were designed to compare the whole range of Dn values and TMP's studies previously. However, at Dn values less than 380_{Dn} cells coating the tubing and valves caused erratic fluctuations in the pressure. At Dn values above 760_{Dn} the permeate recycle pump was unable to equilibrate the axial TMP. Consequently, three Dn values were selected for study. These were 408_{Dn}, 579_{Dn} and 759_{Dn} and subjected to TMP's of 2, 3 and 4 psi. A TMP of 1 psi was not selected as the pure water permeate flux (150 lmh) was not in the range described by Caridis *et al.,* (1997) as that similar to continuous centrifuges. Finally, the effect of viscosity and increased cell mass on the fouling rates was determined with two different OD cell cultures, $OD_{2.5}$ (μ= $1.024\mu_w$) and OD_{16} (μ= $1.157\mu_w$) i.e. increasing the cell content by 540%.

3.7.3.   Results for $OD_{2.5}$ cell cultures

The experimental results can be seen within Table 3.5 and Figures 3-5 and 3-6 where f, f.Re, P_D, ΔP_x and flux data is presented as a function of the flow groups Dn, Gn, γ and process time (t). Considering there was good agreement between the data for both the pure water and cell culture data, it was assumed that the fluid dynamics occurring as a function of Dn also beared close resemblance. Therefore, the conclusions detailed above are also imposed onto the present data.

Dean number		402_{Dn}	2.5_{OD}	579_{Dn}	2.5_{OD}	759_{Dn}	2.5_{OD}	518_{Dn}	16_{OD}
TMP (psi)	Time (mins)	Flux	R	Flux	R	Flux	R	Flux	R
2	1	237	0.54	456	1.13	336	0.97	289	0.71
	5	168	0.38	398	0.99	288	0.83	202	0.49
	20	125	0.29	330	0.82	250	0.72	150	0.37
	Average	144		369		271		195	s
3	1	288	0.39	528	0.92	406	0.71	403	0.68
	5	211	0.29	456	0.79	326	0.57	288	0.49
	20	163	0.22	336	0.58	269	0.47	220	0.37
	Average	187		401		301		279	
4	1	317	0.31	417	0.48	465	0.60	364	0.42
	5	240	0.24	331	0.38	346	0.44	278	0.32
	20	158	0.16	227	0.26	250	0.32	230	0.27
	Average	205		281		308		273	

Table 3.5: Data shows the influence of Dean number (Dn) and TMP on the permeate flux as related to the processing time (t). The data is presented as flux and R. Flux is the observed permeation rate, and R is the ratio of $Flux_t/Flux_{PW}$ where $Flux_{PW}$ is the pure water flux under the same conditions. All experiments were performed by using a single EFD 125 cm^2 cross-flow filtration system which can be seen in Figure 3-1.a. 2L cultures of E. coli DH5α cells ($OD_{2.5}$ and OD_{16}) were grown overnight in sterile LB-amp media at 37°C.

Accordingly, the EFD system demonstrated the ability to process a bacterial cell culture at all the Dn and TMP's values studied. However, further examination of Figures 3-5 and 3-6 show that the fouling rates associated with these parameters are more complex than a simply relationship between Dn number and specific fluid dynamics.

It can seen that whilst operating at 408_{Dn} and 2 psi TMP, equating to a 20 and 45% greater pure water flux than 579 and 759_{Dn}, the EFD system was unable to control the fouling rate and crashed to 29% of the pure water flux after 20 min processing time. However, when considering that 408_{Dn} also represents the lowest shear rate studied, this was expected. On reflection, the position of the maximum radial TMP (resulting from the centrifugal plateau, discussed previously) being located on the outer turn of the helix (the position of maximum shear rate seen within Figure 3-2), suggested that the majority of the permeate was to pass through this position. Therefore, the shear rate in relation the TMP experienced at this position should be discussed. It is known that increases in Dn produce larger increases in shear rate when compared to the cross-plane pressure distribution i.e. Figure 3-2 and Table 3-2. Therefore, higher shear rates should be more able to control deposition rates.

Consequently, the maximum permeation rate is found at 579_{Dn} and 3 psi TMP whilst the optimum control imposed onto the fouling rate was seen at 759_{Dn} and 2 psi TMP. At 528_{Dn}, the EFD system was able to process the cell culture at 528 lmh initially, falling to 336 lmh after 20 minutes. At 579_{Dn} an average of 369, 401 and 281 lmh was seen for the TMP's of 2, 3 and 4 psi. Although this position does not possess the optimum ability to control cell fouling (759_{Dn} and 2 psi), it does demonstrate the optimum ability of the system as opposed to other technologies. When comparing the fouling graphs

to those presented by Caridis *et al.*, (1997), it can be seen that the EFD experiences the initial stages of surface sorption for all the TMP's studied, and therefore maintains a permeate flux of 82% of the pure water flux after 20 minutes. As previously, it is thought that the majority of the permeate has passed through the position located on the outside turn of the helix because of the cross-plane pressure gradient described by Liu *et al.*, (1993). Therefore, it is thought that 579_{Dn} differs to 408_{Dn} by possessing an increased shear rate experienced at this radial position i.e. the primary flow profile being displaced further towards this position of maximum radial TMP.

As stated above, the optimum condition that controlled the rate of cell fouling was found at 759_{Dn}. An average permeate flux of 271, 301 and 308 lmh was sustained over a 20 minute period whilst only falling by 28, 54 and 66% of the pure water flux. This is compared to 31, 42 and 74% for 579_0. As previously, the early stage of surface sorption of a monolayer of bacterial cells was experienced at 759_{Dn} suggesting that the shear rate experienced at the position of maximum radial TMP (the outside of helical turn) was able to control the fouling rate. However, the centrifugal force within the flow plane increased by 72% and 244% above that for 579_{Dn} and 408_{Dn}. It is known that the cross-plane pressure gradient (Table 3-2) increases by 345% between 100_{Dn} and 500_{Dn}. Therefore, it is suggested that at 759_{Dn} the permeate is channelled through an ever decreasing window, but the higher shear rate is more adept to control what should be a higher fouling rate.

Finally, the ability of the EFD system to depolarise the fouled bacterial cells was studied. However, in accordance with that presented by Caridis *et al.*, (1997), only 10% of the fouled flux was recovered after ceasing permeation for 5 minutes i.e. 0 psi TMP. When this study was performed, the value was always approximately 10%. It was found that only 400 ppm NaOCl at 60°C was able to effectively remove fouled material from the membrane.

TMP	Dn	lmh	R	R	R	Flux	Gn	Re	γ	f	P_D	f.Re
		1min	1min	5min	20min	average					(Watt)	
2psi	408	236.8	0.54	0.38	0.29	144	103.9	1154.4	0.0126	0.36	0.16	408
3psi	408	287.6	0.39	0.29	0.22	187				0.34	0.19	385
4psi	408	316.8	0.31	0.24	0.16	205				0.32	0.23	368
2psi	579	456.0	1.13	0.99	0.82	369	147.2	1635.3	0.0106	0.36	0.35	584
3psi	579	528.0	0.92	0.79	0.58	401	-	-	-	0.28	0.36	454
4psi	579	417.6	0.48	0.38	0.26	281	-	-	-	0.32	0.45	516
2psi	759	335.7	0.97	0.83	0.72	271	192.9	2143.7	0.0092	0.27	0.71	570
3psi	759	406.4	0.71	0.56	0.46	301				0.25	0.70	546
4psi	759	464.8	0.60	0.44	0.32	308				0.26	0.74	552

Table 3.6: Data showing the influence that the Dean number has on the experimental flow groups at 408, 579 and 759_{Dn} and for a fouling fluid. $OD_{2.5}$ and OD_{16} cultures of E.coli were grown according to Method 2.6.2 in continuous recycle, maintaining constant viscosity (μ) and density (ρ).

3.8. Fouling fluid with permeation: High OD (16) bacterial cell cultures

3.8.1. Experimental

Finally, this section of work was completed by studying the ability of the EFD to process a higher OD *E. coli* bacterial cell culture, an OD similar to that experience by the EFD modules after concentrating the initial $OD_{2.5}$ cell culture by 540% (i.e. $\mu_{16}=1.157\mu_w$). An OD of 16 was selected as it represented a position where the initial culture volume had been reduced by over 80%, and therefore 80% of the process time. The experiments were performed using the procedure describe previously where the EFD modules initially concentrated an $OD_{2.5}$ bacterial cell culture until the appropriate OD had been reached. The EFD system was subsequently cleaned, washed and equilibrated with sterile LB-amp media (1L, 25°C) where the pure media flux was recorded. As a consequence of the previous experiments, the flow-rate of 484 ml min^{-1} (579_{Dn} previously) was selected where the Dn value is reduced to 518_{Dn} as the viscosity and density increase.

3.8.2. Results

The results of these experiments can be seen within Figure 3-10 and Table 3-5 where the permeate flux has been presented as a function of TMP and process time. As described previously, the ability of the EFD to depolarise the fouled cells was examined, and shown to return only 10% of the fouled flux. This observation is corroborated by Riesmeir *et al.*, (1987), who reported a mechanism by which bacterial cells irreversibly foul onto membranes.

Comparing the OD_{16} and $OD_{2.5}$ data for 579_{Dn} it demonstrates that although the cell concentration had increased by 540%, the fouling rate did not. Rather, over the 20 minute period the EFD was able to support a permeate flux of 195, 279 and 273 lmh for the TMP's of 2, 3 and 4 psi. Comparing these values demonstrates that for OD_{16} culture, the permeation rate drops by 174 (47%), 122 (30%) and 8 (3%) lmh respectively, i.e. still competitive with the other technologies. As previously, the optimum process condition is found when imposing 3 psi TMP over the EFD. Previous studies (Mullubholta *et al.*, 1995) had shown that at low D numbers (8-13) for yeast cells (0.023 and 0.251 wt%), the fluxes were 80 and 45 lmh respectively, 60% and 40% greater than that seen without secondary vortices where the pure water flux was 467 lmh. In comparison, the EFD operating at higher D numbers (44.5_D $OD_{2.5}$ and 40_D at OD_{16}) was able to maintain a flux greater than 336 and 220 lmh for 20 minutes respectively, 419% and 267% greater than that shown by Mullubholta *et al.*, (1995).

3.8.3. Summary

In conclusion, the specific application of processing bacteria, depolarisation effects were shown to be ineffective, so process conditions were selected on the basis of prevention. The optimum condition was seen at 579_{Dn}, when imposing axial TMP's of 2 and 3 psi, i.e. the optimum combination of primary flow and Dean vortices was found to concentrate $OD_{2.5}$ and OD_{16} bacterial cultures. For a TMP of 2 psi, the EFD module processed a 1L $OD_{2.5}$ *E. coli* culture to completion (50 ml) in under 11 minutes (~400 lmh) whilst a TMP of 3psi accomplished the same task in under 10 minutes (~450 lmh). Therefore, the EFD is able to out-perform both economically and practically, continuous centrifuges.

3.9. Diafiltration

Whereas alkaline lysis technique rarely employ diafiltration, the devised affinity purification strategy involved freeze-thaw lysis as an affinity ligand (zinc-finger DNA-binding protein) and was to be expressed within the same cell as the target DNA. Therefore, to maintain the integrity of the affinity ligand and the resulting protein-DNA complex, the cells were diafiltered into TBS pH 7.4 buffer for reasons discussed within Chapter 5. The ability of the EFD system to accomplish this process without the need to transfer the cell paste into a different GMP validated vessel was, therefore, studied.

The process schematic can be seen in Figure 3-1d where 300 ml of the diafiltration buffer is pumped into the feed vessel (50 ml of cells) at the same rate that the permeate is removed to waste to effect a 6-fold diafiltration. The experiments were performed immediately after the previous concentration stage where the membrane is fouled (i.e. no need to chemically clean the membrane). Not surprisingly, the addition of TBS pH 7.4 into the feed tank, did not adversely effect the permeate flux from that seen at the end of the concentration stage. Consequently, for 579_{Dn} the diafiltration was performed at 2 psi (~360 lmh), 3 psi (~400 lmh) and 4 psi (~300 lmh) taking on average 4, 3.6 and 4.8 minutes to complete respectively. In conclusion, the complete concentration and diafiltration stage was completed within 14 minutes at 579_{Dn} and 3 psi TMP.

3.10. Harvesting of plasmid DNA from 'freeze-thaw' bacterial cell lysates

The final section of the EFD work was to test the ability of the module to process a 'freeze-thaw' (Method 2.5.17) bacterial lysate, whilst allowing passage of the therapeutic product through the membrane. The EFD system was operated as before i.e. fouled. This meant the system was brought to equilibrium (1 minute) at 0psi, and slowly subjected to axial TMP. Considering the downstream chromatographic stage required 300 ml static volume, the modules were operated under the previous diafiltration mode until 300 ml (i.e. the highest concentration of product) of permeate was collected and analysed for protein and DNA content.

On average, the target plasmid DNA (8.3 ng μl^{-1}) was present with genomic DNA (~23,000 bp, 36 ng μl^{-1}), cellular proteins (5-100 kDa, 21.4 ng μl^{-1}), and unknown levels of RNA and endotoxin within the post-EFD clarified lysate. The corresponding electrophoresis gels can be seen in Figure 3-12 where the vast majority of large molecular weight genomic DNA (>23,000 bp) was retained by the EFD. This was probably due to DNA aggregation but also shows that the EFD module was able to act as a primary purification stage for removing genomic DNA from the product stream.

3.11. Overall summary

Experiments were designed to validate the use of EFD micro-filtration technology within three key areas of the biotechnology industry whilst providing an understanding of the underlying fluid dynamics occurring within the module. The three key areas were:

- Concentration of a 1L bacterial culture a rate between 150-400 lmh and within 20 minutes,

- Diafiltration of the concentrate into a suitable processing buffer within 10 minutes,

- Clarification of the therapeutic product from solid matter after 'freeze-thaw' lysis.

In the preliminary studies prior to optimisation, the EFD showed the ability to process a 1L $OD_{2.5}$ *E.coli* bacterial cell culture at a rate initially of 420 lmh. However, fast surface sorption of the bacterial cells

onto the membrane reduced this value to 230 lmh after 10 minutes. Although, in a crude way this demonstrated the intrinsic ability of the EFD system to compete with the other technologies, its application for this task is limited to short time periods only.

From confirming the intrinsic ability of the EFD system, an attempt was made to discern the particular fluid dynamics that occur within the EFD's helical membranes and their influence over the permeation rate and the control of deposition rates for fouling materials. Consequently, the friction factor (f), friction (f.Re) and power dissipation (P_D) were determined for distilled water (25°C) flowing through the system at different Dean numbers (Dn). Dn numbers between 187 and 818_{Dn} when under the influence of between 0 and 5 psi transmembrane pressure (TMP). The resulting data demonstrated that the friction factor accurately depicts the radial TMP and therefore the permeation rate. The permeation rate was shown to be at a maximum at 227_{Dn} and a minimum at 818_{Dn}. However, the large increases in power dissipation suggested that the system was in a state of change as Dn increased. It was suggested that at low Dn and D numbers, small increases in Dn cause an increase in the secondary flow strength that in turn causes an increase in the permeation rate. However, as the Dn is increased above 227_{Dn} this influence decreases with a net reduction in the permeation rate. It was seen, when studying numerical solution to near identical problems, that as Dn increased so the centrifugal forces that cause Dean vorticies start to dominate the flow equations. This results in the formation of central centrifugal plateau, which increases the cross-plane pressure gradient, which causes a localised maximum radial TMP towards the outside of the helical turn. Also, this dominance causes the primary flow pattern to move towards the outside wall, so creating an area of high shear at the same position as the radial TMP maximum. The net affect of this was to create a system where the maximum pure water flux (227_{Dn}) did not coincide with the maximum fouling fluid flux (579_{Dn} and 3 psi) nor the position exerting the maximum control over the fouling rate (759_{Dn} and 2 psi). Consequently, when using a fouling mixture of $OD_{2.5}$ and OD_{16} E.coli bacterial cells it was shown that at 579_{Dn} and 3 psi TMP, the EFD system was able to process a 1L bacterial cell culture at an average flux of 401 and 279 lmh respectively.

For the second part, the ability of the EFD module to diafilter the concentrated bacterial cell culture as part of a continuous process was determined, i.e. fouled from the previous concentration stage. It was shown that at 579_{Dn} and 3 psi (the optimum for concentrating the E.coli bacterial cell culture), an average permeate of 400 lmh was maintained for a six-fold buffer exchange to be completed i.e. 300 ml.

Finally, the EFD module was shown to have ability to perform within the third key area, that of clarifying the plasmid DNA from the cellular debris and large fragments of genomic DNA (>23,000 bp). On average, it was shown that 300 ml of the target plasmid DNA (8.3 ng μl^{-1}), genomic DNA (~23,000 bp, 36 ng μl^{-1}), cellular proteins (5-100 kDa, 21.4 ng μl^{-1}), was passed through the EFD into the process stream, processing at an average rate of 120 lmh.

In conclusion, the EFD system was shown to be able to concentrate, diafilter and finally clarify the plasmid DNA from a 1L $OD_{2.5}$ E.coli bacterial cell culture in a average of 26 minutes without the need for cleaning or transference of the process material into different vessels.

4. ADSORPTION OF PLASMID DNA ONTO ANION-EXCHANGE MEMBRANES

4.1. Overview

The purpose of the work detailed within this chapter was to determine the ability of anion-exchange membranes to effect the capture and purification of plasmid DNA from a post-EFD clarified *E. coli* bacterial cell lysate where the target plasmid DNA (8.3 ng μl^{-1}) is present with genomic DNA (23,000 bp, 36 ng μl^{-1}), cellular proteins (5-100 kDa, 21.4 ng μl^{-1}), and unknown levels of RNA and endotoxin. During these studies, the physical parameters influencing the adsorption of DNA onto the surface of the membranes was assessed, their typical binding capacities when challenged with purified calf thymus DNA in buffers of various ionic strength. Consequently, equilibrium binding capacities and breakthrough curves were determined when without the complications of competitive adsorption of the contaminants present within the post-EFD process stream. Finally, the membranes were employed within the overall purification train and challenged with the post-EFD process material. In this way the effectiveness and scalability of the strategy would be determined so indicating the suitability of this strategy within the desired process. In addition, this chapter also includes details of the work performed to convert an existing assay that could effectively determine the concentration and identity of DNA material passing through the EFD and subsequent purification stages. The inclusion of the data gives valuable information when validating the compliance of the purification schemes with the current FDA guidelines concerning genomic DNA contamination.

4.2. Quantification and identification of DNA in *E.coli* cell lysates

4.2.1. Overview

This section includes details of the work performed to convert an existing assay (Charlton, 1999) that accurately and reliably quantified DNA present within culture media and dilute lysate material, to an assay that could also identify the DNA present (i.e. plasmid or genomic). The fluorochrome PicoGreen™ (Molecular Probes) is suggested as the most suitable probe as accuracy and reliability to determine the quantity of DNA when in the presence of dilute bacterial lysate (Charlton, 1999, Singer *et al.*, 1997) has already bees demonstrated. Although the size the of the DNA molecules present within the post-EFD cell lysate ranges between 2,700 to 23,000 base pair (bp), PicoGreen remains a good candidate as the fluorescent signal emitted from the PicoGreen dependant upon intercalation with only a few base pairs of specifically double stranded DNA (Ahn *et al.*, 1996). Considering that PicoGreen has been employed within agarose gel electrophoresis strategies for the identification of products from a PCR reactions (Enger. 1996), the accuracy and reliability of both quantifying and identifying DNA by electrophoretic techniques, whether from pure or crude sources, has never been demonstrated.

However, the fluorescent signal emitted from PicoGreen intercalated into DNA and their resultant mobility within an agarose electrophoresis gel is subject to a number of factors:

- De-mobilising the DNA-PicoGreen complex within the agarose gel,

- Fluorescence emitted from PicoGreen intercalated with DNA,

- Fluorescence emitted from unbound PicoGreen (i.e. background)

- Fluorescence emitted from PicoGreen intercalated with other nucleic acids (i.e. RNA),

- Fluorescence emitted from other sources (protein, media components, etc),

- Reduction in fluorescence caused by the shielding of unknown sources,

Consequently, experiments were designed to determine, where possible, the influence of each of the factors detailed above. Initially this involved developing the assay with purified plasmid DNA samples, demonstrating the mobility of the three conformations found naturally (i.e. super-coiled, open-circular and linear) whilst determining accuracy and reliability of the fluorescent signal emitted by the PicoGreen-DNA complex. Therefore, pure sources of plasmid DNA were prepared from an overnight 1L LB-amp culture of a single *E.coli* DH5α colony (previously transformed with the plasmid pTS) where 'Wizard maxi prep' (Promega) kits were used to purify the plasmid pTS. Crude sources were prepared in a similar way where the 1L culture was processed by EFD technology that resulted in a process material that contains the target plasmid DNA (~8.3 ng μl^{-1}), genomic DNA (23,000 bp, 36 ng μl^{-1}), cellular proteins (5-100 kDa, 21.4 ng μl^{-1}), and unknown levels of RNA and endotoxin.

4.2.2. Pure plasmid DNA

PicoGreen™ (0.5μl) was incubated with the purified samples of pTS DNA (0-50 ng) and suspended in TBS pH 7.4 (20 μl) with sucrose loading buffer (5 μl). The resulting DNA-PicoGreen™ complexes (40 μl max) were run though a 1.5% agarose electrophoresis gel at 20, 40, 60 and 80V to determine their mobility and also observe whether the PicoGreen remained intercalated into the DNA at the higher voltages. Figure 4-1 shows the electrophoresis gel corresponding to 80V where the DNA quantity linearly increases from 0 (lane 1) to 50 ng (lane 18). The agarose gel was analysed by a TUNDRA™ digital imaging system where the fluorescent signal emitted within each individual pixel located within the DNA band is proportional to the quantity of DNA present. The corresponding fluorescence-DNA plot can be seen in Figure 4-2 where the fluorescent signal and consequently the DNA present within each band, whether super-coiled, open-circular, linear or the sum of all three, remains linear and predictable. Identical plots were seen for the subsequent 20, 40, and 60V electrophoresis gels showing that PicoGreen remained intercalated into the DNA. The influence of PicoGreen on the mobility was demonstrated by overlaying agarose gels electrophoresed under identical conditions but where the dye ethidium bromide was used. The resulting images showed that the mobility of plasmid did not vary, whether in the super-coiled, open-circular or linear conformation.

4.2.3. Crude plasmid DNA

Finally PicoGreen was studied when in the presence of a crude *E. coli* cell lysate under identical conditions. To gauge the resulting fluorescent emission, the concentration of plasmid pTS and genomic DNA was determined spectrophotometrically as 44.3 ng μl^{-1}. Figure 3-12 shows the resulting 1.5% agarose electrophoresis gel where the DNA ladder λ Hind III (lane 1) clearly demonstrates that the plasmid DNA (Lanes 3-8) is not hindered by the contaminants present within the lysate. However, a similar calibration plot could not be shown due to the low concentration of plasmid DNA present within the lysis material (i.e. concentration of the DNA would significantly alter the nature of the sample).

4.2.4. Summary

Considering that the ability of PicoGreen to fluoresce and determine the quantity of DNA in cell culture supernatants or dilute cell lysates containing monoclonal antibodies and numerous other unidentified proteins or cellular contaminants had been clearly demonstrated (Charlton, 1999). That Singer et al., (1997) showed that the specific fluorescent enhancement of PicoGreen in the presence of dsDNA is constant and independent of the source organism whilst Ahn et al., (1996) demonstrated that PicoGreen can bind DNA of 150 base pairs (bp) with the same sensitivity and efficiency as larger strands of DNA. The combined data present above suggests that PicoGreen is a suitable candidate for the quantification and identification of DNA present in pure or crude bacterial cell cultures when employing agarose gel electrophoresis techniques.

4.3. Membrane housings

However, the research in this chapter starts with the ability of membrane housings to effect the reproducibility of DNA breakthrough curves. This work was carried out because breakthrough curves for the Sartorius SartoBind Q15 employed within this study could not be reproduced and that other workers had demonstrated similar problems with the membrane housing in question (Charlton, 1999, Gebauer et al., 1997). The data that indicted a failure in the reproducibility of this work and that the membrane housing may be at fault is shown in Figure 4-6a. From this data it can be seen that the breakthrough curves generated using the SartoBind Q15 membrane held in the manufacturers own pre-formed housing were variable for the same set of conditions and that the curves themselves do not appear in the format of conventional breakthrough curves (Suen et al., 1992). Since these membranes are sold as having constant ligand density and affinity, other workers have previously hypothesised and demonstrated that the erratic nature is due to the challenge material not being evenly distribution across the membrane surface (Gebauer et al., 1997, Charlton 1999). The former of these two writers also cited the sub-optimal flow characteristics as a 'major problem that need to be addressed before a successful transition from lab-scale to pilot plant and beyond can be derived'. Where this failure to reproduce had been observed, the workers stated that the geometry of the membrane module needed to be addressed to promote even distribution of the challenge material across the membrane surface that determines the Peclet number experienced within the membrane (Gebauer et al., 1997). The importance of the Peclet number is demonstrated by its definition, defining the ratio of convective to diffusive transport of adsorbates to the adsorbents within the membrane pores (i.e. convective transport>>diffusive transport). Charlton (1999) demonstrated the sub-optimal flow-characteristics within the Sartorius pre-formed housing by challenging the membrane with a negatively charged dye (bromophenol blue) at flow-rates of 5.0 ml min^{-1} and 50.0 ml min^{-1}. The upper of these values is reported by the manufacturer as the maximum flow-rate at which the membrane should be operated. The resulting data showed that the fluid was only distributed over approximately 20% of the membrane surface at 50 ml min^{-1}. However, where the same was observed for the current Sartorius modules, the alternative 0.45 µm UltraBind membranes (Pall Gelman, Ultrabind) that were challenged with the negatively charge dye Cye3 (Amersham) within the two 13 mm and 150 mm stainless steel housings showed a more even distribution of challenge material across the entire membrane surface. The experimental data generated by this work is shown in Figure 4-3 where the distribution of the Cye3 dye within the 13mm housing is approximately uniform but concentrated within the central region within the 150mm housing indicating a radial variation in Peclet. Therefore, this indicates that the subsequent breakthrough curves resulting from challenging the DNA to membranes

located within these housings will be more valid and reproducible than the Sartorius housing. The membranes used for visualisation of fluid dispersal across the UltraBind US450 material were cut from sheets that were purchased from Pall Gelman.

However, these results yielded useful information but offered only qualitative descriptions of the distribution of challenge material across the surface of the membranes. Therefore, the fluid distribution problem within the pre-formed Sartorius and 13mm Millipore housings were studied numerically with the aid of the fluid dynamic package CFX-4 (AEA Technology). CFX-4 is a Computational Fluid Dynamic (CFD) package that allows a 3-D Computer Aided Design (CAD) image to be converted into a finite element mesh where a subsequent solution domain to which the momentum, heat and mass transfer equations can be applied and solved. CFX-4 is particularly effective in solving porous and solid wall problems such as the currently employed membrane modules. Therefore, after accurately measurements were taken, the geometry's of the Sartorius and Millipore housings and membranes were inputted into the CFX-4 domain and the corresponding finite element mesh generated. Once the appropriate boundary conditions were built into the solver, the steady-state momentum and continuity equations were solved (i.e. water at 25°C, solid boundary wall, no slip at the wall, porous membrane with internal resistance (1×10^9), incompressible Newtonian fluid operating within an isothermal system). The solutions to the two housings can be seen within Figure 4-4,5 indicating the failure of the Sartorius pre-formed housing to even partially distribute the fluid flow across the membrane surface at the recommended operating conditions. The data demonstrates that the membrane surface experiences significant radial variations in the Peclet number (i.e. proportional to the interstitial velocity) that is a characteristic of the poor distribution of fluid and finally observed in the erratic experimental breakthrough curves. Clearly, the 3-D solution of the fluid distribution within the Sartorius housing (50 ml min^{-1}) demonstrates that that the fluid jets through the central section of the membrane with little distribution towards the outside areas. From Figure (4-4c), the numerical data shows that only the central 20% of the membrane experienced flow (i.e. comparable with Charlton's (1999) studies). Therefore, the erratic nature of the breakthrough curve under identical conditions is probably due to disturbances in the flow patterns so that distribution of fluid across the membrane surface changes with an decrease or increase in the observed capacity. However, this does not detract from the fact that the Sartorius housing cannot be scaled beyond the laboratory because of the reasons detailed above.

However, in accordance with the experimental visualisation (Figure 4-5) of the fluid distribution within the 13mm Millipore housing, the corresponding numerical solution demonstrated, and also supports, the ability of the housing to more evenly disperse the fluid across the membrane surface. But, the numerical plot generated by the CFX-4 program also predicts that the Millipore housing will experience radial variations in the Peclet number as the interstitial velocity reduces from the centre of the membrane towards the outer wall. Although it is likely that such fluid dispersal across the 13 mm membrane would enhance the adsorption of the challenge material as opposed to the Sartorius housing, the experimental data would still result in the premature breakthrough of adsorbates as the absorbents within the central region that experience higher Peclet numbers become saturated first. However, this does suggest that the housings where the fluid is more evenly distributed of fluid would provide a more successful transition from lab-scale to pilot plant and beyond, especially if the membrane were stacked to reduce the fast breakthrough within the central region.

4.3. Sartorius Sartobind Q15

The Sartorius SartoBind Q15 membrane was designed specifically as an anion exchange matrix to promote the more rapid adsorption of negatively charged molecules than the equivalent column based ion-exchange matrices, consequently, it should be expected to display minimal non-ionic (i.e. hydrophobic) interactions. The operational and equilibrium binding capacity was determined by challenging the membrane with known quantities of pure calf thymus DNA (ctDNA), ctDNA and bovine serum albumin (BSA) simulating a competitive process, and a crude *E.coli* cell lysate containing the plasmid pTS, genomic DNA, cellular proteins and unknown quantities of endotoxin and RNA. The SartoBind Q15 membrane remained located within the pre-formed housing was initially studied as a part of a continuous process where the process material was challenged to the adsorbates in a single pass. The calf thymus DNA, suspended in TE pH 7.4 buffer, was challenged at a concentration of 1 μg ctDNA ml^{-1}. Accordingly, to determine whether any enhancements in the fluid distribution could be achieved, the flow-rates and corresponding superficial velocities were varied above and below the manufacturers recommendations (i.e. 10 – 90 ml min^{-1}). The DNA and protein concentration within the effluent was analysed continuously by DNA (Method 2.5.14) and protein assays (Method 2.5.13).

4.3.1. Challenge of calf thymus DNA

The subsequent breakthrough curves and binding capacities under the various conditions and challenges are shown in Table 4-1 and Figure 4-6b respectively. Breakthrough for the continuous process (single pass of challenge material) was taken as the point at which the effluent concentration of DNA was 10% of the challenge concentration. This point represents the operational capacity and, where possible, cited as the quantity of DNA adsorbed per square millimetre at breakthrough. The equilibrium capacity is defined as the quantity of DNA captured when the DNA concentration within the effluent is 100% that of the DNA within the challenge.

The resulting pure ctDNA data and adsorption profiles (Table 4-1, Figure 4-7,8) suggest that the adsorption of DNA onto the membrane is by electrostatic interaction only as there was no enhanced adsorption of DNA from the challenge when containing 100 mM and 1M salt (NaCl) that would normally be expected to promote hydrophobic interactions. If hydrophobic interactions were present, the challenge material would be adsorbed onto the membrane at high ionic strength (salt concentration) and eluted at low ionic strength solutions. For this reason, tests were not performed using polysorbate 80, a molecule normally used to confirm the presence of hydrophobic interactions. However, the resulting breakthrough curves were erratic and unfavourable when challenged with ctDNA for all the physio-chemical and flow conditions tested. In most cases, breakthrough occurred either immediately or after less than 100 μg of ctDNA had been challenged to the membrane surface and was immediate followed by a rapid rise in ctDNA concentration above 10% of the challenge concentration. Therefore, the operational capacity could not be determined accurately. Arnold *et al.*, (1985) demonstrated that ligands are used more efficiently at the point at which the DNA is completely removed from the solution. In consideration of this, the data indicates that the membrane surface was not being used as efficiently as possible and shown by the previous data seen in Figure 4-4. Considering that the SartoBind Q15 housing could not be altered, the problem of inefficient use of available ligands could be addressed in one of three ways. Firstly by expanding the diameter of the membrane surface with the result that the slope of the breakthrough curve would become shallower. Secondly, to stack layers of adsorbent that would result in the shifting of breakthrough curves to the right whilst the gradient remains constant. This has the effect of allowing the membranes at the top of

the stack to adsorb more DNA before breakthrough is realised at the base (although the membranes at the base will always behave sub-optimally). Thirdly, by recycling the effluent back through the membrane that would result in the breakthrough curves being disqualified and the equilibrium binding capacity being reached without excessive loss of the desired DNA. However, even by integrating these techniques into the process the SartoBind Q15 membranes located within the Sartorius housing will always behave sup-optimally due to the distribution of fluid across the membrane surface.

4.3.2. Challenge of process material

Nevertheless, the SartoBind Q15 membrane differs from many other membranes in that it is able to be regenerated after use rather than to be disposed of, therefore offering significant economic advantages. In consideration of this property and the data generated from the ctDNA challenge experiments, the SartoBind Q15 membrane was employed within the purification train for the removal of plasmid DNA from the post-EFD process material. The overall performance of the SartoBind Q15 membrane when challenged with process material was assessed in two ways. In the first series of experiments, the membrane was challenged with pure ctDNA (1 μg ml^{-1}) and BSA (50 μg ml^{-1}) to simulate the competitive environment. The flow-rate was maintained at the maximum as stated by the manufacturer for all the experiments (i.e. 50 ml min^{-1}) and the material suspending in TBS buffered at pH 7.4. The resulting performance can be seen in Table 4-1 and Figure 4-9 where the equilibrium binding capacity was determined as 44 μg of ctDNA and approximately 1150 μg of BSA after immediate breakthrough (>10%) of both species. In the second series of experiments, the SartoBind Q15 membrane was challenged with a crude *E.coli* cell lysate containing the plasmid pTS (8.3 μg μl^{-1}), genomic DNA (23,000 bp, 36 ng μl^{-1}) and cellular proteins (5-100 kDa, 21.4 ng μl^{-1}). The concentration and identity (Figures 3-12, 13) of the DNA and proteins was determined in samples prior to the process step and afterwards. However, the presence of RNA or endotoxin was not determined. Were the strategy to be used within the manufacturing of DNA for gene therapy, these would need to be quantified as part of the FDA regulations concerning the levels of contamination present within a therapeutic dose. Considering that the membrane was expected to bind significant quantities of cellular protein, the effluent was continuously recycled to determine the equilibrium binding capacity. This was done to determine whether the membrane could be employed for the preliminary capture of DNA considering that purification was not possible. However, the immediate breakthrough of both DNA and protein confirmed that the SartoBind Q15 membrane was rapidly saturated with protein rather than the desired plasmid DNA. So much so, that use of the membrane within the within a DNA harvesting stage could not result in a significant quantity of DNA being absorbed from the process material. The presence of cellular protein within the post EFD process material indicated that the DNA had to compete for sites with the other species that were capable of ionic interactions with the surface of the membrane. It was not surprising therefore to find that the anion-exchange membrane in the purification stage could only adsorb 1.86% of the DNA, plasmid or genomic, present within the process material (i.e. the SartoBind Q15 membrane is not suitable for capturing DNA within a plasmid DNA purification strategy). The corresponding 12% polyacrylamide electrophoresis gel of the cellular protein present in the challenge and eluted material can be seen in Figure 4-10.

4.4. Pall Gelman UltraBind™

Considering the failure of the Sartorius SartoBind Q15 membrane to effect the capture of significant quantities of DNA from a crude *E.coli* lysis process material, other anion-exchange membranes were

tested for this purpose. The 0.45 μm Pall Gelman UltraBind US450 membrane was designed specifically as a generic matrix for the covalent immobilisation of proteins for the affinity purification of enzyme-antibody conjugates. Containing active aldehyde groups (0.9 nmol cm^{-2}) that permanently bind available amine groups at pH 7.4, positively charged polymers were immobilised onto the matrix to effect the electrostatic adsorption of DNA molecules within the current purification strategy. As such, the monomer L-lysine (146.2 M$_w$) and the polymers polyethyleneimine (60,000 M$_w$), and three different length poly-L-lysine (500-2,000, 29,800, 111,000 M$_w$) molecules were covalently immobilised onto individual 13 mm and 150 mm membranes. Considering the breakthrough curves generated by the previous membrane, the UltraBind membranes were studies for their equilibrium binding capacity as part of a batch process where the challenge material and subsequent effluent is recycled through the membrane. The equilibrium binding capacity for ctDNA was determined in the same way as that for the SartoBind Q15 membrane, except the superficial velocity of the challenge material across the surface of the membrane was lowered (0.003 cm s^{-1}) thereby ensuring that the membrane did not compress when positioned onto the supports within the 13 mm and 150 mm housings. The equilibrium binding capacities for the various positively charged ligands for ctDNA are shown in Table 4-1. However, when the membranes were positioned within the 13mm housing they compressed immediately into the support. For this reason, all tests were performed within the 150 mm housing where the ensuing superficial velocity of the challenge material had been previously shown (Figure 4-3b) to disperse the fluid across the entire membrane. Although Figure 4-3b also indicates that the challenge material is not equally dispersed across the surface of the membrane, passing through the central regions preferentially, this should not influence the equilibrium binding capacity if sufficient time is permitted for the adsorbates to become saturated.

4.5.1. Challenge of Calf thymus DNA

Initially the adsorption of calf thymus DNA (1 μg ctDNA ml^{-1}) when suspended in TBS pH 7.4 buffer was examined, recycling the challenge material and effluent through the membranes at 36 ml min^{-1} (0.003 cm s^{-1}) until the equilibrium binding capacity was established. For the L-lysine (146.7 M$_w$) membrane the binding capacity was shown to be 233 μg, corresponding to 0.013 μg ctDNA mm^{-2}, 65% less than that of the SartoBind Q15 membrane operating under the identical physio-chemical conditions. The binding capacity's of the 500-2000, 29800 and 111,000 M$_w$ 150mm poly-L-lysine membranes were shown to be 834, 1730 and 7426 μg respectively, corresponding to 0.047, 0.098 and 0.420 μg ctDNA mm^{-2}. The 150 mm PEI membrane demonstrated the maximum where 8054 μg DNA was adsorbed corresponding to a binding capacity of 0.456 μg ctDNA mm^{-2}, 23% greater than the SartoBind Q15 membrane.

However, an increase in pressure drop across all the membranes was noted as DNA was being adsorbed (typically increasing from 0.5 psi at the start of the experiment and increasing to 2 psi towards the end). It was also observed that any further increases in the pressure drop increasing above 2 psi resulted in the membrane irreversibly compressing into the support. Interestingly, such a response was not observed for the SartoBind Q15 membrane or the low molecular weight (147.6 M$_w$) L-lysine membrane. This phenomenon may be explained by the well-documented fact that the higher molecular weight charged polymers, such as PEI and poly-L-lysine, precipitate DNA (Atkinson and Jack, 1973). Therefore, the increase in pressure may well have been caused by the cumulative aggregation of DNA within the pores that would also result in a loss of membrane capacity. This indicates that the observed binding capacities may possibly be lower than that theoretically possible.

4.5.2. Challenge of process material

As with the SartoBind Q15 membrane, the 111,000 M_w poly-L-lysine membrane was integrated into the post-EFD process stream and subsequently challenged with a 300 ml crude *E. coli* cell lysate, previously suspended in TBS pH 7.4, and as part of a batch operation. The crude cell lysate challenge (300 ml) contained the plasmid pTS (8.3 µg µl^{-1}), genomic DNA (23,000 bp, 36 ng µl^{-1}) and cellular proteins (5-100 kDa, 21.4 ng µl^{-1}), where the concentration and identities (Figures 3.12-13) were determined in samples prior to the purification stage and after the equilibrium binding capacity had been established. The equilibrium capacity was shown to be 280 µg (0.016 µg DNA mm^{-2}) of genomic and plasmid DNA and 1110 µg (0.063 µg protein mm^{-2}) of cellular protein. Considering that the previous increase in pressure (0.5-2 psi) was not noted, the rapid saturation of the membrane with the cellular proteins potentially hindered the aggregation of the genomic DNA within the pores as observed previously. However, the slight enhancement in DNA bound possible reflects the quantity of plasmid adsorbed, that due to its size would not aggregate and cause pore blockage. The full array of cellular proteins adsorbed and subsequently eluted from the matrix can be seen in Figure 4-10 and lane 4.

4.5.3. Summary

Therefore, presence of cellular protein within the post-EFD process material indicated that the DNA molecules had to compete with the other species that were also capable of ionic interactions with the surface of the membrane. It was not surprising therefore to find that the anion-exchange membrane in the purification stage could only adsorb 11.84% of the DNA, plasmid and genomic, from the crude lysate process material. Therefore, the integration of such anion-exchange membranes into the purification scheme for plasmid DNA demonstrates unequivocally that they are unable to adsorb significant quantities of DNA, preferentially adsorbing other negatively charged contaminants with higher affinity. Therefore, the anion-exchange membranes do not find any application within the preliminary purification stages of plasmid DNA manufacture for the gene therapy market.

Sartorius Sartobind Q15 (1473 mm^2):

Pure DNA Binding: Calf thymus DNA (1 µg ctDNA ml^{-1}) challenge in TE pH 7.4 buffer.

V cm s^{-1}	NaCl (nM)	Binding capacity (µg)	A (µg mm^{-2})	V cm s^{-1} (ml min^{-1})	NaCl (mM)	Binding capacity (µg)	A (µg mm^{-2})
0.034	0	459	0.94	0.170	0	399	0.23
0.068	-	470	0.96	-	20	565	0.48
0.068	-	537	1.09	-	40	521	0.35
0.102	-	641	1.31	-	60	544	0.37
0.136	-	486	0.99	-	80	587	0.40
0.170	-	389	0.79	-	100	574	0.39
0.204	-	415	0.85	-	140	543	0.37
0.238	-	335	0.68	-	250	489	0.33
0.272	-	468	0.95	-	500	426	0.29
0.306	-	404	0.82	-	1000	34	0.02

Competitive binding: Calf thymus DNA (1µg ctDNA µl^{-1}) and bovine serum albumin (50 µg BSA µl^{-1}).

| | | | | DNA | 0.170 | 140 | 47 | 0.03 |
| | | | | Protein | - | - | 1350 | 0.92 |

Crude lysate: Plasmid (8.3µg µl^{-1}), genomic DNA (23,000bp, 36 ng µl^{-1}), cellular proteins (21.4 ng µl^{-1}).

| | | | | DNA | 0.170 | 140 | 44 | 0.03 |
| | | | | Protein | - | - | 1150 | 0.78 |

Pall Gelman Ultrabind (17671mm^2):

Pure DNA challenge: Calf thymus DNA (1 µg ml^{-1}) in TE pH 7.4 buffer.

Immobilised Ligand	Molecular weight							
PEI	60,000 M$_w$			0.003	140	8054	0.456
L-lysine	146.2 M$_w$			-	-	233	0.013
Poly-L-lysine	500-2,000 M$_w$			-	-	834	0.047
Poly-L-lysine	29,800 M$_w$			-	-	1730	0.098
Poly-L-lysine	111,000 M$_w$			-	-	7426	0.420

Crude lysate: Plasmid (8.3µg µl^{-1}), genomic DNA (23,000bp, 36ng µl^{-1}), cellular proteins (21.4ng µl^{-1})

| Poly-L-lysine | 111000 | DNA | | 0.003 | 140 | 280 | 0.016 |
| - | - | Protein | | - | - | 1110 | 0.063 |

Table 4-1: Summary table listing the total capacity of the Sartorius Sartobind Q15 module and Pall Gelman Ultrabind US450 membrane, positioned within a 150mm housing, when challenged with either calf thymus DNA in various test streams with and without bovine serum albumin (BSA), or a crude E.coli cell lysate. The membranes were challenged with DNA and protein at concentrations as stated within the table with solutions of various ionic strengths. All crude lysate experiments were performed in TBS pH7.4 buffer. Where V is the superficial velocity, A is the equilibrium binding capacity per square centimetre of membrane.

5. Purification of plasmid DNA using sequence-specific DNA-binding proteins

5.1. Overview

In the previous chapter, it was clearly demonstrated that anion-exchange chromatography was ineffective in isolating plasmid DNA from two of the four classes of molecules (i.e. genomic DNA and cellular protein) that should be quantified and minimised during the manufacturing of plasmid DNA for gene therapy (Durland and Eastman, 1998). Although non-specific strategies other than anion-exchange have been developed, such as hydrophobic interaction chromatography (Diogo et al., 2000), they have also been shown to be ineffective in isolating plasmid DNA, since they lack the specificity and affinity that characterise the current protein purification processes (Yang, et al., 1998). Currently, the affinity-based purification of plasmid DNA from E.coli has relied upon short triplex-forming oligonucleotides as affinity-ligands (Wils et al., 1997, Schelup and Cooney, 1998; 1999). Whilst exhibiting high specificity for the target DNA sequence, they lack the necessary tight DNA-binding properties that are exhibited by DNA-binding proteins to immobilise the plasmid onto a solid support. However, effective techniques have been demonstrated where immobilised DNA affinity-ligands have been used to selectively purify sequence-specific DNA-binding proteins and restriction endonucleases from a clarified cell lysate (Pierrou et al., 1995, Pozidis et al., 1993). Therefore, using immobilised DNA-binding proteins within a solid matrix could potentially provide an effective DNA chromatography to target a recognition sequence within plasmid DNA with sufficient specificity and affinity to discriminate against genomic DNA and cellular protein present in a crude E.coli cell lysate.

Consequently, this chapter details the work performed to integrate a sequence-specific DNA-binding protein into a single-stage DNA chromatography procedure to isolate plasmid DNA from E.coli cells whilst minimising the contamination from genomic DNA and cellular protein. A gene encoding the consensus sequence zinc finger protein described by Berg and co-workers (1993) was obtained from D. Palfrey (Aston University). The encoded zinc-finger protein recognises and binds the to nine base-pair (bp) sequence 5'-GGG-GCG-GCT-3' with a dissociation constant of $K_D = 2$ nM (Shi and Berg, 1995). To aid expression/purification of this protein, the gene encoding the zinc finger had been inserted into the expression vector pGEX-2TK (Amersham Pharmacia) by D. Palfrey to generate a zinc-finger/glutathione S-transferase (GST) gene fusion. Thus, the encoded fusion protein was able to bind the recognition sequence and a glutathione (GSH) affinity-matrix simultaneously (Sepharose 4B, Amersham Pharmacia). Consequently, after incubating the DNA and protein with the GSH-matrix, the immobilised protein-DNA complex could be competitively eluted from the GSH-matrix with excess reduced-glutathione (rGSH). Subsequent analysis for genomic DNA and cellular protein should determine the overall effectiveness of this technique.

Experiments were initially designed to demonstrate the ability of the zinc-finger fusion protein to recognise and bind a 23 bp oligonucleotide. Resulting from the information gathered from this experiment, the 29 bp oligonucleotide was in inserted into the plasmid pUC19 (named pTS) where pure sources were incubated with the fusion protein to demonstrate whether the recognition sequence could be located and bound with sufficient affinity as to capture the protein-DNA complex with a GSH affinity matrix i.e. the GSH binding the GST section of the fusion protein. In comparison, identical experiments were performed employing pUC19 to demonstrate the specificity of the fusion protein for pTS DNA alone. Subsequently, a crude E.coli cell lysate containing the plasmid pTS was employed as the challenge material. Finally the effectiveness and scalability of the strategy was demonstrated by

challenging the pTS DNA released by 1L of *E.coli* bacterial cell culture, clarified from the solid matter by an EFD micro-filtration module and challenged to the fusion protein and a GSH affinity membrane.

5.2. Cloning the target sequence into the plasmid pUC19

Previous studies (Desjarlais and Berg, 1993) had demonstrated the specificity of the consensus zinc-finger protein for the 9 bp recognition sequence, binding with a dissociation constant of 2 nM. However, the ability of the protein to bind the recognition sequence when located within plasmid (supercoiled) DNA had not been demonstrated. Consequently, a plasmid carrying the recognition sequence was manufactured by inserting a suitable 29 bp oligonucleotide into the *Sma*I restriction site of the plasmid pUC19 (2686 bp). The insert can be seen below containing the 9bp recognition sequence:

5'-TTT-TTT-TTT-TTG-GGG-CGG-CTT-TTT-TTT-TT-3'

The double stranded 29 bp insert was manufactured by annealing together 50 pmols of the complimentary single-stranded (ss) DNA (MWG Biotech) in de-ionised water (50 μl total) (Method 2.5.2). The annealed product (46 μl) was then 'filled-in' and 'blunt-ended' with dNTP's and ATP (Method 2.5.7). The blunt ended product (2.8 pmol) was then ligated (1unit ligase, 1x ligase buffer) into pre-phosphatased pUC19 (2.8 pmol; (MBI Fermentas)) overnight at 16°C (Method 2.5.9). The ligated product was transformed into competent DH5α cells (Method 2.5.1), plated out onto LB-agar containing 50 μg ml^{-1} ampicillin (Method 2.2.3) and incubated overnight at 37°C. Both the modified and native pUC19 plasmids carry the ampicillin resistance gene so screening out untransformed cells. Singles colonies of the transformed cells were cultured at 37°C overnight in 50 ml LB-amp media (Method 2.2.3) and the subsequent plasmid DNA templates screened by Polymerase Chain Reactions (PCR) (Method 2.5.7).

Prior to PCR analysis, transformed cells are plated out onto LB-agar containing 50 μg ml^{-1} ampicillin where PCR is performed using cells from a single transformed colony. PCR is a technique that amplifies small sections within a DNA template many thousands of times quickly and reliably. A small section within the DNA template (10 ng of template) located around the *Sma*I restriction site was amplified (~200 bp with the insert and ~170 bp without) by the action of forward and reverse primers and the enzyme *Taq* DNA polymerase (Method 2.5.7). The subsequent products of the PCR reactions were analysed by 1.5% agarose gel electrophoresis (Method 2.4.1), separating the products on the basis of their size to visually determine whether the 29 bp oligonucleotide had been inserted. The results can be seen in Figure 5-1a. Figure 5-1a demonstrates that lanes 5,6,7,8,13,14 and 15 contain PCR products of the required size of ~ 200 bp (i.e. ~30 bp larger than the control pUC19). Plasmids were prepared by 'Wizard' technology from the clones amplified in lanes 4,12 and 14 of Figure 5-1a and the purified plasmids were themselves examined by agarose gel electrophoresis (Figure 5-1b), the clones seen in lanes 4, 12 and 14 were sequenced using similar PCR techniques but with ^{32}P labelled termination dNTP's (Method 2.5.7). These ^{32}P-dNTP's contain no 3'-terminus so randomly terminate the amplification process initiated by the forward and reverse primers (1μM) with thermosequenase (0.5 units). The radioactive product was analysed within a sequencing gel (Method 2.4.2) and placed in contact with photographic film to expose the position of the ^{32}P-dNTP's. The photographic film can be seen in Figure 5-2 where the correct recognition-sequence (Lane 1=A, 2=C, 3=G and 4=T) can be read from top to bottom based on the vertical displacement of the DNA bands. Although the C lane has failed, the sequence found within the A, G, and T lane implies that the correct

sequence has been inserted in the plasmid pUC19 (i.e. pTS DNA). The plasmid in lane 14 of Figure 5-1b was named pTS and was selected for use in future experiments.

5.3. Manufacture of the zinc-finger fusion protein (GST-ZF)

The vector pGEX-2TK (50 ng) carrying the gene encoding the fusion-protein was transformed (Method 2.5.1) into competent BL21 *E.coli* cells and incubated (37°C) overnight on LB-amp plates (Method 2.2.3). A single transformed colony was inoculated into 200 ml pre-warmed LB-media containing ampicillin (50µg/ml), glucose (0.2% w/v) and was grown overnight (37°C). The overnight 200 ml culture was further inoculated into 1800 ml pre-warmed LB-amp media containing 0.2 mM IPTG, grown overnight (30°C) and harvested in a 4°C fixed rotor centrifuge at 5,000 rpm for 10 mins. (Expression of the fusion-gene is controlled by the *Lac* promoter, the addition of IPTG induces expression by cleaving off the *LacI* protein from the repressor site. The control of this promoter is slightly 'leaky'). After harvesting, the cell pellet was washed (3x 20 ml chilled PBS pH 7.4) and re-suspended in 20 ml chilled PBS pH 7.4 and finally lysed by six cycles of 'freeze-thaw' (liquid nitrogen) to released the fusion-protein from the cells (Method 2.5.17). Zinc finger fusion protein was purified from the resulting lysate (Method 2.5.12). The purified protein was stored in a polypropylene microfuge tube at −20°C until needed. The size of the purified protein was analysed within the 12% polyacrylamide denaturing electrophoresis gel (Method 2.4.3) (Figure 5-8). The protein (lane 3) and protein ladder (lane 1) was denatured by incubation in SDS loading buffer at 95°C for 2 minutes. The protein was electrophoresed within the denaturing gel at 100V and visualised by staining with Coomassie blue (70°C) for 20 minutes and washing off the excess (ethanol: acetic acid 60:40) until the protein bands became visible. The gel (Figure 5-8) showed that the purified product was predominantly 36.5 kDa protein with traces of 28 kDa and 26 kDa bands, possibly representing degraded fusion product. Quantification was achieved with Bradford reagent and subsequent adsorption at 595 nm (UV spectrophotometer) (Method 2.5.13).

5.4. Preliminary studies

5.4.1. Characterisation of the GST-ZF fusion protein

The validity of using the zinc-finger fusion-protein as an affinity-ligand was assessed by a gel shift assay, determining its specificity for the recognition sequence by the apparent mobility of any protein-DNA complex and free DNA within an electrophoresis gel. The gel mobility assay was performed with the 29 bp oligonucleotide previously inserted into pUC19, but with the addition of the fluorescent probe Cye3 (Amersham) attached to the 3'-terminus on one of the ssDNA i.e. one probe per dsDNA molecule. The single stranded DNA (MWG Biotech) containing the fluorescent probe was:

5'-TT-TTT-TTT-TTT-GGG-GCG-GCT-TTT-TTT-TTTCy3-3'
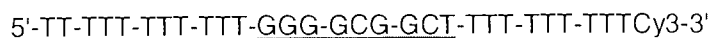
The double-stranded (ds) oligonucleotide was manufactured by annealing 50 fmols of the complimentary single DNA strands together (95°C; 3 min) in pure water (50 µl) and allowing to cool slowly to room temperature. After loading the fusion-protein (46.7 fmol) into the electrophoresis gel (12% non-denaturing polyacrylamide, 15 min), the zinc-finger was exposed to the recognition sequence by running the Cye3-labelled oligonucleotide (47.4 fmol) through the fusion-protein. This either resulted in the DNA being bound or passed through the fusion-protein (i.e. the protein is much larger than the DNA). Figure 5-3 shows the position of the bound DNA, unbound DNA (lane 3) and calibration sample (lane 2) after the gel had been identified and quantified by a TUNDRA™ digital

imaging system, exciting the Cye3 probe at 495 nm and visualising at 535 nm. The quantity of DNA molecules present within the gel was calculated by computing the intensity from each digital pixel within the fluorescent DNA bands (i.e. the intensity per pixel is directly proportional to the number of DNA molecules present within that digital pixel). The sum of the emitted-intensity per digital pixel within the bound and unbound (lane 3, 47.4 fmol) was shown to be equal to the single calibration band (lane 2, 47.4 fmol). Consequently, the quantity of DNA within each gel-shift bands was determined by expressing the measured intensity units as a linear function of the calibration intensity. The quantitative results can be seen within Table 5-1 and the electrophoresis gel in Figure 5-3.

Sample	Fusion protein challenge (fmol)	DNA challenge Lane 2 (fmol)	Unbound DNA Lane 3 (lower) (fmol)	Bound DNA Lane 3 (upper) (fmol)
Quantity	46.67	47.40	41.06	6.44 (13.6%)

Table 5-1: Qualitative analysis of the target-sequence bound (i.e. retarded) by the fusion-protein within a 12% polyacrylamide pH7.4 gel mobility assay. The fluorescent signal emitted by the Cye3 probe was quantified by a TUNDRA™ digital imaging system, exciting the Cye3 probe at 495nm and visualising at 535 nm. Lane 2: 47.4 fmol oligonucleotide challenge for intensity calibrations purposes, lane 3: 6.44 fmol of oligonucleotide bound (upper band) by the zinc-finger fusion protein whilst 41fmols passes unretarded.

The location of the zinc-finger protein being situated with the de-mobilised DNA was confirmed by staining (70°C, 20 min) the gel with Coomassie blue (Method 2.4.5), demonstrating that it was indeed the influence of the protein that had de-mobilised the DNA (data not shown). Previously (Berg *et al.*, 1993), the functionality of the zinc-finger protein had only been demonstrated without the presence of the GST fusion, this result clearly shows that the zinc-finger fusion-protein (46.7 fmol) recognises the 9 bp sequence and binds 13.6% (6.44 fmol) of the challenge.

When initially identifying the purified fusion-protein (Figure 5-8), three visible bands were observed, one representing the intact zinc-finger fusion-protein (38.5 kDa) and the other two as degraded fusion products (<38.5 kDa) or other cellular proteins with affinity for GSH (i.e. they had been adsorbed and subsequently eluted from the GSH-matrix by rGSH). Densiometric measurements of the protein bands indicated that approximately 80% of the final product was the fusion-protein in the presence of 20% contamination. In addition, the actual quality of the intact zinc-finger fusion-protein was unknown. Consequently, the relatively small quantity of DNA bound (13.6%) by the equimolar fusion-protein challenge is potentially reflects/indicates the actual quality of prepared zinc-finger protein when expressed and purified according to the procedure seen in Method 2.5.11.

5.5.   Development of a sequence-specific DNA chromatography

Although demonstrating recognition of the target sequence, the above results had not demonstrated if the fusion protein could locate and bind the target sequence within a plasmid with sufficient affinity to immobilise that plasmid onto the GSH-matrix. Therefore, experiments were developed to study the affinity of the zinc-finger protein for the recognition sequence located within the plasmid pTS whilst discriminating against the control pUC19. Additionally, to determine the significance of protein mobility in locating the recognition sequence, experiments determining the quantity of DNA isolated when the protein is allowed to retain full mobility, simulating the normal action of transcription factors within cells,

were compared to situations where the protein was initially adsorbed onto the GSH-matrix and challenged with pTS DNA. The resulting data could then be used to determine whether the affinity ligand should be expressed within the same bacterial cell as the target DNA or whether they should be manufactured separately.

From studying the plasmid map, it was noticed that the control plasmid (pUC19) contains seven of the nine bases within the recognition sequence, GGG-GCG-G(AG), potentially being recognised by the first two zinc-fingers and the first residue on the third zinc-finger. However, previous DNA foot-printing experiments (Berg *et al.*, 1993) had demonstrated that the zinc-finger protein recognised this sequence with a dissociation constant of 15nM i.e. significantly more that the actual recognition sequence (650%). This indicates that the selectivity of the zinc-finger fusion-protein is for pTS DNA alone. The results from the DNA foot-printing experiments (Berg *et al.*, 1993) can be seen within Table 5-2.

Binding site	Dissociation constant K_D (nM)
GGG-GCG-GCT	2
GGG-GCG-GGG	15
GCG-GCG-GCG	1000

Table 5-2: Dissociation constants calculated from the equilibrium isotherms (Desjarlais and Berg, 1993) for interactions between the zinc-finger protein and three related binding sites. Although the zinc-finger protein is identical to Berg's, the current protein has been fused to glutathione S-transferase to incorporate a secondary affinity site so the protein-DNA complex can be adsorbed onto a glutathione affinity-matrix.

5.5.1.   Binding studies: Zinc-finger fusion-protein with pTS and pUC19

Ordinarily the specificity of the fusion-protein for the GSH-matrix would have been determined, however, since the identical matrix had previously purified the fusion-protein, this was deemed unnecessary. The experimental studies initially focused on demonstrating the ability of the fusion-protein to recognise the 9 bp sequence within pTS DNA with sufficient affinity to isolate that plasmid in preference to pUC19, which naturally contains 7 bp of the 9 bp recognition sequence. The exact quantities of the fusion-protein were incubated with the two plasmids independently of each other, as agarose gel electrophoresis lacks the sensitivity to discern between plasmids varying by 29 bp in size.

Two affinity processes are involved in the purification; binding of the zinc-finger to the recognition sequence within pTS and the binding of the GST to the immobilised GSH. Therefore, the process could be performed in two distinct ways:

- By binding the zinc-finger fusion protein to the plasmid DNA in a homogeneous, solution phase process, followed by capture of the resulting complex onto the GSH affinity matrix, or

- By first preparing a zinc-finger solid phase adsorbent by the binding of the protein to the GSH adsorbent, followed by the adsorption of the plasmid DNA onto this functionalised matrix.

Both procedures were tested. When allowing the protein and matrix to complex initially, the experiments were performed according to the following protocol. The GSH-matrix (8 µl) was copiously

washed (3x 1 ml), centrifuged and finally re-suspended in the challenge buffer (20 µl). To this mixture, the fusion protein (~140 fmol) was added and incubated at room temperature (5 min) to allow the protein to be adsorbed onto the matrix. The plasmid was then added (115.6 fmol) and incubated at room temperature (5 mins). After washing (3x1 ml buffer and 5000 rpm centrifugation), the protein-DNA complex was eluted twice in 50 mM r-GSH (20 µl) buffer and the resulting plasmid DNA examined by agarose gel electrophoretic assays (Method 2.4.1). The plasmid was qualified and quantified by PicoGreen™ intercalation under a TUNDRA™ digital imaging system (Method 2.4.7).

When challenging the protein to the DNA initially, an identical procedure was performed but where the protein (~140 fmol) and DNA (115.6 fmol) were allowed to couple, incubated with the GSH-matrix (7 µl), washed (3x 1 ml buffer) and finally eluted (2x 20 µl) with rGSH elution buffer.

5.5.2. Results

Table 5-3 shows the quantified data for the preliminary experiments that were performed. The protein-DNA complexes were eluted from the GSH-matrix and analysed by the DNA electrophoresis assay. The eluted DNA was incubated with the fluorescent probe PicoGreen™ (0.5 µl), electrophoresed through an agarose gel and visualised by exciting the probe at 495 nm and recording the resulting emission at 535 nm. The quantification and identification of DNA was performed within a TUNDRA™ digital imaging system, displaying a calibration accuracy to 2 ng double stranded DNA (i.e. ~1 fmol pTS DNA). The calibrated signal emitted by the PicoGreen™-DNA complex, demonstrating that the intensity is directly proportional to the quantity of DNA present, allowed the resulting agarose electrophoresis gels to be calibrated by a single calibration lane of known quantity of DNA.

Plasmid	Buffer			Challenge (fmol)		Elution (fmol)		
	TBS	PBS	Tween[20]	DNA	Protein	Protein–DNA	Protein–matrix	Lane
Study 1: Figure 5-4								
pTS	✓		0.05%	115.6	137.0	9.95		8
pUC19	✓		0.05%	115.6	137.0	Trace		12
Figure 5-5								
pTS	✓		0.03%	115.6	137.0	7.28		1,2
pTS	✓		0.05%	115.6	137.0	9.95		5,6
pUC19	✓		0.03%	115.6	137.0	0.0		3,4
pUC19	✓		0.05%	115.6	137.0	0.0		7,8
Study 2: Figure 5-7								
pTS		✓	0.00%	187.5	480	26.3	1.0	2,6
pTS	✓		0.03%	187.5	480	22.7	34.2	3,7
pTS	✓		0.05%	187.5	480	43.5	24.2	4,8
Study 3: Figure5-4								
pTS	✓		0.05%	55.0	137.0	3.2		6
pUC19	✓		0.05%	55.0	137.0	0.0		10

Table 5-3: Summary table listing the quantities of pTS and pUC19 purified by the GST-ZF fusion-protein within the buffers PBS and TBS pH7.4 of various Tween[20] concentrations challenger procedure. The eluates were analysed by the agarose gel electrophoretic assay and quantified by intercalated PicoGreen™, excitation and analysed at 495 nm under a TUNDRA™ digital imaging device. Pure DNA samples were prepared by 'Wizard maxi-prep' (Promega) and quantified by UV adsorption at 260 nm in quartz cuvettes (1 absorption unit ~ 50 µg ml^{-1}).

The data demonstrated that the optimum binding kinetics were promoted when the DNA is incubated with the protein initiailly.

5.5.3.   Study 1: Preliminary study

During the preliminary studies, a suitable experimental procedure was developed to reduce the non-specific interaction between the DNA and GSH-matrix. When incubating (25°C, 5 min) either the pTS or pUC19 DNA (115.6 fmol, 20 µl) with the GSH-matrix (10 µl) suspended in TBS pH 7.4, washing (3x 1 ml TBS, 2,000 rpm) and subsequently eluting (2x 20 ml) with rGSH elution buffer (50 mM), DNA was adsorbed/retained and eluted from the matrix independently of the fusion-protein (~5 fmol). However, subsequent increases in the centrifugal speed when washing the adsorbed complex (4,000 rpm) reduced the quantity of DNA eluted from the matrix considerably to non-quantifiable levels (i.e. <1 fmol). Consequently, every subsequent wash was performed at the higher centrifugal speed to increase the centrifugal induced shear that can remove non-specifically adsorbed species from the matrix. The source of the non-specific interactions between the DNA and GSH-matrix is thought to be due to the single amine group located within GSH (Figure 5-12), protonated at pH 7.4 and therefore able to provide weak electrostatic interactions with the cationic backbone of any DNA species. Consequently, the significance of this mechanism for non-specific adsorption may increase when challenging the matrix with crude *E.coli* cell lysates, potentially resulting in the co-purification of smaller contaminating molecules that cannot be removed from the matrix by the shear induced by the increased centrifugal force.

Initially, the fusion-protein (137 fmol) and plasmid DNA (115.6 fmol) were allowed to complex, incubated with the GSH-matrix (7 µl), washed (3x 1 ml buffer) and finally eluted (1x 20 µl rGSH buffer) according to the procedure described previously. The buffer TBS pH 7.4 containing 0.05% Tween[20] was used during this complete study. The resulting elutions were incubated with PicoGreen™ (0.5 µl, 1 min) and run within a 1% agarose electrophoresis gel (Figure 5-4). The resulting DNA bands were quantified by the TUNDRA™ digital imaging system, calibrating the signal with that seen for pure pTS 115.6 fmol, lane 2) (Table 5-3). The results clearly show that the zinc-finger fusion-protein located and recognised the pTS DNA with sufficient affinity to immobilise 9.95 fmol of the resulting protein-pTS DNA complex onto the GSH-matrix whilst immobilising only trace (i.e. <1 fmol) quantities of the pUC19 DNA, therefore acting as a highly selective affinity ligand. However, it is thought that the pUC19 seen within lane 12 has been non-specifically absorbed and eluted from the GSH-matrix rather than by the fusion-protein.

The above experiments were subsequently repeated to determine whether the trace quantities of pUC19 DNA that were seen could be minimised by further increases in the centrifugal speed (5,000 rpm) during the washing stage. As previously, the experiments were performed within TBS pH7.4 containing either 0.03% or 0.05% Tween[20]. The resulting electrophoresis gel can be seen with Figure 5-5 and the total quantity of DNA within the first and second elution can be seen within Table 5-3. As previously, the signal emitted from pure pTS (300 ng) seen in Figure 5-4 (lane 2) was used to calibrate the signal emitted within Figure 5-5. Lanes 1-2 show the first and second pTS (0.03% Tween[20]) elutions, lanes 3-4 the first and second pUC19 (0.03% Tween[20]) elutions, lanes 5-6 the pTS elution (0.05% Tween[20]) and lanes 7-8 the pUC19 elution (0.05% Tween[20]). The quantified data shows that the zinc-finger fusion-protein isolated 7.28 fmol and 9.95 fmol of pTS DNA within 0.03% and 0.05% Tween[20] TBS buffers whilst isolating no visible (i.e. <<1 fmol) of the control pUC19 DNA (Table 5-3). This result conclusively demonstrates the ability of the zinc-finger fusion-protein to act as a highly selective affinity ligand for pTS alone, discriminating against native pUC19 plasmid that carries 7bp of the 9bp recognition sequence.

When comparing the calibration (lane 2) and elution lanes (lane 3-8) within Figure 5-5 a mobility shift of the plasmid DNA is apparent. Therefore, the validity of quantification process relies upon the assumption that the two bands present within the elution is solely due to the DNA present within the challenge. Considering that the elution differed only in fusion-protein and rGSH content to the challenge, a series of experiments were devised to determine the impact that these two molecules have on the mobility of the plasmid within the agarose electrophoresis gel. The resulting electrophoresis gel can be seen in Figure 5-6, where pure samples of pTS DNA (115.6 fmol) were incubated (25°C, 5min) with the fusion-protein alone (137, 274 and 411 fmol), rGSH alone (1 μmol) and finally fusion-protein (137 fmol) and rGSH (1 μmol) together. Clearly, the addition of both the fusion-protein and rGSH result in the same effect, de-mobilising the three pure DNA bands (super-coiled, open-circular and linear) present in the challenge (lane 2), into two and finally one band as the fusion-protein or rGSH content is increased. Although it appears that the mobility of the protein-DNA complexes is similar to that of open-circular and finally linear (slowest) plasmid DNA, their actual mobility is slightly less suggesting that the DNA had not being opened or linearised by the fusion-protein of rGSH. Consequent quantification (Method 2.4.7) of the DNA present within the gel demonstrated that, although the fusion-protein and rGSH influenced the mobility of the DNA, they did not impact on the signal emitted by the intercalated PicoGreen™ i.e. the assay retained the ability to quantify the DNA present within the gel. Therefore, the apparent mobility shift is a consequence of complexation between the plasmid and r-GSH.

5.5.4.   Series 2: Optimisation of the binding buffer, affinity promoter and binding order

The influence of various Tween[20] concentrations (0%, 0.03%, 0.05%), buffers (TBS and PBS pH 7.4) and the binding procedure was studied to identify potential areas for optimising DNA yields (i.e. the binding of the fusion-protein to the DNA or fusion-protein to the GSH-matrix initially). The experiments were performed according to the procedure described previously. To increase the sensitivity of the experiment, the quantity of fusion-protein (480 fmol) and plasmid DNA (187.5 fmol) was increased. The resulting protein-DNA complex was adsorbed and eluted from the GSH-matrix and analysed by the agarose gel electrophoresis assay defined previously (Section 2.4.7). The resulting electrophoresis gel can be seen in Figure 5-7 and the quantified data within Table 5-3. The resulting data suggests that binding procedure employed does significantly influence the quantity of pTS DNA isolated within the PBS buffer, isolating 26.3 fmol to 1 fmol, whilst becoming less significant within TBS buffers. However, the buffer TBS pH 7.4 containing 0.05% Tween[20] proved to be the optimum condition tested, isolating 43.5 fmol (23.2%) of the 187.5 fmol challenge but still only utilising 9%, assuming one fusion-protein to target sequence and subsequent adsorption, of the fusion-protein present within the challenge. Therefore, it appears that significant increases in the quantity of pTS DNA purified will require the fusion-protein to be present in large excess.

5.5.5.   Study 3: Purification of pTS from post EFD cell lysis

Having demonstrated that previously-purified plasmid DNA could be isolated using the zinc finger fusion protein as an affinity ligand, it was now attempted to purify plasmid DNA directly from cells. Challenge material was prepared by transforming the plasmids pUC19 and pTS into competent DH5α cells and plating out overnight (37°C) onto LB-agar containing 50 μg ml^{-1} ampicillin. The transformed colonies were cultured overnight (37°C) in LB-amp media, processed and diafiltered into TBS pH 7.4 by an EFD micro-filtration module and finally lysed by six cycles of freeze-thaw lysis. The resulting cell

lysate was clarified from the cellular debris within the same EFD modules. The DNA and cellular protein present within the clarified cell lysate can be seen within Figures 5-9 and 5-10 where a single band of genomic DNA (>23,000 bp; 36 ng μl^{-1}) and the cellular protein (5-100 kDa; 21.4 ng μl^{-1}) are present with the pTS or pUC19 plasmid (8.3 ng μl^{-1}). The levels of RNA or endotoxin could not be measured.

The process conditions were selected from the previous studies, which had demonstrated that plasmid DNA within TBS pH 7.4 containing 0.05% Tween[20] when allowed to complex with the fusion-protein initially presented the most favourable binding kinetics. Consequently, the clarified cell lysis material (55 fmol) was incubated (5°C, 5 min) with the fusion-protein (137 fmol) and allowed to complex. The resulting mixture was adsorbed (25°C, 5 min) onto the GST-matrix (10 μl), washed (3x1 ml TBS pH 7.4. 0.05% Tween[20]) and finally eluted (2x 20 μl, 70 mM rGSH elution buffer). The resulting protein-DNA complex was analysed by the agarose gel electrophoresis assay (Figure 5-4) where it was shown that the fusion-protein (137 fmol) isolated 3.2 fmol of the pTS DNA (lane 6) challenge completely from the genomic DNA (~23,000 bp; 36 ng μl^{-1}) present in the cell lysate. Also, the identical pUC19 challenge (55 fmol) isolated only trace (i.e. <<1 fmol DNA) quantities of plasmid DNA (lane 10) with no traces of the genomic DNA present in the crude *E.coli* cell lysate. However, the low sensitivity of the subsequent protein assay (Method 2.5.13) could not detect or identify the presence of any cellular proteins that were co-purified with the plasmid DNA.

Although this does not categorically demonstrate the ability of the this technique to isolate plasmid DNA from the other three contaminants described by the FDA as substances that should be minimised and quantified during plasmid DNA manufacture, it does indicate the potential for using DNA-binding proteins as sequence-specific affinity ligands. The results clearly demonstrate the ability of the fusion-protein to locate and recognise the target sequence with sufficient affinity to isolate pTS DNA from pUC19 and genomic DNA within crude *E.coli* cell lysates.

5.6.   Large scale manufacture of plasmid DNA

Consequently, the scale of the process was increased to determine whether the technique could be within a commercial manufacturing process, purifying plasmid DNA sequence-specifically from the genomic DNA and cellular protein contaminant that can be quantified and identified as part of the electrophoretic assays. Although the previous studies failed to provide conclusive evidence that the technique did not co-purify cellular proteins due to the sensitivity of protein assays, by increasing the scale and any subsequent co-purification of contaminants, the technique was rigorously tested to determine the actual ability in relation to crude *E.coli* cell lysates. Therefore, the complete manufacturing procedure was simulated, challenge the technique with plasmid DNA from 1L of clarified *E.coli* cell lysis material.

However, the presence of DNase's and protease's within an *E.coli* cell lysate, capable of degrading the affinity ligand and target plasmid, forces the consideration of process time on the quality and quantity of plasmid DNA isolated by the procedure. Consequently, it was decided to transfer from the static GSH-matrix system that is reliant on slow pore diffusion for transporting protein-DNA complexes to the GSH-membrane system (176.7 cm^2) promoting the faster convective transportation of adsorbates through small pores. When residence time becomes critical, membrane processes offer significant advantages. They are designed to limit the influences of pressure-drop and intra-bed diffusion normally characteristic of packed beds, by forcing the adsorbent through fine pores

promoting fast convective transport of adsorbates to the active sites. Coupling this with the fast association kinetics displayed by GSH and GST, a membrane system should significantly reduce the loading, washing and elution time to minimal value (Suen *et al.*, 1992) i.e. reducing the contact of the protein-DNA complex with degrading DNase's and protease's. The GSH-membrane is held in a stainless steel housing (176.7 cm^2; Millipore), connected to a peristaltic pump (Millipore) and pressure gauge (Cole Palmer) by Tygon™ tubing (Masterflex). The holding volume of the entire system was measured at 50 ml.

5.6.1. Manufacture of a GSH-affinity membrane

As GSH-membranes are not commercially available, they had to be manufactured from sheets of UltraBind™ US450 (Pall Gelman, 0.45 μm pore size, 0.45-0.75 mm thickness) membrane. The UltraBind™ US450 membrane, functionalised by aldehyde groups, is able to covalently bind free amine groups located within proteins (135 μg of IgG per cm^2 capacity) and therefore able to covalently bind GSH. Circular sheets (176.7 cm^2, ~23.9 mg IgG capacity) of the UltraBind™ membranes were cut and according to the manufacturers recommendations and incubated (25°C) with GSH (25 mg, Sigma UK) in PBS pH 7.4 (50 ml) under gentle agitation for 2 hours. Subsequent protein assays (Method 2.5.13) of the bound and unbound material demonstrated that ~23 mg of the GSH challenge had been adsorbed onto the UltraBind™ membrane. To determine the functionality of the prepared GSH-membrane, pure GST (10 nmol) of known activity within the buffer PBS pH7.4 (50 ml) was passed through the membrane (37ml min^{-1}) for 20 minutes until the equilibrium concentration had been reached. The adsorbed GST was washed (2x 300 ml PBS pH7.4) and eluted by circulating rGSH (50 nmol) elution buffer (2x 50 ml) through the system and membrane. The resulting quantity and activity of the GST adsorbed onto the GSH-membrane was determined by an immuno-affinity assay, monitoring the conjugation of GSH with 1-chloro-2,4-dintrobenzene (CDNB) as catalysed by GST. The reaction was performed within a 1 ml quartz cuvette and the activity of the GST recorded by monitoring the change in molar adsorption at 340nm with time (i.e. directly proportional to the reaction rate). The assay was calibrated by performing the assay with a known GST standard where the reaction rate is directly proportional to the units of active GST present. The subsequent assay determined that the GSH-membrane contained approximately 8 nmol of site able to adsorb active GST. Theoretically this corresponds to the GSH-membrane adsorbing 8 nmol of the fusion-protein or 14 mg of plasmid DNA-protein complex assuming one protein-DNA complex per active site.

5.6.2. Large-scale manufacture of the zinc-finger fusion-protein and pTS DNA

Considering that the GSH-membrane is potentially able to adsorb 8nmol of fusion-protein, the maximum quantity of cell culture (4 L) from a single batch operation was used to manufacture the affinity ligand for one single challenge. The procedure defined within Methods 2.5.11 was used to manufacture and purify the fusion-protein. The vector pGEX-2TK was transformed into competent Bl21 *E.coli* cells and plated out onto LB-agar plate containing 50 μg ml^{-1} ampicillin and grown overnight (37°C). A single colony was inoculated into 2x 200 ml LB-amp media containing 0.2% w/v glucose and grown overnight (37°C) under agitation. The resulting cell culture was transferred into 2x 1800 ml LB-amp media and induced with 0.2 mM IPTG, grown overnight (30°C) and subsequently harvested at 5000 rpm within a chilled (4°C) centrifuge. After washing (3x 20 ml PBS pH7.4) and freeze-thaw cell lysis, the resulting supernatant containing the zinc-finger fusion-protein was adsorbed onto 4 ml of GSH-matrix, washed (3x 20 ml PBS pH7.4) and finally eluted with rGSH elution buffer

(2x4 ml, 50 mM). Finally the rGSH was dialysed from the zinc-finger fusion-protein by three successive (10%, 20% and 50%) glycerol-PBS pH 7.4 solution over a 48 hour period. Quantification (Method 2.5.13, 2.4.3) of the purified protein showed that of the 168μg (4.58 nmol) that had been purified, 80% was the undegraded zinc-finger fusion-protein. The correspond electrophoresis gel (12% polyacrylamide denaturing) can be seen within Figure 5-8 (Lane 3). The two smaller bands seen below the fusion-protein are potentially the degraded fusion product that retained activity for the GSH-matrix.

5.6.3.   Experimental

As previously, the crude source of pTS DNA was derived from 1L of transformed *E.coli* DH5α cells (Methods 2.5.1) To simulate the desired two-stage manufacturing and affinity purification process, the 1L cell culture was processed by the EFD micro-filtration module in-line with the affinity purification system. Again, the DNA and protein within the challenge was quantified and analysed by agarose gel electrophoresis and suitable assays. The DNA, after densiometric tests to determine the signal emitted by the ethidium bromide intercalated into DNA (Figure 5-10), indicated that of the 13.28 mg passed through the EFD, 10.28 mg was genomic DNA of specifically 23,000 bp molecular weight (36 ng μl^{-1}) and 2.5 mg (1.4 nmol) of the plasmid pTS (8.3 μg ml^{-1}). The corresponding protein assay and electrophoresis gel seen in Figure 5-9 identified that 6.4 mg of 5-100 kDa cellular protein were present at a concentration of 21.4 ng μl^{-1}. (The levels of RNA or endotoxin could not be substantiated).

As demonstrated previously, by allowing the fusion-protein and plasmid to complex within the buffer TBS pH 7.4 containing 0.05% Tween[20] initially, optimum binding kinetics was promoted for all the conditions tested. Therefore, the zinc-finger fusion-protein (4.58 nmol) was allowed to complex (25°C, 5 min) with the DNA within the crude *E.coli* cell lysate (300 ml containing 0.05% Tween[20] under gentle stirring within the holding vessel. During which time, the GSH-membrane was equilibrated with TBS pH 7.4 0.05% Tween[20] (500 ml) at 37 ml min^{-1}, a flow-rate that proved effective when using similar anion-exchange membranes (Chapter 4). It was observed previously that increasing the flow-rate above 37 ml min^{-1} tended to compress the UltraBind™ membrane into the metal support, resulting in permanently compressed membrane. The resulting protein-DNA complex (300 ml) was challenged to the GSH-membrane by circulating (37 ml min^{-1}) the mixture through the system. The concentration of DNA within the challenge was monitored constantly (UV adsorption at 260 nm) until the equilibrium quantity of DNA had been adsorbed (i.e. constant 260nm adsorption). Immediately the membrane was washed (600 ml TBS pH 7.4, 0,05% Tween[20]) at 37ml min^{-1} and the adsorbed material eluted with rGSH elution buffer (2x 50 ml, 50 nM). The resulting eluates were analysed for DNA and protein content by DNA/protein assays (Method 2.5.13, 2.5.14) and electrophoresis techniques (Method 2.4.1, 2.4.3).

5.6.4.   Results

The complete results of the quantification and identification assays can be seen in Table 5-4 whilst Figure 5-11 shows the DNA present in the elution. The corresponding electrophoresis gel to determine the identity of contamination proteins resulted in no visible bands so was not included. The quantity of DNA determined by the densiometric assay was checked by measuring the molar absorbance at 280nm within quartz cuvettes and calibrated by known quantities of calf thymus DNA. Similarly, the quantity of protein determined by the protein assay was calibrated against known quantities of BSA.

		DNA (μg)	(nmol)	Protein (μg)
Challenge		13280	-	7164.2
	Genomic	~10780	-	-
	pTS	~2500	1.40	-
Fusion-protein		-	-	167.0
Unabsorbed		12240	-	6425.4
Adsorbed		1040	0.57	768.8
Eluted		943	0.52	406.72
Without the fusion-protein within the challenge that is assumed to be either adsorbed into the GSH matrix or DNA		-	-	239.7
Total		**943 (37.7%)**		**239.7 (3.4%)**

Table 5-4: The complete experimental data for large-scale purification of plasmid DNA from crude E.coli cell lysates using the sequence-specific DNA-binding protein GST-ZF. Protein was assayed using Bradford reagent (BioRad) and 12% polyacrylamide gels. No visible signs of protein are seen within the gels after 10-fold concentration of the eluate. DNA was quantified by UV adsorption (260/280) and agarose gel electrophoretic assay after incubation with IPTG (1M 60°C) and 10-fold concentration. No genomic DNA only pTS DNA was present in the eluate.

5.6.5. DNA adsorbed and eluted from the UltraBind™ glutathione-membrane

The data seen within Table 5-4 and Figure 5-11 clearly demonstrates the ability of this sequence-specific purification technique, although not displaying any preference for the type of plasmid DNA (i.e. linear, open-circular or the desired super-coiled), isolating 943 μg (38%) of the 2500 μg (estimated by densiometric measurements of the resulting agarose electrophoresis gel) of pTS DNA completely from the 10.28 mg of genomic DNA (23,000 bp) present within the crude *E.coli* lysate. The corresponding 1% agarose electrophoresis gel can be seen in Figure 5-11 where lane 2 shows the wizard-prepared pTS DNA, lane 4 the first elution and lane 5 the second.

Initially, the lack of visible DNA within the corresponding electrophoresis gels indicated that the presence of rGSH hindered the intercalation of PicoGreen™ or ethidium bromide with the DNA. Therefore, the rGSH and fusion-protein were cleaved off the DNA by incubating (60°C, 5 mins) the eluate (500 μl) with IPTG (1 M) with the cleaved rGSH and fusion-protein being filtered from the DNA (A serendipitous discovery had previously demonstrated that that IPTG and heat released the GSH from the plasmid DNA). The mixture was loaded (500 μl) into the spin-column (100 kDa cut-off), centrifuged (4,000g, 10 min) to retain the DNA (i.e. >100 kDa) and subsequently reversed and re-centrifuged into a clean micro-tube to discharge the retained DNA (20 μl). This was performed for the two 50 ml eluates with the resulting mixture run through a 0.5% agarose electrophoresis gel containing ethidium bromide. Figure 5-11 shows the electrophoresis gel as describe previously.

5.6.6. Protein Eluted from the UltraBind™ glutathione-membrane

Previously, no protein was identified of quantified when using the GST-matrix due to the sensitivity of the assay (Method 2.5.13). However, by increasing the scale by 25-times, it has been demonstrated that the technique co-purified 768.8 μg (6.3%) of the 6425 μg cellular proteins present within the clarified *E.coli* cell lysate. Considering that 186 μg (7.7 ng μl^{-1}) of this is potentially the fusion-protein of degraded protein added into the challenge, (i.e. had been previously purified by a GSH-matrix), it is suggested that the technique actually co-purified 406.7 μg (4.07 ng μl^{-1}) of cellular proteins equating to a clearance of 96.3%. Previously, an UltraBind™ anion exchange membrane utilising 111,000 Mw poly-L-lysine ligands under similar condition adsorbed 11500 μg from an identical challenge (i.e. 28-times the quantity).

However, considering that the protein-DNA complex occupied a maximum of 5% of the active GSH-sites (0.4 nmol), the majority of the GSH-membrane remained vacant. Previously, it was demonstrated how rGSH and subsequently any positively charge protein (Charlton, 1999), could interact with plasmid DNA within a series of gel mobility studies. It was hypothesised that these interactions were predominantly due to electrostatic interactions between the protonated amine group (i.e. the same amine group present within GSH). Therefore, it is expected that the remaining 95% of active GSH sites are available for such non-specific interactions that could potentially be competed off the immobilised GSH by the excess of rGSH present. Therefore, this value could be potentially reduced if the majority of the available GSH sites were occupied. However, this does not detract from the specificity demonstrated by the technique in locating and recognising pTS with sufficient affinity so to isolate that plasmid completely from genomic DNA and 97.6% of the cellular proteins present within a crude *E.coli* cell lysate.

5.7. Summary

Experiments were designed to validate a fluorescence based assay employing PicoGreen™ for the quantification and identification of DNA within pure and crude sources of DNA. By incubating the PicoGreen™ with the DNA source and running through an agarose electrophoresis gel, it was demonstrated that the influence of culture media, salt and cellular proteins (fusion-protein and rGSH) were negligible on the linear and predictable signal emitted from the intercalated PicoGreen™. However, the assay was not able to identify DNA that had been de-mobilised until IPTG and subsequent filtration had removed fusion-protein/rGSH from the DNA.

In a series of studies in which the fusion-protein was challenged to a pure sources of 29 bp oligonucleotide and eventually pTS DNA both containing the 9 bp recognition sequence, it was clearly demonstrated that the fusion-protein located and recognised the target sequence with sufficient affinity to immobilise the corresponding protein-DNA complex onto a GSH-matrix. It was shown that the optimum condition displayed by the technique was achieved when allowing the DNA and fusion-protein to complex within TBS pH 7.4 containing 0.05% Tween[20], challenging too the matrix and increasing the centrifugal speeds when washing to reduce the non-specific purification of DNA to negligible quantities. The technique demonstrated that the fusion-protein performed as a highly selective affinity ligand for pTS alone, differentiating against the 7 of the 9 bp present in native pUC19 for the complete recognition sequence that had been previously inserted into pUC19 to create the plasmid pTS.

To determine the ability of the technique to locate and recognise pTS DNA within a crude E.coli lysate, the fusion-protein was challenged to pTS and pUC19 lysis material generated by freeze-thaw lysis and subsequent clarification with the EFD micro-filtration module. The results confirmed the ability to purify solely pTS, this time differentiating against pUC19 in the presence of large quantities of genomic DNA and cellular protein.

Finally the ability of the technique to be scaled towards an actual manufacturing process was studied. The complete two-stage process was performed, initially concentrating a 1L culture of E.coli DH5α cells, diafiltration into TBS pH 7.4, freeze-thaw lysis and subsequent clarification of the released pTS DNA from the cellular debris, by a single EFD micro-filtration column and within 26 minutes. The resulting mixture was incubated with fusion protein, challenged to and eluted from a GSH-membrane resulting in the isolation of approximately 1 mg of pTS plasmid, completely purified form genomic DNA and 96.4% of the cellular proteins within 36 minutes. The contaminating proteins are potentially positively charged species that have either interacted with the DNA or GSH-matrix and been subsequently co-purified with the product. However, it was shown that the technique does not differentiate between the type of plasmid, purifying linear, open-circular and the desired super-coiled DNA.

Therefore, the complete technique was able to process a 1L culture of E.coli cells within 1 hour to manufacture ~1 mg of pTS DNA, free from genomic DNA and 96.4% of the cellular proteins. This work suggests that this type of affinity purification of plasmid DNA, utilising sequence-specific DNA binding proteins as affinity ligands, will have an application within the Biotechnology industry desiring to manufacture plasmid DNA for the gene therapy market.

6. DISCUSSION

A single objective defines the research scenario, the development of a generic manufacturing process for the purification of plasmid DNA for use in human gene therapy. However, this single objective conveniently spilt into two separate issues. First the ability of an EFD cross-flow micro-filtration module to effect the concentration and diafiltration of an *E.coli* bacterial cell culture, and finally to partition the plasmid DNA released from the cellular debris after lysis. Second, to develop a highly specific affinity technique for the purification of the plasmid DNA from the post-EFD clarified process material (i.e. reducing the numerous non-specific purification stages currently employed).

The combination of these two issues meant that the numerous centrifugation, precipitation, and non-specific chromatographic stages that are currently being employed for this purpose could be reduced, whilst issues that directly affect the granting of a licence to market such therapeutic DNA, including safety, reproducibility, and efficacy could be promoted.

The initial work in this thesis was executed to determine the ability of the EFD micro-filtration module to effect the manufacturers design remit, and ability to execute the desired strategies (i.e. concentration, diafiltration, and clarification). The design remit was that the helical membranes within the EFD were to promote centrifugal instabilities (Dean vortices) to effect the concentration of bacterial cells at the membrane wall to reduce and control the fouling rates characteristic of standard filtration stages, and also promote flux enhancements. This was achieved by challenging the EFD system initially with pure DI water, maintaining zero transmembrane pressure, and determining the experimental friction factor, power usage and friction as the Dean number was increase between 187_{Dn} and 818_{Dn}. Second by operating the EFD system under constant axial transmembrane pressure to determine the effect of fluid dynamics on the pure water flux. Third by challenging the EFD system with $OD_{2.5}$ and OD_{16} bacterial cell cultures to determine the ability of the fluid dynamics to effect concentration de-polarisation and to control the resulting fouling rates. It was demonstrated that the fluid dynamics (Dean vortices) occurring within the EFD as a function of the Dean number, manufactured indicative trends in the friction factor, permeate flux and power usage. It was shown that friction factor, the pressure exerted by a fluid element on the wall of the membrane, accurately predicted the permeate flux, demonstrating that combinations of primary and secondary flow combine to either increase or decrease the average radial transmembrane pressure experienced within the membrane. It was seen that as Dn number increased above 227_{Dn} that the system transferred from system experiencing equal increase in centrifugal and viscous forces (i.e. secondary flows increasing) to one where the centrifugal forces start to compete and eventually dominate the viscous forces that results in a distortion in the original flow patterns. The results were compared to numerical studies, a series expansion method that predicted the primary and secondary flows at low Dn numbers ($10-120_{Dn}$), and studies developed by Liu *et al.*, (1993) that demonstrated the orientation of primary and secondary flows at higher Dn numbers ($100-900_{Dn}$).

By challenging the EFD system with bacterial cells ($OD_{2.5}$ and OD_{16}), it was clearly demonstrated that the combinations of primary and secondary flows and the resulting shear profile had an enormous effect of the ability of the module to control the permeate flux. It was shown that at lower Dn numbers, where the pure water data recorded the highest flux enhancements, the shear profile generated was unable to control the fouling rates, resulting in premature blinding of the membrane. However, when the flow-rate (i.e. shear profile) was increased, an increase that previously resulted in a reduction in

the pure water flux, the EFD module was able to successfully control the fouling rates to process the bacterial cells for long periods of time at permeate rates close to the pure water flux. This trend remained as the Dean number was further increased (759_{Dn}) although the pure water flux was reduced. The trends were identical for both $OD_{2.5}$ and OD_{16} bacterial cell cultures.

Finally, after selecting the optimum processing condition, it was shown that the EFD system was able to concentrate a bacterial cell culture (1 L) to completion (50 ml) in less than 10 minutes, and processing at an average rate close to 400 lmh (i.e. competitive with established technologies).

The next piece of work was performed to determine the ability of the EFD module to diafilter the harvested cells into TBS pH 7.4, immediately after the concentration stage. It was shown that the permeate flux experienced at the conclusion of the concentration stage was maintained when diafiltering the cells, concluding a 6-fold buffer exchange (300 ml) in less than 5 minutes without the need to transfer the process material from the system.

The final piece of work employing the EFD system was to effect the clarification of cellular debris from the process steam after the bacterial cells had been disrupted by freeze-thaw lysis techniques. After diluting the lysis material into the process buffer (300 ml), it was shown that the EFD processes the lysate, passing the plasmid DNA, supercoiled etc, cellular proteins, and a single band of genomic DNA (~23,000 bp) into the process stream, whilst retaining larger genomic DNA within the retentate.

On the basis of the data generated in the final study, an electrophoretic assay for DNA was developed. Since DNA was present as different sized molecules, it was first necessary to determine the size of DNA passing through the EFD module. This was achieved by electrophoretic separation of the DNA is agarose, staining with ethidium bromide, and determining the concentration by densiometric measurements to generate qualitative results. The DNA in the post-EFD process stream was shown to be the plasmid DNA of supercoiled, open-circular, and linear conformation, with one contaminating band of genomic DNA of >23,000 bp is size. It was shown that higher molecular weight genomic DNA was substantially cleared from the process stream after passage through the EFD. On this basis, the fluorochrome PicoGreen was employed which was able to generate fluorescent signals when intercalated into dsDNA without incurring interference from other biomolecules (Ahn *et al.*, 1996, Charlton, 1999, Singer *et al.*, 1997).

Singer *et al.*, (1997) have shown that the specific fluorescent enhancement of PicoGreen in the presence of linear dsDNA is constant and independent of the source organism. Ahn *et al.*, (1996) demonstrated that PicoGreen can bind DNA of 150 base pairs with the same sensitivity and efficiency as larger strands of DNA. However, Enger (1996) demonstrated that PicoGreen, upon intercalation into dsDNA, can be run within a agarose electrophoresis gel to determine the concentration and identification of PCR products. In addition, Charlton (1999) demonstrated that the signal emitted from PicoGreen was unaffected by monoclonal antibodies, host cell protein, culture broth and dilute cell lysate. Experimental procedures in this thesis demonstrate that PicoGreen can be used to quantify and identify dsDNA within agarose electrophoresis gels. The combined data demonstrates that PicoGreen can be used to quantify and identify dsDNA from a variety of sources by agarose gel electrophoretic techniques.

However, due to a malfunction in the detection equipment, the assay was unable to be employed for the determination of DNA passing through the EFD module. Therefore, ethidium bromide and densiometric measurements determined that approximately 83% (2.5 mg) of the plasmid DNA (8.3 ng

μl^{-1}), 10.8 mg of genomic DNA (~23,000 bp, 36 ng μl^{-1}), and 7.2 mg of cellular proteins (5-100 kDa, 21.4 ng μl^{-1}) were passed into the post-EFD process stream. Therefore, the affinity purification technique would need to differentiate between the two types of DNA present without binding the cellular proteins.

The second issue defined by the project objectives was to develop a reliable affinity purification technique to effect the capture of plasmid DNA from the process stream containing the genomic DNA and cellular proteins. For this purpose, certain anion-exchange membranes were employed in various test streams where their performance was assessed. The data showed that the anion-exchange membranes were indeed capable binding significant quantities of pure ctDNA. However, the Sartorius SartoBind Q15 membrane and housing, shown to bind predominantly by electrostatic interactions by increasing the ionic strength of the buffer, suffered from adverse adsorption profiles where breakthrough was almost immediate for all conditions tested. As this was shown to be a fluid distribution problem, also shown by Charlton (1999), the membranes were subsequently operated as a batch operation where the effluent was recycled into the feed stream (i.e. determination of the equilibrium binding capacity).

Consequently, the equilibrium binding capacities were determined as, 0.48 μg mm^{-2} for the SartoBind Q15 membrane, and 0.013 μg mm^{-2}, 0.047 μg mm^{-2}, 0.098 μg mm^{-2}, 0.42 μg mm^{-2} and 0.46 μg mm^{-2} for the Pall Gelman UltraBind membranes containing 146.2 M_w l-lysine ligands, 500-2000 M_w poly-L-lysine ligands, 36,000 M_w poly-L-lysine ligands, 111,000 M_w poly-L-lysine ligands, and 60,000 M_w PEI ligands respectively. However, when challenging the membranes with the post-EFD process stream, the data showed that they were unable to effect the separation of plasmid DNA, preferentially binding large quantities of cellular proteins whilst only capturing small quantities of DNA, plasmid and genomic.

Therefore, the final work in this thesis was executed to develop a sequence specific affinity chromatographic technique. For this purpose a gene encoding the consensus sequence zinc finger protein described by Berg and co-workers (1993) was obtained from D. Palfrey (Aston University). The previous workers had shown that the encoded zinc-finger protein recognises and binds the to nine base-pair (bp) sequence 5'–GGG-GCG-GCT-3' with a dissociation constant of K_D = 2 nM (Shi and Berg, 1995). To aid expression/purification of this protein, the gene encoding the zinc finger had been inserted into the expression vector pGEX-2TK (Amersham Pharmacia) by D. Palfrey to generate a zinc-finger/glutathione S-transferase (GST) gene fusion. Thus, the encoded fusion protein was able to bind the recognition sequence and a glutathione (GSH) affinity-matrix simultaneously (Sepharose 4B, Amersham Pharmacia). Whilst a gel mobility assay demonstrated that the fusion-protein had affinity for the recognition sequence, the ability of the fusion-protein was explicitly shown after successfully differentiating between pTS and native pUC19, the template plasmid containing 7bp of the 9bp responsible for recognition. To conclude the small-scale studies, the technique was challenged with the crude process material where it was demonstrated that the fusion-protein (137 fmol) was able to locate and bind 5 fmols of pTS DNA and only trace quantities of pUC19 DNA with no contamination from genomic DNA.

On the basis of the data generated in the small-scale studies, the technique was scaled 250-fold where a 1L bacterial cell culture was processed by the EFD micro-filtration modules, the resulting process material incubated with the fusion-protein (167 μg) and challenged to a glutathione membrane that had been previously demonstrated as functional towards GST. It was shown that the affinity

purification technique was able to capture 943 µg (38%) of supercoiled, open-circular, and linear pTS DNA, 240 µg (3.4%) of cellular protein whilst showing no traces of genomic DNA from the 10.8 mg present on the challenge.

In conclusion, the integrated process for the purification of plasmid DNA for use in human gene therapy was able to capture approximately 1 mg of plasmid DNA, showing complete clearance from genomic DNA, and resulting in the removal of 96.7% of cellular protein. The entire process was achieved by two integrated stages and occupied less than one hour from of process time.

6.1. Recommendations for future work

In consideration of the fact that research within this area is an on going process, certain recommendation can be made concerning the direction of the future work resulting from the findings or omissions described herein. The suggestions for future work, in accordance with the initial objectives, can be conveniently dived into two. First relating directly to the EFD micro-filtration system, and second to the affinity purification strategy.

With regards to the EFD module, there is clear evidence here that the geometry of the module has a major impact on the overall performance of the EFD system. Although it was demonstrated that the EFD system was able to exceed the abilities of the current membrane systems sufficiently enough to compete with existing technologies, the evidence suggests that the disharmony between the optimal wall shear stress ($>579_{Dn}$) and the maximum flux enhancements (227_{Dn}) results in the EFD performing sub-optimally. Considering that these two issues are related to the cross-flow rate and the internal geometry of the helical membrane, it is suggested that future work could be approached by modelling the EFD in 3-D in order to determine the exact point where the optimum shear rates, secondary flows, and primary flows coincide to create the maximum flux enhancement and the concentration de-polarisation effect. Depending on the findings of the numerical study, the geometry of the helical membranes should be altered to determine whether the experimental performance could be improved that would result in a larger flux being able to be maintained for longer time periods. In addition, latex beads should be used within these studies rather than bacterial cells (i.e. removing irreversible fouling characteristics from the study).

Regardless of these studies, the EFD system should be tested with larger scale bacterial cell cultures to determine whether the results are reproducible under the more realistic simulation of large-scale manufacturing processes. Therefore, banks of the EFD modules should be studied, whether employed in series or parallel, to determine the configuration of the optimal process train. In addition to these studies, the diafiltration of the bacterial cells to remove adventitious material from the subsequent purification stages should be demonstrated. Incorporating relevant assays to determine the efficiency, safety, and efficacy of the process, information that would be necessary before a manufacturing license could be presented.

Concerning the partitioning of the plasmid DNA from the bacterial lysis material, the EFD system should be extended and be rigorously tested in order to determine whether active 'gel layers' can be employed to actively discriminate against the larger molecular weight genomic DNA seen previously present in the process material. The reproducibility of the operation should also be adequately demonstrated.

With specific reference to the purification of plasmid DNA from the crude *E.coli* cell lysate, the goal must be to develop a robust procedure that is simple to operate in manufacturing and reliably produce plasmid DNA products of satisfactory therapeutic grade. Considering that it is not yet known to what extent the feedstock needs to be conditions to ensure that the subsequent affinity systems will operate most effectively, the feedstock should be conditioned in a variety of ways in order to determine their influence of the subsequent affinity purification strategy. In addition, the influence that diafiltration has on the feedstock to reduce contamination from soluble adventitious components in the growth medium should also be demonstrated.

Ideally, the affinity system should be able to operate directly with the feedstock from the lysis stage, in either an expanded bed or membrane chromatographic system. Therefore, the general aspects of affinity plasmid purification, using the zinc-finger fusion-protein as an effective model, should be performed. To simulate a process where the affinity ligand is expressed within the host cell (i.e. promoting the most favourable binding kinetics), the recognition sequence should either be inserted into the pGEX2TK vector that codes for the zinc-finger fusion protein, or the gene encoding the fusion protein should be inserted in the bacterial genome. This would effectively simulate the normal action of DNA binding proteins within the host cell, therefore reducing the need for external affinity ligand manufacture, purification, and subsequent validation in terms of safety, efficacy etc.

With specific reference to the scenario where the affinity ligand is expressed within the therapeutic plasmid host cell, the effect of process variables on the purity and integrity of DNA released, and the suitability of the product obtained for use in subsequent high-resolution separation procedures should be investigated. The information gathered should be used to determine the optimal residence times of process liquids in the lysis of the flow system, and the need for any other separation stages prior to final formulation of the DNA dose.

However, this study has not precisely identified the level of contamination from the adventitious material that has been specified by the FDA as material that must be quantified and minimised during such manufacturing procedures. In consideration of the demands legislated for by the FDA concerning the purity of plasmid DNA for gene therapy, a strategy for demonstrating the purity, efficacy, and safety of the developed process, especially in terms of endotoxin and RNA contamination, will have to be demonstrated. Therefore, the future work will have to employ relevant endotoxin and RNA assays for the accurate determination of such adventitious material. In addition, these assays will have to be shown to accurately, and reliably, quantify such material throughout the course of the process in order to determine the efficacy of all the separate stages employed within the overall process.

As a final note, the effectiveness of the zinc-finger protein was shown to be compromised by its fusion to glutathione S-transferase (GST), a molecule that was shown to possess some affinity for DNA. Therefore, it is suggested that the future work should also include the development of either other fusion protein fuse the zinc finger protein to, or the employment of a different protein that can be expressed by the host cell and be functional towards two affinity sites.

7. APPENDICES

7.1 Appendix 1: The structure of DNA

The structure of the DNA molecule was first determined by Watson and Crick in 1953. DNA is a double helix where each strand consists of 2'-deoxyribose molecules linked together by phosphodiester bonds between the 3' hydroxyl group of one and the 5' hydroxyl group of the next. The purine and pyrimidine bases (attached to the 1 position of deoxyribose) project toward the centre of the molecule, holding the two strands together by hydrogen bonding between specific purine-pyrimidine pairs. Guanine is pared with cytosine (G-C) and adenine is paired with thymine (A-T). When the bases are present in their energetically most favourable form only these pairs can fit within the hydrogen-bonding distances. The two hydrogen bonds that are formed between adenine and thymine, and the three hydrogen bonds that are formed between guanine and cytosine.

adenine   thymine   guanine   cytosine
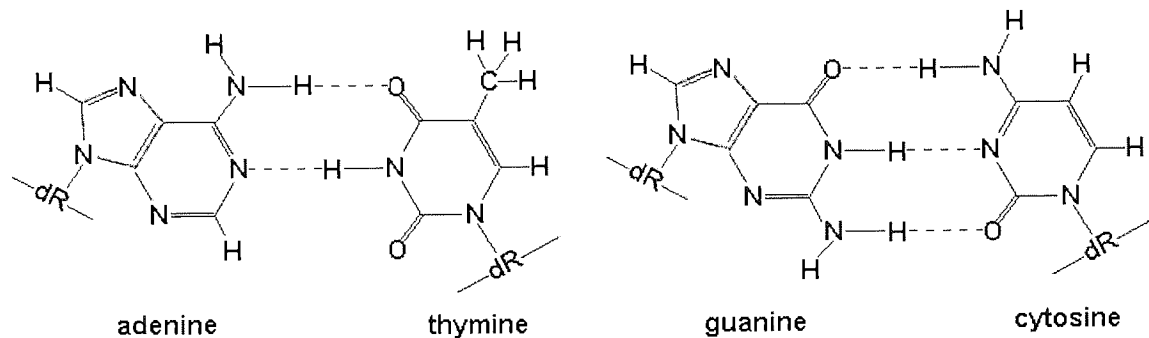
Figure A1-1: The pairing of adenine with thymine and guanine and cytosine by hydrogen bonding. The deoxyribose groups of the sugar-phosphate backbone of the double helix is represented by dR. The hydrogen bonds re shown by the dotted line.

Appendix 2: Schematic of pharmaceutical grade plasmid DNA

Fermentation

↓

Cell paste

↓

Alkaline lysis

↓

Precipitate with 2-propanol

↓

Resuspend and precipitate impurities with ammonium acetate

↓

Precipitate plasmid with PEG-8000

↓

Sephacryl S-1000 chromatography

↓

Formulate

↓

Sterile final dosage form
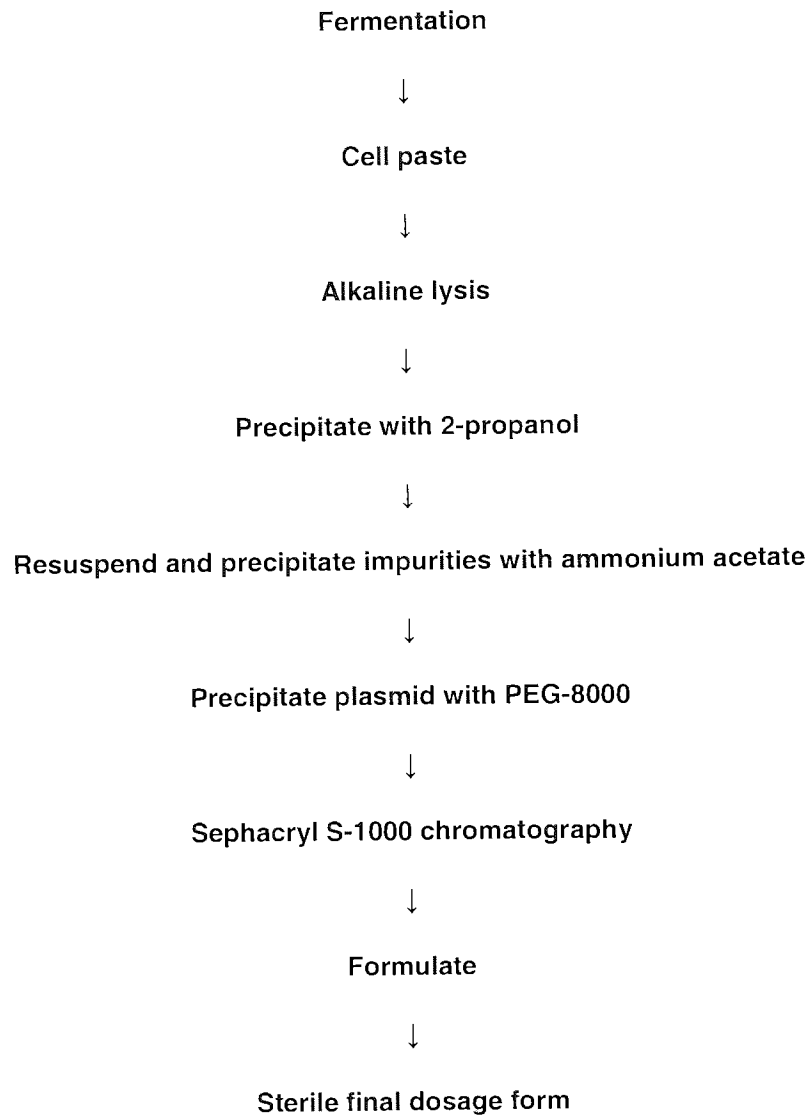
Figure A2-1: Schematic of a general process purifying pharmaceutical grade plasmid DNA.

7.3. Appendix 3: Mathematical formulation of the 'fully developed flow within helical pipes' problem

The schematic below shows an helical coil and the orientations of the reference systems that was used by Liu *et al.*, (1993) in describing the Cartesian co-ordinate system (x_1, x_2, x_3).
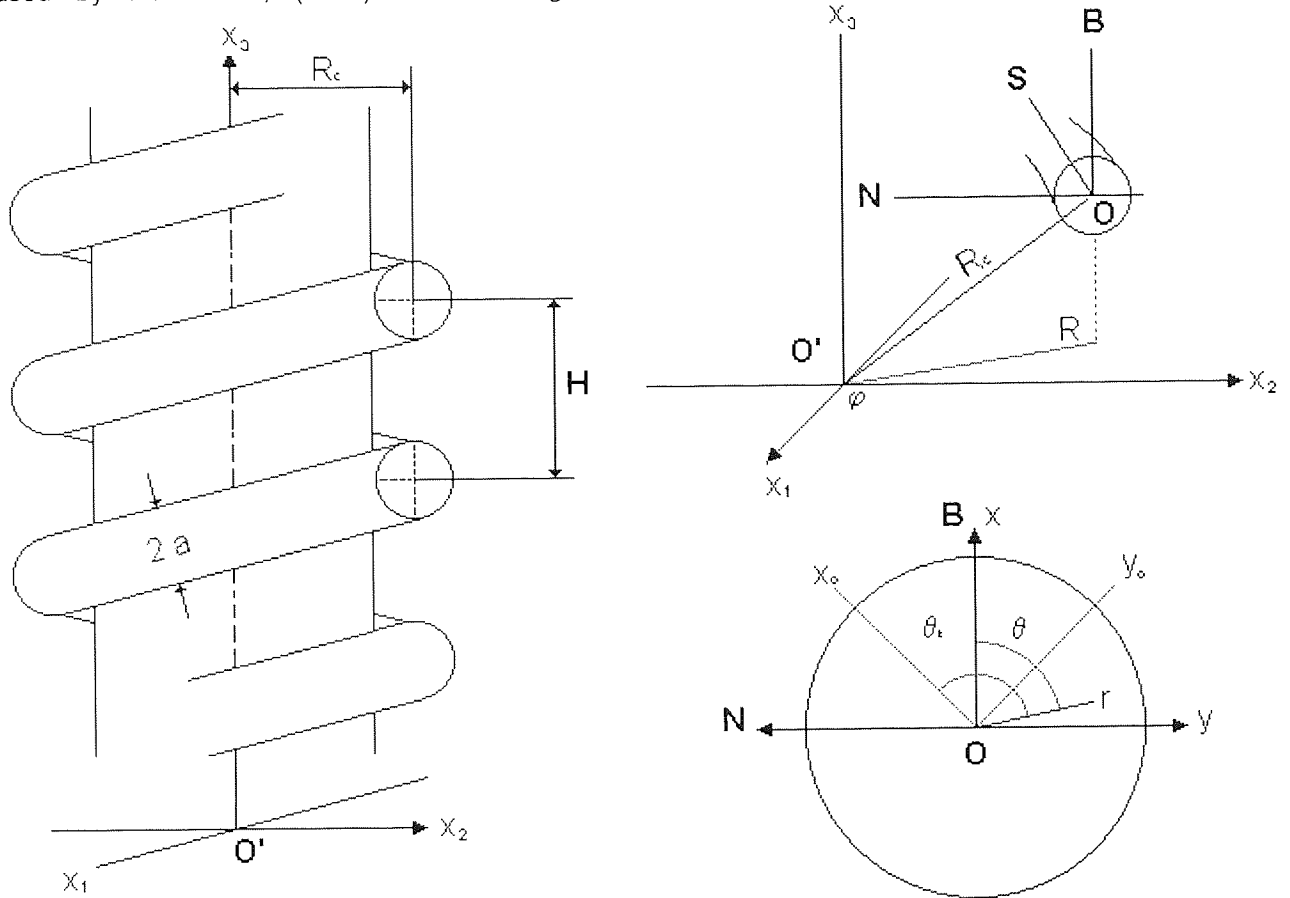

Figure A3-1: A helical tube and Germano co-ordinate system (1982)

The local vectors that originate on the generic curve of the helix were described as:

$$R = \left(R_c \cos \varphi, R_c \sin \varphi, bs\right) \tag{A3.1}$$

$$T = dR/ds = \left(-\left(\lambda R_c\right)^{0.5} \sin \varphi, \left(\lambda R_c\right)^{0.5} \cos \varphi, b\right) \tag{A3.2}$$

$$N = \frac{1}{\lambda}\frac{dT}{ds} = \left(-\cos \varphi, -\sin \varphi, 0\right) \tag{A3.3}$$

$$B = T \times N = \left(b \sin \varphi, b \cos \varphi, \left(\lambda R_c\right)^{0.5}\right) \tag{A3.4}$$

$$\varphi = s \Big/ \left[R_c^2 + \left(H/2\pi\right)^2\right]^{0.5} \tag{A3.5}$$

Where $b = (\eta H/2\pi)^{0.5}$; R is the global co-ordinate vector at the point O on the curve; the generic curve is the track of a particle moving along the centre of the helical pipe; T (shown as s above), N and B are the tangential, normal and bi-normal to the generic curve respectively; s is the dimensionless curve length parameter along the generic curve, l and h are the dimensionless curvature ratio and torsion, R_c and H are the dimensionless radius of curvature and the dimensionless pitch for the helix. Liu *et al.*, (1993) considered a loose coiling analysis to identify the dominant parameter from the curvature ratio (λ), the torsion (η) and the Reynolds number Re. Where:

$\lambda \to 0$ and $\eta \to 0$, while $\text{Re} \to +\text{I}, \lambda \to 0$

<div align="right">(A3.6)</div>

After introducing the following re-scaled velocity fields:

$u_1 = u, u_2 = \text{Re}\upsilon, u_3 = \text{Re}w, P = \text{Re}p.$

<div align="right">(A3.7)</div>

Hence, they ommitted any axial variation and related the normalised pressure gradient directly to the friction factor.

$$f\,\text{Re} = -4\frac{\partial p}{\partial s} = -\frac{a\,\text{Re}}{\rho\,U^2}\frac{\partial p'}{\partial s'}$$

<div align="right">(A3.8)</div>

Where f is the fanning friction factor. The following equations were obtained:

Continuity

$$\frac{1}{r}\frac{\partial(u_3 - \text{Re}\,\eta r u_1)}{\partial\theta} + \frac{1}{r}\frac{\partial(r u_2)}{\partial r} = 0$$

<div align="right">(A3.9)</div>

Momentum

$$M\phi = \frac{\partial\phi}{\partial t} + \frac{1}{r}\frac{\partial}{\partial r}\left[r\left(u_2\phi - \frac{\partial\phi}{\partial r}\right)\right] + \frac{1}{r}\frac{\partial}{\partial\theta}\left[(u_3 - \text{Re}\,\eta r u_1)\phi - \frac{1}{r}\frac{\partial\phi}{\partial\theta}\right]$$

<div align="right">(A3.10)</div>

s-momentum

$$\phi = u_1, d_\phi = 0, S_\phi = 0.25f\,\text{Re}$$

<div align="right">(A3.11)</div>

r-momentum

$$\phi = u_2, d_\phi = \frac{1}{r^2}, S_\phi = -\frac{\partial P}{\partial\theta} + \text{Re}^2\lambda\sin\theta u_1^2 + \frac{u_3}{r} + \text{Re}\,\lambda\eta\cos\theta u_1 - \frac{2}{r^2}\frac{\partial u_3}{\partial\theta}$$

<div align="right">(A3.12)</div>

θ-momentum

$$\phi = u_3, d_\phi = \frac{u_2}{r} + \frac{1}{r^2}, S_\phi = -\frac{\partial P}{\partial\theta} + \text{Re}^2\lambda\cos\theta u_1^2 - \text{Re}(\lambda r + \sin\theta)\lambda\eta u_1 - \frac{2}{r^2}\frac{\partial u_2}{\partial\theta}$$

<div align="right">(A3.13)</div>

After introducing the Germano number and the generalised Dean number and making the loose coiling assumption, the reduced flow equations became:

Continuity

$$\frac{1}{r}\frac{\partial(u_3 - Gn r u_1)}{\partial\theta} + \frac{1}{r}\frac{\partial(r u_2)}{\partial r} = 0$$

<div align="right">(A3.14)</div>

Momentum

$$M\phi = \frac{\partial\phi}{\partial t} + \frac{1}{r}\frac{\partial}{\partial r}\left[r\left(u_2\phi - \frac{\partial\phi}{\partial r}\right)\right] + \frac{1}{r}\frac{\partial}{\partial\theta}\left[(u_3 - Gn r u_1)\phi - \frac{1}{r}\frac{\partial\phi}{\partial\theta}\right]$$

<div align="right">(A3.15)</div>

s-momentum

$$\phi = u_1, d_\phi = 0, S_\phi = 0.25f\,\text{Re}$$

<div align="right">(A3.16)</div>

r-momentum

$$\phi = u_2, d_\phi = \frac{1}{r^2}, S_\phi = -\frac{\partial P}{\partial \theta} + Dn^2 \sin\theta u_1^2 + \frac{u_3}{r} - \frac{2}{r^2}\frac{\partial u_3}{\partial \theta} \qquad (A3.17)$$

θ-momentum

$$\phi = u_3, d_\phi = \frac{u_2}{r} + \frac{1}{r^2}, S_\phi = -\frac{\partial P}{\partial \theta} + Dn^2 \cos\theta u_1^2 - \frac{2}{r^2}\frac{\partial u_2}{\partial \theta} \qquad (A3.18)$$

The flow group (γ) number is determined when noting that the Germano number always appears in the form (u_3-Gnru$_1$). Since the norms of u_3 and u_1 are functions of Dn, it becomes necessary to relate the Germano number and the Dean number in order to find out when the Germano number is important. Liu *et al.*, (1993) noted that Reξ= u_3-Gnru$_1$, where ξ is the body-centred azimuthal velocity component. Although ξ is not an orthogonal velocity component, the writers stated that it was the momentum/energy velocity in the azimuthal direction. They deduced the importance of Gn from the momentum equations, applying the M operator as defined by (A3.15) on the above and making use of (A3.16) and (A3.18), leading to:

$$Re\,M\xi = Mu_3 - GnM(u_3) \propto Dn^2 - CGnf\,Re \qquad (A3.19)$$

This reduces when applying the normalised pressure gradient whilst assuming negligible torsion:

$$Re\,M\xi \propto Dn^2\left(1 - A_1 GnDn^{-1.5}\right) \qquad (A3.20)$$

Where A_1 is a constant. Therefore, for the Germano number to have a noticeable influence on the helical flow field, GnDn$^{-1.5}$ must be large and is subsequently redefined as the flow group γ:

$$\gamma = \frac{Gn}{Dn^{1.5}} = \frac{\eta}{(\lambda Dn)^{0.5}} \qquad (A3.21)$$

## 7.4. Appendix 4: Dean vortex problem solved by a series expansion method (Kao. H. 1987)
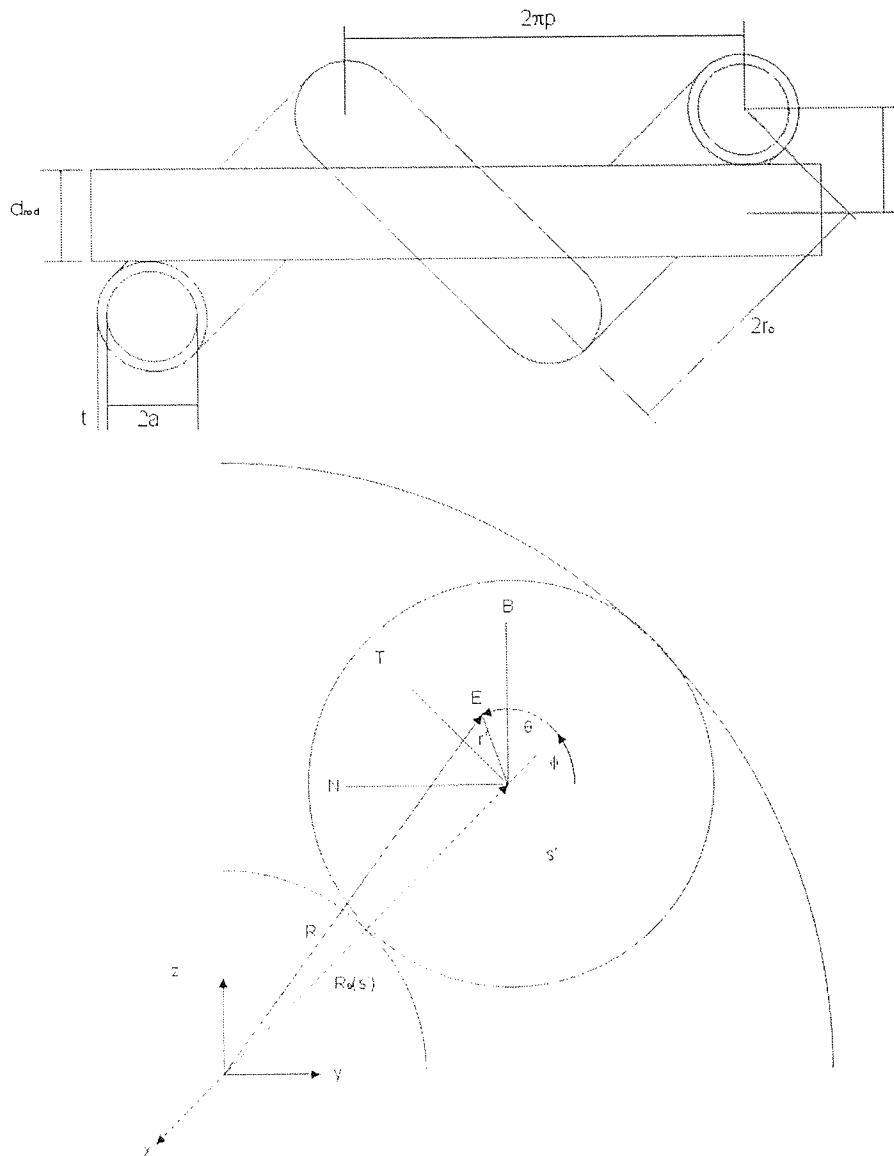
Figure A4.1: The helical coordinate system used by Kao. (1987)

The governing equations seen in Appendix 3 were substantially simplified by Kao. H., 1987, by introducing a series expansion method. Assuming that the velocity components u_x, u_y and u_z are of the same order of magnitude and that $\varepsilon < 1$, $\lambda < 1$ and $\beta^{1/2} = \lambda/(2\ \varepsilon)^{0.5} = 0$.

$$\bar{\omega} = \omega_0 + K\omega_1 + K\omega_2 + K\omega_3 + K\omega_3 + \ldots \quad (A4.1)$$

$$\bar{\psi} = \psi_0 + K\psi_1 + K\psi_2 + K\psi_3 + K\psi_3 + \ldots \quad (A4.2)$$

Where ω is the primary flow component and ψ a modified stream function (secondary flow). After the introduction of the relevant boundary conditions the solutions were cited as followed:

$$\omega_0 = 1 - r^2 \quad (A4.3)$$

$$\psi_0 = 0 \quad (A4.4)$$

$$\psi_1 = \frac{1}{144}\left(r - \frac{9}{4}r^3 + \frac{3}{2}r^5 - \frac{1}{4}r^7\right)\sin(\alpha) \tag{A4.5}$$

$$\omega_1 = \frac{1}{576}\left(\frac{19}{40}r - r^3 + \frac{3}{4}r^5 - \frac{1}{4}r^7 + \frac{1}{40}r^9\right)\cos(\alpha) \tag{A4.6}$$

$$\psi_2 = \frac{\beta^{1/2}}{4 * 576}\left(-\frac{13}{60}r + \frac{79}{60}r^3 - \frac{49}{30}r^5 + \frac{13}{14}r^7 - \frac{47}{180}r^9 + \frac{17}{660}r^{11}\right)\cos(\alpha) \tag{A4.7}$$

$$\omega_2 = \frac{\beta^{1/2}}{4 * 576}\left(\frac{176565}{225225}r + \frac{13}{90}r^2 - \frac{79}{150}r^4 + \frac{7}{15}r^6 - \frac{13}{63}r^8 + \frac{47}{990}r^{10} - \frac{17}{4290}r^{12}\right)\cos(\alpha)$$
$$+ \frac{\beta^{1/2}}{4 * 576}\left(\frac{14789}{118800}r - \frac{19}{80}r^3 + \frac{139}{720}r^5 - \frac{9}{80}r^7 + \frac{11}{280}r^9 - \frac{79}{10800}r^{11} + \frac{3}{6160}r^{13}\right)\sin(\alpha) \tag{A4.8}$$

$$\psi_3 = \frac{1}{320 * 576}\left(1.3412r^2 - 3.0982r^4 + \frac{9}{4}r^6 - \frac{7}{12}r^8 + \frac{5}{48}r^{10} - \frac{1}{70}r^{12} + \frac{1}{2016}r^{147}\right)\sin(2\alpha)$$
$$+ \frac{\beta^{1/2}}{320 * 576}\left(\begin{array}{l}1.9688r - 0.6506r^3 - 0.1926r^4 + 0.2006r^6 - 0.07407r^8 \\ + 0.01667r^{10} - 0.00221r^{12} + 0.00012r^{14}\end{array}\right)\cos(2\alpha) +$$
$$\frac{\beta}{320 * 576}\left(\begin{array}{l}0.69529r + 2.4420r^3 - 4.675r^5 + 4.0559r^7 - 2.0986r^9 \\ + 0.65595r^{11} - 0.11402r^{13} + 0.00778r^{15}\end{array}\right)\sin(\alpha) \tag{A4.9}$$

The series solutions were inputted into a MatLab M-file and solved according to the EFD geometry. The graphical solutions can be seen in Figures 3.2-3 where the shear rate within the flow field was determined by differentiating the axial velocity component and times by negative viscosity.

$$\tau_{rs} = -\eta\frac{d\varpi}{dr} \tag{A4.10}$$

9. References

Ahn, S.J., Costa, J., and Emanuel, J.R. PicoGreen quantification of DNA: effective evaluation of samples pre- and post-PCR. *Nucleic Acids Research.* **24(13):** 2623-2625, 1996.

Arnold, F.H., Blanch, H.W., and Wilke, C.R. Analysis of affinity separations. I: Predicting the performance of affinity adsorbers. *Chemical Engineering Journal.* **30:** B9-B23, 1985.

Atkinson, A. Jack, G.W. Precipitation of nucleic acids with polyethyleneimine and the chromatography of nucleic acids and proteins on immobilised polyethyleneimine. *Biochemica and Biophysica Acta.* **308:** 41-52, 1973.

Bara. B., Nandakumar. K., Masliyah. J.H. An experimental and numerical study of the Dean problem: flow development towards two-dimensional multiple solutions. *Journal of Fluid Mechanics.* **244:** 339-376, 1992.

Baumann. C.G., Bloomfield. V.A. Large-scale purification of plasmid DNA for biophysical and molecular biology studies. *Biotechniques.* **19:** 884-890, 1995.

Baumgartner. I. Constitutive expression of phVEGF165 following intramuscular gene transfer promoescollateral vessel development in patients with critical limb ishchaemia. *Circulation.* **98:** 2800-2804, 1998. Abstract.

Belfort. G. Fluid dynamics in membrane filtration: recent developments. *Journal of Membrane Science.* **40:** 123, 1989.

Belfort. G., Chung. K.Y. Dean vortices in curved tube flow: 5. 3-D MRI and numerical analysis of the velocity field. *AIChE Journal.* **39:** 1592-1602, 1993.

Belfort. G., Pimbley. J.M., Greiner. A., Chung. K.Y. Diagnosis of membrane fouling using rotating annular filter 1. Cell culture media. *Journal of Membrane Science.* **77:** 23, 1993.

Belfort. G., Pimbley. J.M., Griener. A., Chung. K.Y. Diagnosis of membrane fouling using a rotating annular filter. 1. Cell culture media. *Journal of Membrane Science.* **77:** 1-22, 1993.

Belfort. G., Pimbley. J.M., Griener. A., Chung. K.Y. Diagnosis of membrane fouling using a rotating annular filter. 2. Dilute particle suspensions of known particle size. *Journal of Membrane Science.* **77:** 23-39, 1993.

Berg. J.M., Desjarlais. J.R. Use of zinc-finger consensus sequence framework and specificity rules to design specific DNA binding proteins. *Proc. Natl. Acad. Sci.* **90:** 2256-2260, 1993.

Bhattacharjee. S., Kim. A.S., Elimelech. M. Concentration polarisation of interacting solute particles in cross-flow membrane filtration. *Journal of Colloid and Interface Science.* **212:** 81-99, 1999.

Blaese. R.M., Culver. K.W., Miller. A.D., Carter. C.S., Fleisher. T., Clerici. M. T-lymphocyte directed gene therapy for ADA⁻ SCID: initial trial results after 4 years. *Science.* **270:** 475-480, 1995.

Briefs, K.-G and Kula, M,-R. Fast protein chromatography on analytical and preparative scale using modified microporous membranes. *Chemical Engineering Science.* **47:** v141-149, 1992.

Caridis. K.A., Papathanasiou. T.D. Pressure effects in cross-flow micro-filtration of suspension of whole bacterial cells. *Bioprocess Engineering.* **16:** 199-208, 1997.

Charlton, H.R. Characterisation of a harvesting step for monoclonal antibodies from mammalian cell culture. *PhD thesis,* 1997.

Charlton, H.R., Relton, J.M., and Slater, N.K.H. Fluorometric determination of DNA in mammalian cell cultures by PicoGreen. *Biotechnology Techniques, in press.* 1999.

Chen. W., an. R. The characteristics of laminar flow in a helical circular pipe. *Journal of Fluid Mechanics.* **244:** 241-256, 1992.

Chung. Brewster. M.E., Belfort. G. Dean vortices with wall flux in a curved channel membrane system. 3. Concentration polarisation in a spiral reverse osmosis slit. *Journal of Chemical Engineering of Japan.* **31:** 683-693, 1998.

Chung. Brewster. M.E., Belfort. G. Dean vortices with wall flux in a curved channel membrane system. 1.A new approach to membrane module design. *Journal of Membrane Science. 91:* 127-137, 1993.

Chung. K.Y., Bates. R., Belfort. G. Dean vortices with wall flux in a curved channel membrane system. 4. Effect of vortices on permeation fluxes of suspensions in micro-porous membranes. *Journal of Membrane Science.* **81:** 139-150, 1993.

Chung. K.Y., Edelstein. W.A., Belfort. G. Dean vortices with wall flux in a curved channel membrane system. 6. Two dimensional magnetic resonance imaging of the velocity field in a curved impermeable slit. *Journal of Membrane Science.* **91:** 151-162, 1993.

Crowder. M.L., Gooding. C.H. Spiral would, hollow fibre membrane modules: A new approach to higher mass transfer efficiency. *Journal of Membrane Science.* **137:** 17-29, 1997.

Dean. W.R. Fluid motion in a curved channel. *Pro. Roy. Soc. London A.* **121:** 402, 1928.

Dean. W.R. Fluid motion in a curved channel. *Pro. Roy. Soc. London A.* **A121:** 402 1927.

Diogo, MM., Queiroz, J.A., Monteiro, G.A., Martons, S.A.M., Ferreira, G.N.M., Parazeres, D.M.F. Purification of a cystic fibrosis plasmid vector for gene therapy using hydrophobic interaction chromatography. *Biotechnology and Bioengineering.* **68:** 576-583, 2000.

Dortant. P.M., Claasen. I.J., Van Kreyl. C.F., Van Steenis. G., Wester. P.W. Risk assessment on the carcinogenic potential of hybridoma cell DNA: implications for residual contaminant cellular DNA in biological products. *Biologicals.* **25:** 381-390, 1997.

Dunham. I. The DNA sequence of the human chromosome 22. *Nature.* **402:** 489-495, 1999.

Durland, R.H., Eastman, E.M. *Adv. Drug Del. Rev.* **30:** 33-48, 1998.

Dutton, M.D., Varhol, R.J., Dixon, D.G. Technical considerations for the use of ethidium bromide in the quantitative analysis of nucleic acids. *Analytical Biochemistry.* **230:** 353-355, 1995.

Dyer. M.R., Herrling. P.L. Progress and potential for gene-based medicines. *Molecular Therapy.* **1:** 213-224, 2000.

Elrod-Erickson. M., Rould. M.A., Neludova. L., Pabo. C.O. Zif268 protein DNA complex refined at 1.6 A: A model system for understanding zinc-finger DNA interactions. *Structure.* **4:** 1171-1180, 1996.

Elrod-Erickson. M., Benson. T.E., Pabo. C.O. High resolution structures of variant Zif268 protein-DNA complexes: Implications for understanding zinc finger-DNA recognition. *Structure.* **4:** 451-464, 1998.

Enger, O. Use of fluorescent dye PicoGreen for quantification of PCR products after agarose gel electrophoresis. *Biotechniques.* **21:**372-374, 1996.

Finlay. W.H., Keller. J.B., Ferziger. J.H. Instability and transition in curved channel flow. *Journal of Fluid Mechanics.* **194:** 417-456, 1988.

Ferreira, G.N.M., Cabral, J.M.S., Prazeres, D.M.F. Development of process flow sheets for the purification of supercoiled plasmids for gene therapy applications. *Biotech. Prog.* **15(4):** 725-731, 1999.

Ferreira, G.N.M., Cabral, J.M.S., Prazeres, D.M.F. Anion exchange purification of plasmid DNA using expanded bed adsorption. *Bioseparations.* **9:** 1-6, 2000.

Ferreira, G.N.M., Cabral, J.M.S., Prazeres, D.M.F. Purification of supercoiled plasmid DNA using chromatographic processes. *Journal of Molecular Recognition.* **11(1-6):** 250-251, 1998.

Forman. S.M., DeBernardez. E.R., Feldberg. R.S., Swartz. R.W. Cross-flow filtration for the separation of inclusion bodies from soluble proteins in recombinant *E.coli* cell lysate. *Journal of Membrane Science.* **48:** 263-279, 1990.

Garem, A., Daufin, G., Maubois, J.L., Leonil, J. Selective separation of amino acids with a charged inorganic nanofiltration membrane: effect of physicochemical parameters on selectivity. *Biotechnology and Bioengineering.* **54:**181-189, 1997.

Gebauer, K.H., Thommes, J., and Kula, M. Plasma protein fractionation with advanced membrane adsorbents. *Biotechnology and Bioengineering.* **54:**291-302, 1997.

Germano. M. On the effect of torsion on helical pipe flow. *Journal of Fluid Mechanics.* **125:** 1-8, 1982.

Germano. M. The Dean equations extended to a helical pipe flow. *Journal of fluid Mechanics.* **203:** 289, 1988.

Gnielinski, V. Correlation's for the pressure drop in helically coiled tubes. *Intl. Chem. Engg.* **26(1):** 36, 1986.

Gomez-Navarro, J., Curiel, D.T., Douglas, J.T. Gene therapy for cancer. *European Journal of Cancer* **35 (14):** 2039-2057, 1999,

Guidance for Industry Guidance for Human Somatic Cell Therapy and Gene Therapy. FDA. 1998.

Hoeg. J.M. Guidelines for trails of gene therapy and somatic gene therapy in cardiovascular disease. *The American Journal of Cardiology.* **81:** 60F-63F, 1998.

Hoovers, J.M.N., Mannens, M., John, R., Bliek, J., Van-Hexningen, V., Porteus, D.J., Leschot, N.J., Westerweld, A., Little, P.F.R. High resolution localisation of 69 potential human zinc-finger protein genes: A number are clustered. *Genomics* **12:** 254-263, 1992.

Points to consider in Human Somatic Cell Therapy and Gene Therapy, 1991; *Code of Federal regulations* 21, 1994.

Horn. N.A., Meek. J.A., Budahazi. G., Marquet. M. Cancer gene therapy using plasmid DNA: purification of DNA for human clinical trials. *Human Gene Therapy.* **6:** 565-573, 1995.

Huttl. T.J., Wagner, C., Freidrich. R. Navier-Stokes solutions of laminar flows based on orthogonal helical co-ordinates. *International Journal for Numerical Methods in Fluids.* **29:** 749-763, 1999.

Ito, H. Laminar flow in curved pipes. *Zeit. Angew. Math. Mech.* **49:** 653, 1969.

Jiao. D., Sharma. M.M. Mechanism of cake build-up in cross-flow filtration of colloidal suspensions. *Journal of Colloidal and Interface Science.* **162:** 454-462, 1994.

Kao. H. Torsion effect on fully developed flow in a helical pipe. *Journal of Fluid Mechanics.* **184: 335-356, 1987.**

Keulega. G.H., Beij. K.H. Pressure losses for fluid in curved pipes. *J. Res. N.B.S.* **18:** 89, 1937.

Klug. A., Schwabe. J.W.R. Zinc fingers. *The FASEB Journal.* **9:** 597-604, 1995.

Kluge. T., Kalra. A., Belfort. G. Viscosity effects on Dean vortex membrane micro-filtration. *AIChE Journal.* **45:** 1913-1926, 1999.

Kluge. T., Rezende. C., Wood. D., Belfort. G. Protein transmission during Dean vortex micro-filtration of yeast suspensions. *Biotechnology and Bioengineering.* **65:** 649-658, 1999.

Krieg. A.M.J. Direct immunologic activities of CpG DNA and implications for gene therapy. *Journal of Gene Medicine.* **1:** 56-63, 1999.

Krusteva. E.D., Doneva. T.A., Vassilieff. C.S. Pseudo-plasticity of filter cakes explains cross-flow micro-filtration. *Colloids and Surfaces A: Physiochemical and Engineering Aspects.* **149:** 499-506, 1999.

Kuakuvi. D.N., Moulin. P., Charbit. F. Dean vortices: a comparison of woven versus helical and straight hollow fibre membrane modules. *Journal of Membrane Science.* **171:** 59-65, 2000.

Lee. M.S., Gippert. G.P., Soman. K.V., Case. D.A., Wright. P.E. Three-dimensional solution structure of a single zinc-finger DNA-binding domain. *Science.* **254:** 635-637, 1989.

Levy, M.S., Collins, I.J., Tsai. J.T., Shamlou, P.A., Ward, J.M., Dunnill, P. Removal of contaminant nucleic acids by nitro-cellulose filtration during pharmaceutical-grade plasmid DNA processing. *J. Biotechnology.* **76(2-3):** 197-205, 2000.

Liu. S., Masliyah. J.H. Axially invariant laminar flow in helical pipes with a finite pitch. *Journal of Fluid Mechanics.* **251:** 315-353, 1993.

Lu. W., Hwang. K. Cake formation in 2-D cross-flow filtration. *AIChE Journal.* **41:** 1443-1455, 1995.

Mallubholta. H., Belfort. G. Flux enhancements during Dean vortex microfiltration. 8. Further diagnostics. *Journal of Fluid Mechanics.* **125:** 75-91, 1997.

Mallubholta. H., Hoffmann. S., Schmidt. M., Vente. J., Belfort. G. Flux enhancements during Dean vortex tubular membrane nanofiltration. 10. Design, construction, and system characterisation. *Journal of Membrane Science.* **141:** 183-195, 1998.

Mallubhotla, H., Nunes, E., Belfort, G., Microfiltration of yeast suspensions with self-cleaning spiral vortices: Possibilities for new membrane module design. *Biotechnology and Bioengineering.* **48:** 375-385, 1995.

Manno. P., Moulin. P., Rouch. J.C., Clifton. M., Aptel. P. Flux improvements by Dean vortices: ultrafiltration of colloidal suspensions and macromolecular solutions. *Journal of Membrane Science.* **156:** 109-130, 1999.

Manno. P., Moulin. P., Rouch. J.C., Clifton. M., Aptel. P. Mass transfer in helically wound hollow fibre ultrafiltration modules. Yeast suspensions. *Separation and purification Technology.* **14:** 175-182, 1998.

Manno. P., Moulin. P., Rouch. J.C., Clifton. M., Aptel. P. The use of dean vortices in coiled hollow-fibre ultra-filtration membranes for waste and waste-water treatment. *Desalination.* **118:** 73-80, 1998.

Meagher. M.M., Barlett. R.T., Rai. V.R., Khan. F.R. Extraction of rIL-2 inclusion bodies from E.coli using cross-flow filtration. *Biotechnology and Bioengineering.* **43:** 969-977, 1994.

Miller. J., McLaughlan. A.D., Klug. A. Repetitive zinc-binding domains in the protein transcription factor IIIA for Xenopus oocytes. *EMBO Journal.* **4:** 1609-1614, 1985.

Mondor. M,, Moresoli. C. Theoretical analysis of the influence of the axial variation in transmembrane pressure in cross-flow filtration of rigid spheres. *Journal of Membrane Science.* **152:** 71-87, 1999.

Monteiro, G.A., Ferreira, G.N.M., Cabral, J.M.S., Prazeres, D.M.F. Analysis and use of endogenous nuclease activities in *Escherichia coli* lysates during the primary isolation of plasmids for gene therapy. *Biotech. Bioeng.* **66(3):** 189-194, 1999.

Moulin. P., Manno. P., Rouch. J.C., Serra. C., Clifton. M.J., Aptel. P. Flux improvements by Dean vortices: Ultra-filtration of colloidal suspensions and macromolecular solutions. Journal of Membrane *Science.* **156:** 109-130, 1999.

Mountain. A. Gene therapy. *Trends in Biotechnology.* **18:** 119-128, 2000.

Mullubholta. H., Schmidt. M., Lee. K.H., Belfort. G. Flux enhancements during Dean vortex tubular nano-filtration: 13. Effects of concentration and solute type. J*ournal of membrane Science.* **153:** 259-269, 1999.

Nardelli. J., Gibson. T., Charnay. P. Zinc finger-DNA recognition: analysis of base specificity by site-directed mutagenesis. *Nucleic Acids Research.* **20:** 4137-4144, 1992.

Ollivier, M., Stadler, J. Large scale purification of plasmid DNA for use in gene therapy. A*dv. Exp. Med. Bio.* **451:** 487-192, 1998.

Pavletich. N.P., Pabo. C.O. Zinc finger-DNA recognition: structure of a Zif268-DNA complex at 2.1A. *Science.* **252:** 809-817, 1991.

Points to Consider in the Characterisation of Cell Lines Used to Produce Biologicals, 1993.

Points to Consider in the Characterisation of Cell Lines Used to Produce Biologicals, 1993.

Points to consider in the Production and testing of new drugs and biologicals produced by recombinant DNA technology, 1995.

Pierrou, S., Enerback, S., Carlsson, O. Selection of high-affinity binding sites for sequence-specific, DNA binding proteins from random oligonucleotides. *Analytical Biochemistry.* **229:** 99-105, 1995.

Pozidis, C., Vlatakis, G. Sequence-specific DNA affinity chromatography: application of a group-specific adsorbent for the isolation of restriction endonucleases. *J. Chromatography.* **630:** 151-157, 1993.

Prazeres, D.M.F., Ferreira, G.N.M., Monteiro, G.A., Cooney, C.L., Cabral, J.M.S. Large-scale production of pharmaceutical-grade plasmid DNA for gene therapy: problems and bottlenecks. *Trends in Biotechnology.* **17(4):** 169-174, 1999.

Reismeier. B., Kroner. K.H., Kula. M.R. Studies on secondary layer formation and its characterisation during cross-flow filtration of microbial cells. *Journal of Membrane Science.* **34:** 248-266, 1987.

Sambrook, J., Fritsch, E.F., Maniatis, T. Molecular cloning: A laboratory manual. Cold Spring Harbour Laboratory Press, Cold Spring Harbour, N.Y., 1989

Schleup, T., Cooney, C.L. *Nucleic Acids Research.* **26:** 4524-4528, 1998.

Schleup, T., Cooney, C.L. *Bioseparations.* **7:** 317-326, 1999.

Schluep. T., Widmer. F. Initial transient effects during cross-flow micro-filtration of yeast suspensions. *Journal of membrane Science.* **115:** 133-145, 1996.

Sethi. S., Wiesner. M.R. Modelling of transient permeate flux in cross-flow membrane filtration incorporating multiple particle transport mechanisms. *Journal of Membrane Science.* **136:** 191-205, 1997.

Sharp, P.A., Sugden B., Sambrook, J. Detection of two restriction endonuclease activities in *Haemophilis parainfluenzae* using analytical agarose-ethidium bromide electrophoresis. *Biochemistry* **12:** 3055-3063, 1973.

Sherwood. C.S., Haynes. C.A., Turner. R.F.N. A nanogram-level micro-volume DNA assay based on the monomeric cyanine dye PO-PRO-3 iodide. *Biotechniques.* **18:** 136-141, 1995.

Singer, V.L., Jones, L.J., Yue, S.T., and Haughland, R.P. Characterisation of PicoGreen reagent and development of a fluorescence-based solution assay for double stranded DNA quantification. *Analytical Biochemistry.* **249:**228-238, 1997.

Soh. W.Y., Berger. S.A. Laminar entrance flow in a curved pipe. *Journal of Fluid Mechanics.* **148:** 109-135, 1984.

Song. L. Permeate flux in cross-flow ultrafiltration under intermediate pressures. *Journal of Colloid and Interface Science.* **214:** 251-263, 1999.

Spink. N., Brown. D.G., Skelly. J.V., Neidle. S. Sequence-dependant effects in drug-DNA interactions: The crystal structure of Hoechst 33258 bound to the d(CGCAAATTTGCG)2 duplex. *Nucleic Acids Research.* **22:** 1607-1612, 1994

Stadler, J. Large scale purification of plasmid DNA for gene therapy. *Cancer Gene Therapy.* **4(5):** 328, 1997.

Stryer, Biochemistry 3rd Ed, 1988

Suen, S.Y., Etzel, M.R. A mathematical analysis of affinity membrane bioseparations. *Chemical Engineering Science* **47:** 1355-1364, 1992.

Schwabe, J.W.R. The role of water in protein-DNA interactions. *Current opinion in Structural Biology* **7:** 125-134, 1997.

Tanny. G.B., Mirelman. D., Pistole. T. Improved filtration technique for concentrating and harvesting bacteria. *Applied Environ Microbiol.* **40:** 269-273, 1980.

Targett. M.J., Retallick. W.B., Churchill. S.W. Flow through curved rectangular channels of large aspect ratio. *AIChE Journal.* **41:** 1061-1070, 1995.

Thommes. J., Kula. M.R. Membrane chromatography: An integrative concept in the downstream processing of proteins. *Biotechnology Progress.* **11:** 357-367, 1995

Van Dyke. M. Extended Stokes series: laminar flow through a loosely coiled pipe. *Journal of Fluid Mechanics.* **86:**129-145, 1978.

Varley, D.L., Hitchcock, A.G., Weiss, A.M.E., Horler, W.A., Cowell, R., Peddie, L., Sharpe, G.S., Thatcher, D.R., Hanak, J.A.J. Production of plasmid DNA for human gene therapy using modified alkaline cell lysis and expanded bed anion exchange chromatography. *Bioseparations.* **8(1-5):** 209-217, 1998.

Wang. C.Y. On low-Reynolds-number flow in a helical pipe. *Journal of Fluid Mechanics.* **108:** 185-194, 1981.

Wils, P., Escriou, V., Warney, A., Lacroix, F., Lagneaux, D., Ollivier, M., Crouzet, J., Mayauz, J,F., Scherman, D. *Gene Therapy.* **4:** 323-330, 1997.

Yamamoto. K., Yanase. S., Jiang. R. Stability of the flow in a helical tube. *Fluid Dynamics Research.* **22:** 153-170, 1998.

Yang, Y., Chase, H.A., Liu, G. Selection of affinity ligands for protein purification from proteolytic digests. *Biotechnology Techniques.* **12(3):** 245-251, 1998.
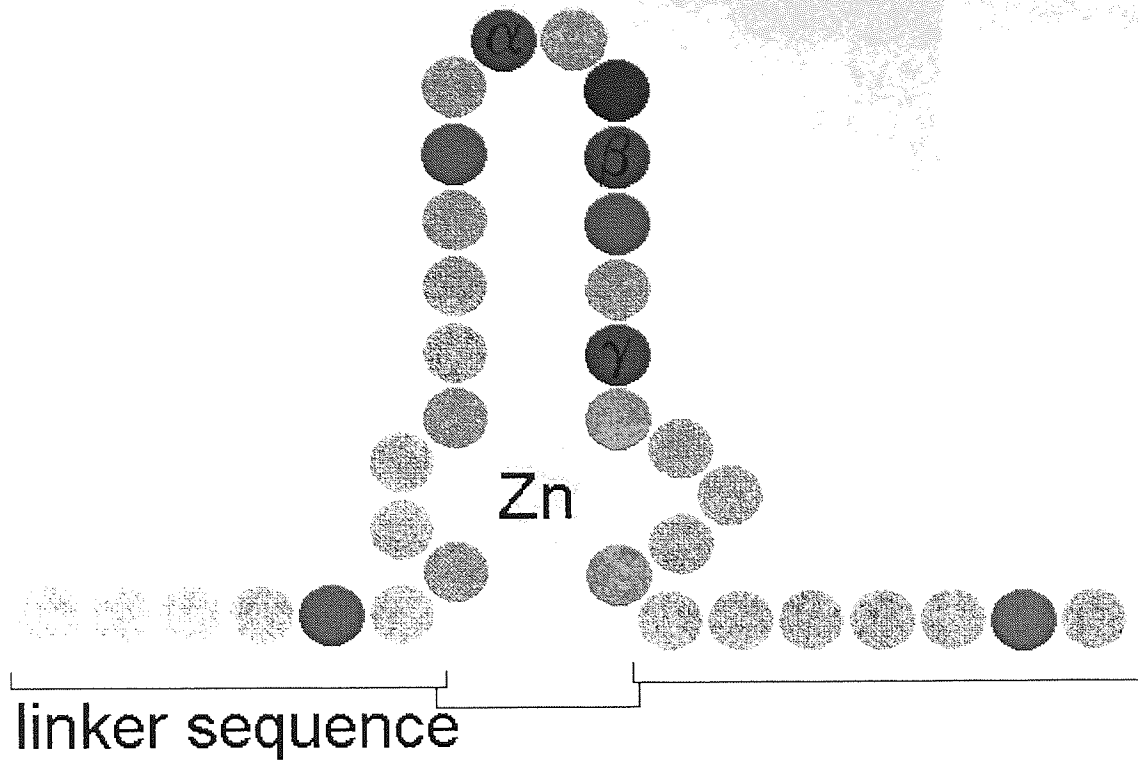
Fig 1-1: Structure of the zinc finger mini domain (Miller et al,. 1985). The linkers usually connect arrays of zinc fingers together (Berg, 1993). DNA contact residue (●), cysteine residue (●), histidine residue (●), conserved hydrophobic residue (●), DNA contacting residue (●) that is occasionally involved in the specificity of the binding of the zinc-finger motif to the DNA.
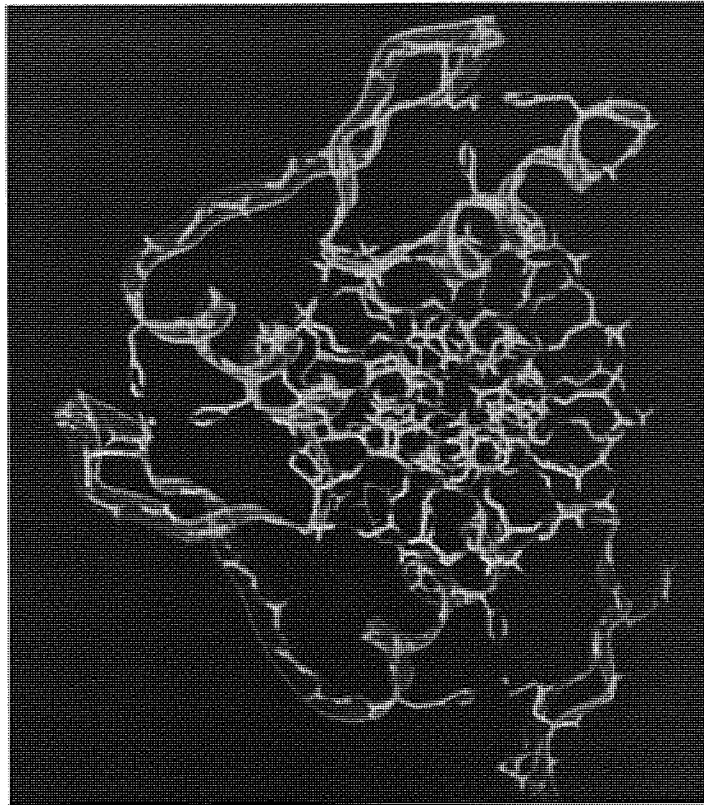
Figure 1-2: The crystal structure of the Zif268:DNA complex. Shows the insertion of the α-helix into the major groove of the DNA. The structure has been downloaded form Brookhaven data-base (Brookhaven ref. Pdb1zaa.ent).
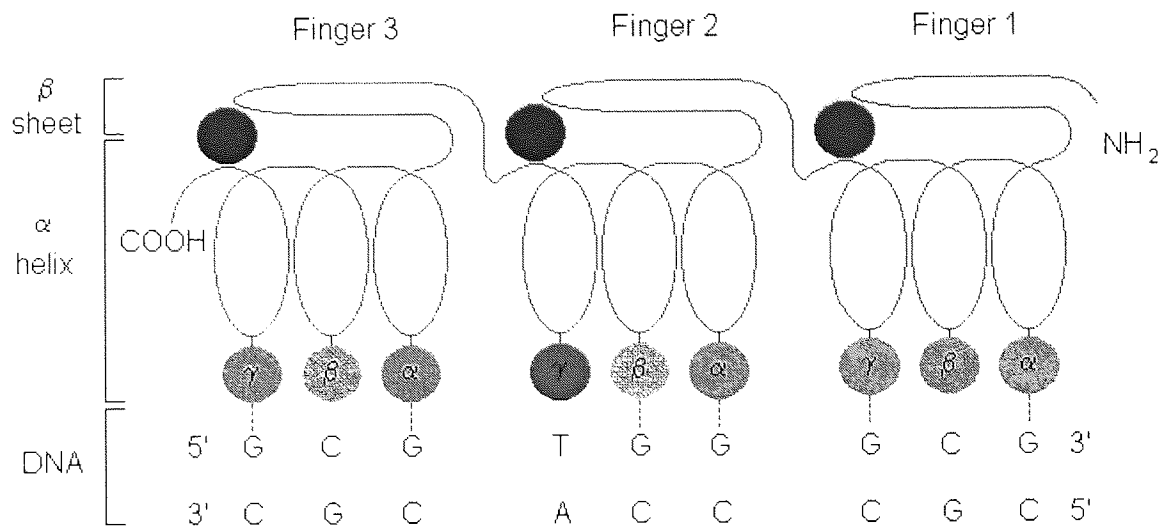
Figure 1-3: Anti-parallel binding of the zinc finger motifs of Zif268 to the target DNA sequence (Pavletich and Pabo, 1991). Where Arginine (●), Threonine (●), Glutamic acid (●), Histidine (●), and zinc ion (●) are co-ordinated between the conserved cysteine and histidine residues (Fig 1.1). Hydrogen bonds between the contacting residues and the DNA bases are represented by ( ).

α   β   γ

MERPYACPVESCD<u>R</u>RFS**R**S**D**ELT**R**<u>H</u>IRIHTGOK

PFQCRI - - CM<u>R</u>NFS**R**S**H**LTT<u>H</u>IRTHTGEK

PFACDI - - CG<u>R</u>KFA**R**S**D**ERK**R**<u>H</u>TKIHTRQKD

β - sheet   β - sheet   α - helix

Figure 1-4: Amino acid sequence of Zif268 (Pavletich and Pabo, 1991). Zinc co-ordinating residues shown in bold. Contacting residues (α, β and γ) shown in red. Underlined residues make contact to the phosphate backbone. Greyed residues make contact to the bases.

NH_2-MEKLRNGSGDPGKKK-

QHACPECGKSFQSSDLQRHQRTHTGEK-

PYKCPECGKSFRSDELQRHQRTHTGEK-

PYKCPECGKSFRSDHLSRHQRTHQNKK-COOH

                    13   16   19

Predicted binding site   5'-G G G - G C G - G C T - 3'

                              COOH -R H R - R E R - R D Q - NH_2

Figure 1-5: Amino acid sequence of the zinc finger protein, ZF. The amino acid contacting residues are shown in red. (Berg and Desjarlais, 1993)

Figure 1-6: Equilibrium binding isotherms showing the interaction of the ZF protein QDR-RER-RHR with three related binding sites. The dissociation constants calculated by Berg et al., (1993) are GGG-GCG-GCT = 2 nM, GGG-GCG-GGG = 15 nM and GCG-GCG-GCG is 1 μM. All DNA foot-printing data has been quoted from Berg and Desjarlais, 1993.

a. Continuous recycling of permeate with the system
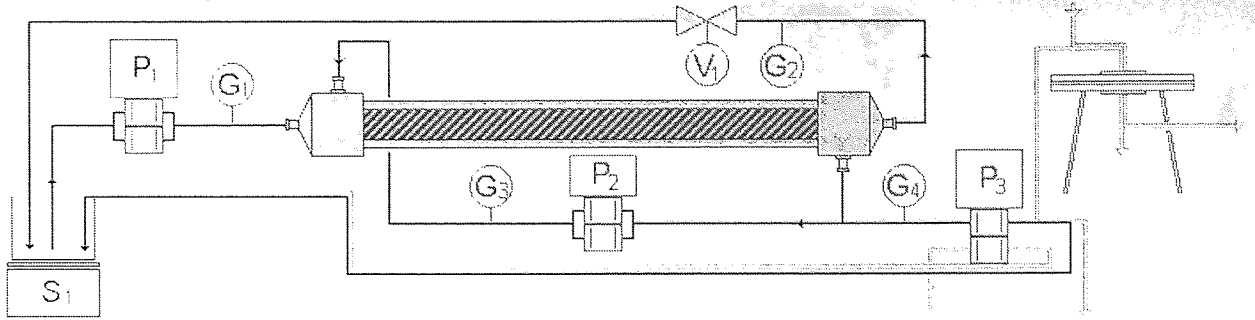
b. Concentration of and E.coli bacterial culture
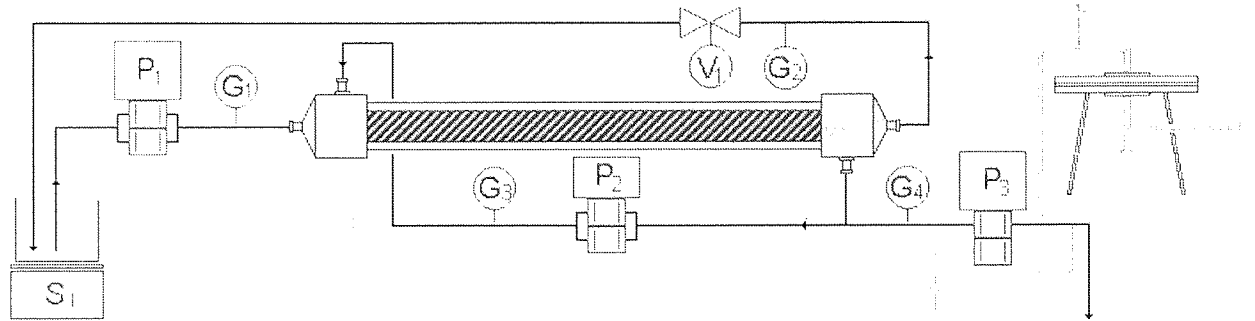
c. Dia-filtration of E.coli cells into the purification buffer
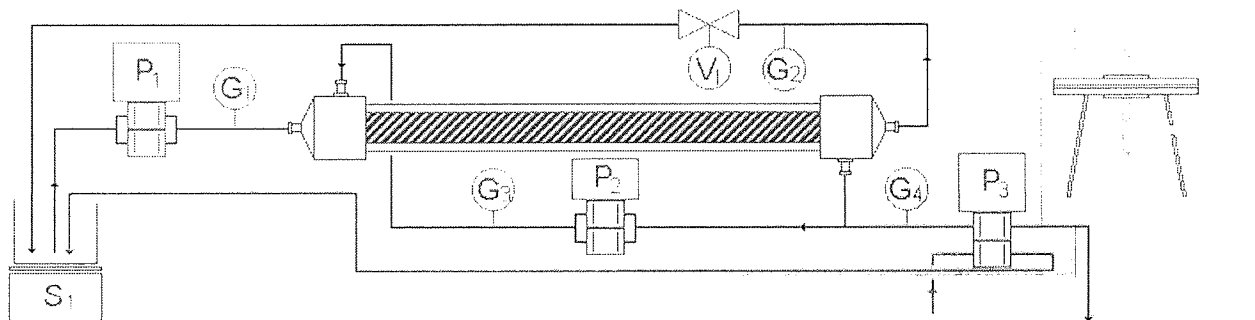
d. Purification of plamsid DNA from the cell lysate
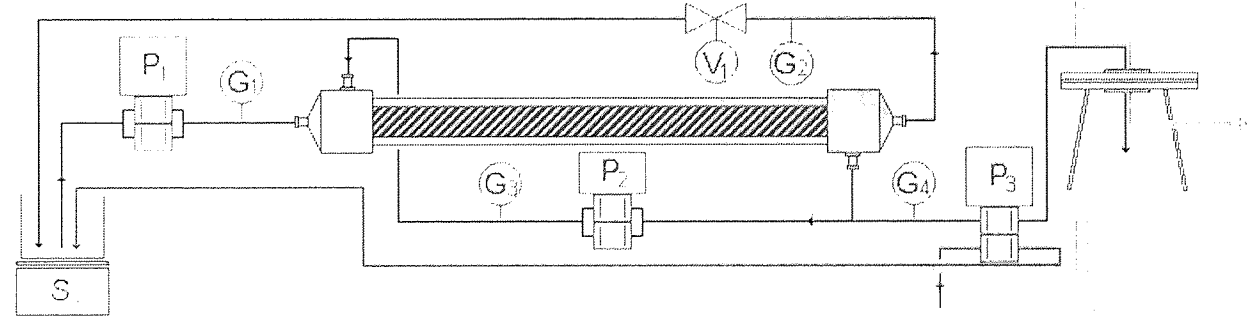
Figure 3-1: Schematic showing the four processing stages used by the EFD (Millipore, UK) cross-flow micro-filtration system to harvest plasmid DNA from a bacterial cell culture. The retentate lines (——), permeate lines (——) and processing buffer lines (——) show the direction of flow around the system.

a. Primary flow profile
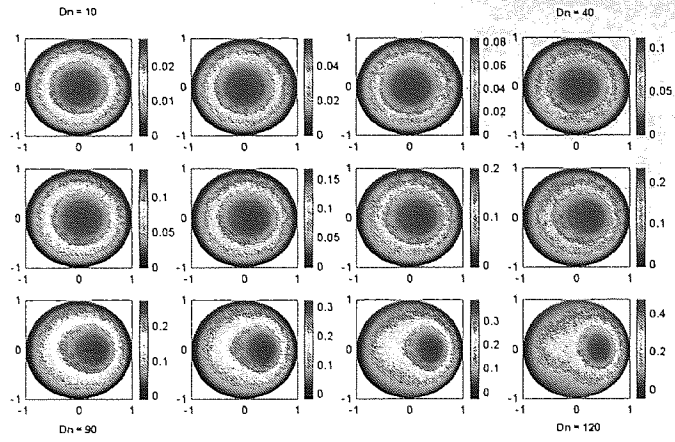
b Secondary flow profile.
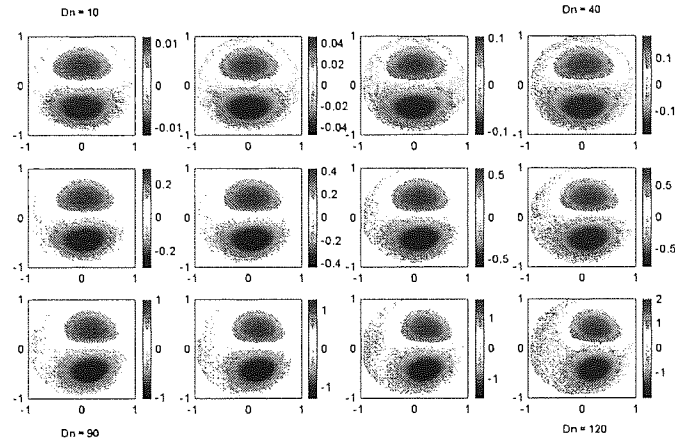
c. Shear profile
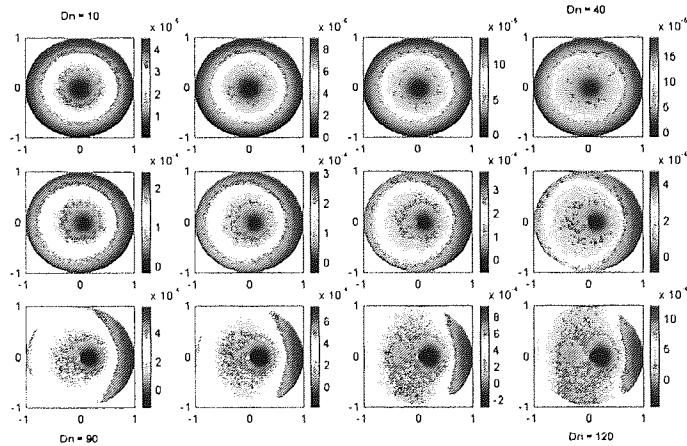
Figure 3-2: Showing the nummerical effect that increasing the Dean number (Dn) (10<Dn<120) has on the primary flows, secondary flows, and shear profiles within the EFD (Millip[ore, UK) cross-flow microfiltration module. The numerical solution was given by the series expansion method (Appendix 4)) where the curvaure (λ =0.2) and torion (η =0.09) are defined by equations 3.4 and 3.5 for the range 10<Dn<120. The inside and outside of the helical turn are positioned at x=-1 and x=+1.

a.
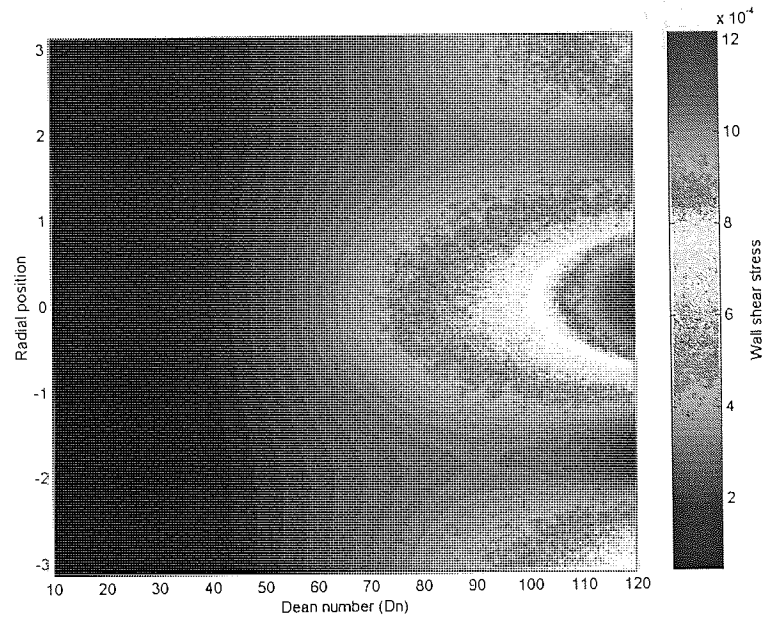
b.
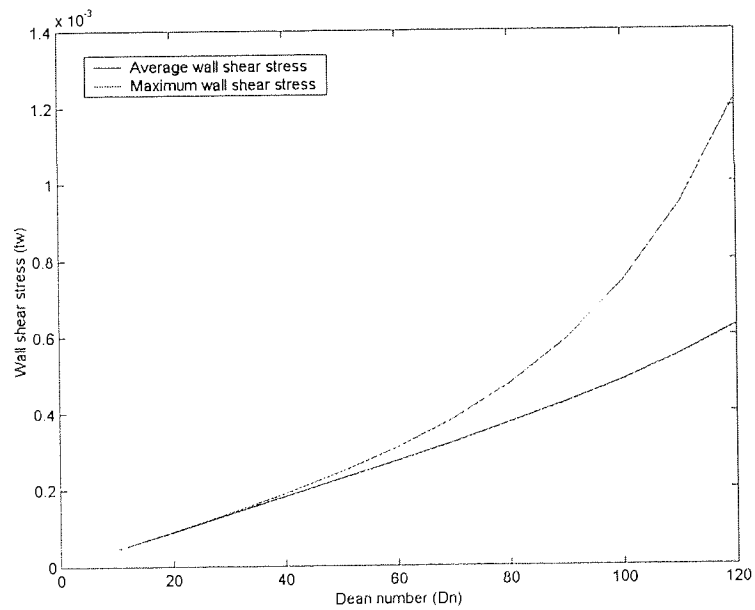
Figure 3-3: Showing the nummerical effect that increasing the Dean number (Dn) (10<Dn<120) has on the shear profile and wall stress within the EFD (Millipore, UK) cross-flow micro-filtration system. The numerical solution was given by a series expansion method (Appendix 4) where the curvaure (λ =0.2) and torion (η =0.09) are defined by equations 3.4 and 3.5. The inside and outside of the helical turn are positioned at r=-3 and r=0, corresponding to x=-1 and x=+1 seen in the previous figures.

111
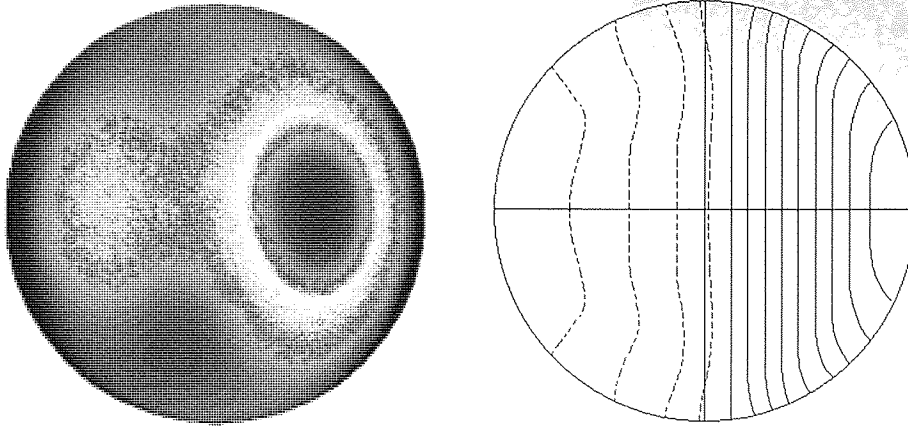
Figure: 3-4: Showing the effect of Dean number (Dn) on the pressure experienced within a flow channel of similar geometry to that found in an EFD module. The nummerical solution was taken from Liu et al., (1993) where Dn = 500, $\lambda=0.2$, $\eta=0.1$, $p_{min}=-35.54$ and $p_{max}=94.16$.

a.

b.

c.

◇ 0 psi   □ 1 psi   2 psi   3 psi   ⋆ 4 psi   ○ 5 psi   ▲ Cells 2psi   ◆ Cells 3psi   ■ Cells 4psi   ◆ Numerical   ■ LMH 1psi
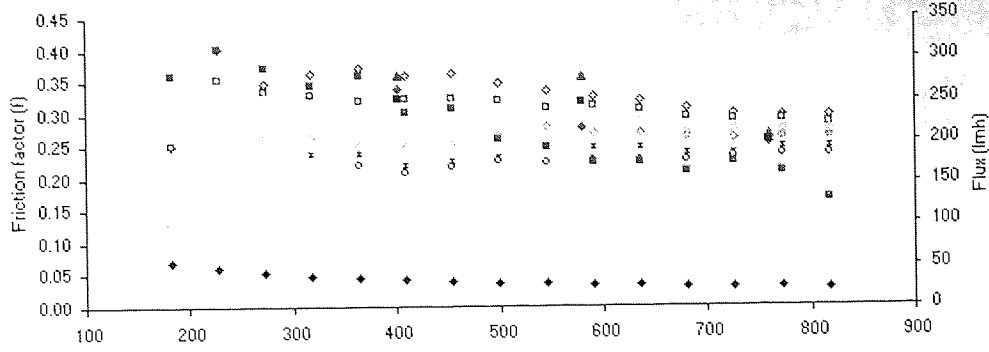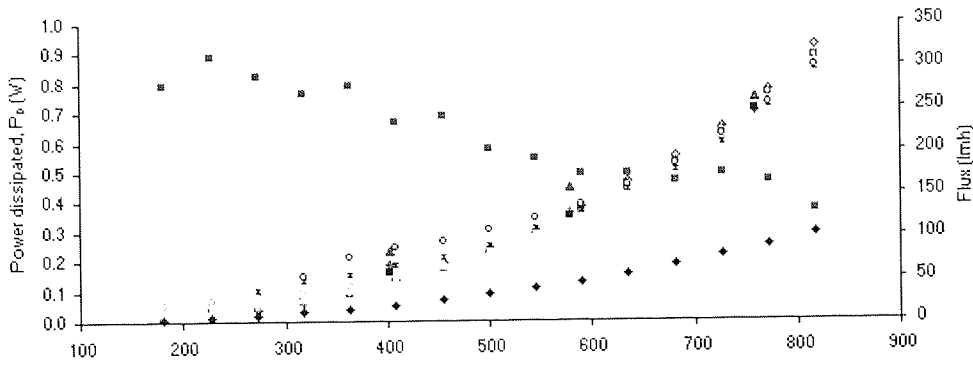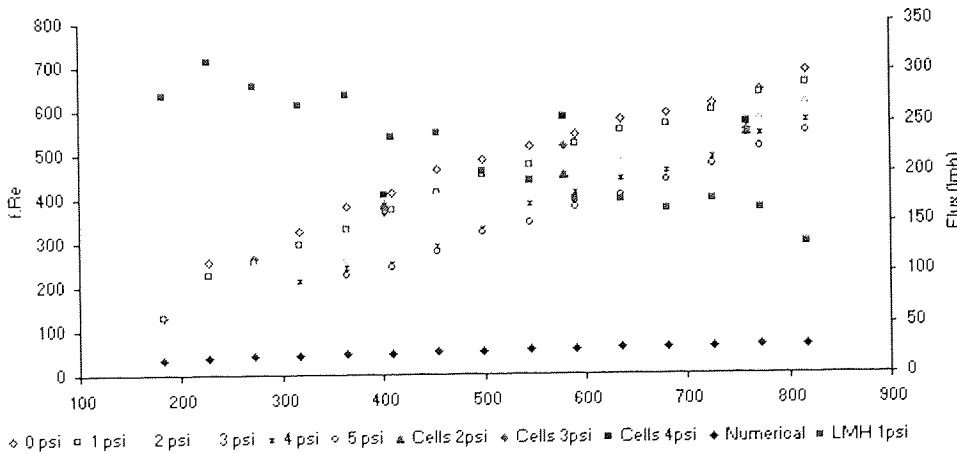
Figure 3.5: The effect of Dean number (Dn) on the experimental friction factor (f), friction (f.Re) and power dissipation (P_D) for pure water with (1-5 psi axail TMP) and without (0 psi axial TMP) permeation, and an E.coli bacterial cell culture ($OD_{2.5}$) within the EFD (Millipore, UK) cross-flow microfiltration system. The data is shown in relation to pure water flux under 1 psi axial TMP (LMH 1 psi) and the numerical correlation (Numerical shown in equation 3.20).

113

a.

b.

c.

◇ 0 psi   ▫ 1 psi   2 psi   3 psi   ✕ 4 psi   ○ 5 psi   ▲ Cells 2psi   ✦ Cells 3psi   ■ Cells 4psi   ◆ Numerical   ■ LMH 1psi
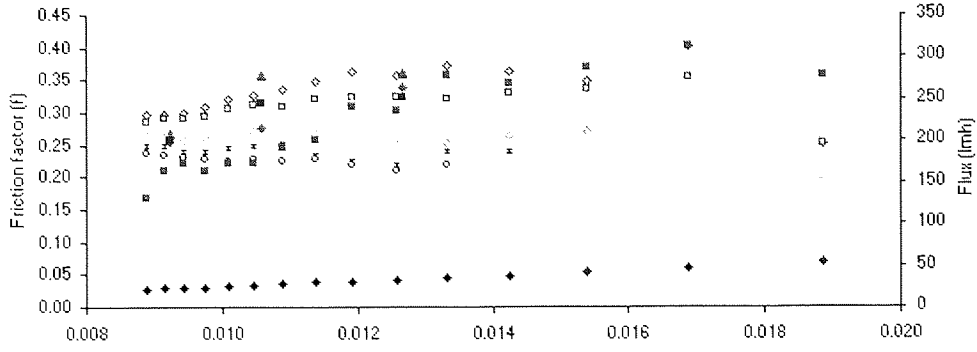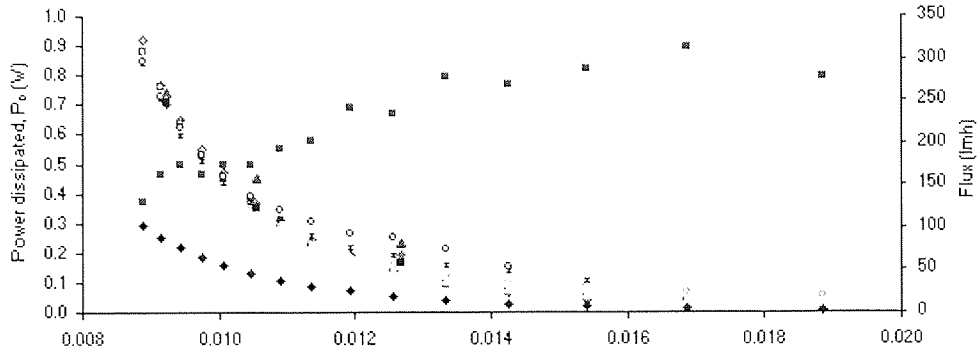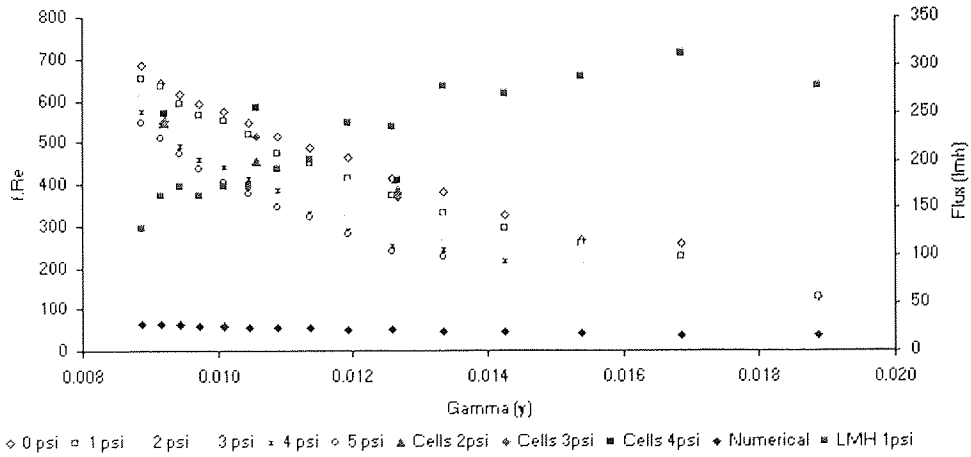
Figure 3-6: The effect of Gamma (γ) on the experimental friction factor (f), friction (f.Re) and power dissipation (P_D) for pure water with (1-5 psi axail TMP) and without (0 psi axial TMP) permeation, and an E.coli bacterial cell culture (OD 2.5) within an EFD (Millipore, UK) cross-flow micro-filtration system. The data is shown in relation to pure water flux under 1psi axial TMP (LMH 1 psi) and the numerical correlation (Numerical) shown in equation 3.20.
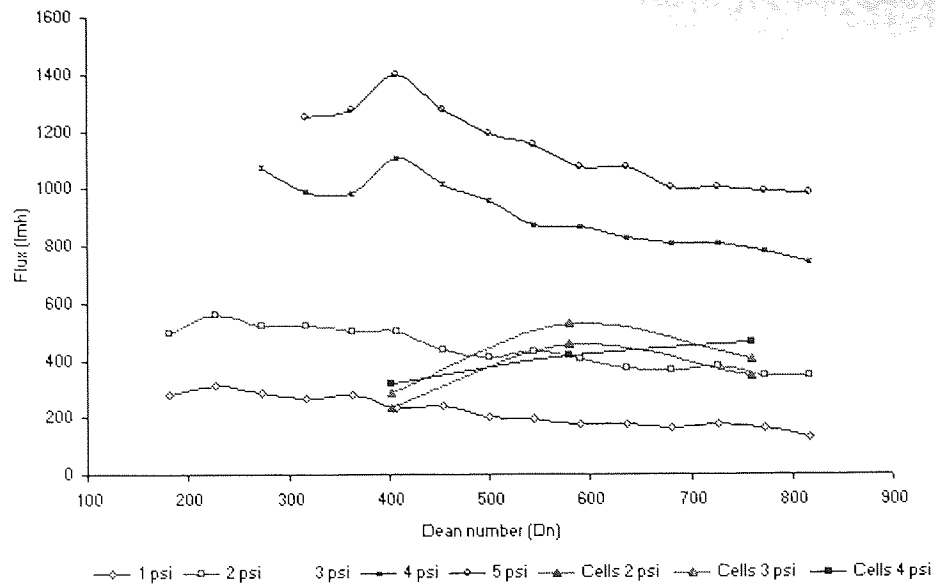
Figure 3-7: The effect of the Dean number (Dn) on the permeate flux (lmh) for pure water with (1-5 psi axial TMP) and without permeation (0 psi axial TMP), and an E.coli bacterial cell culture (OD 2.5) when processed by an EFD (Millipore, UK) cross-flow mirco-filtration module.
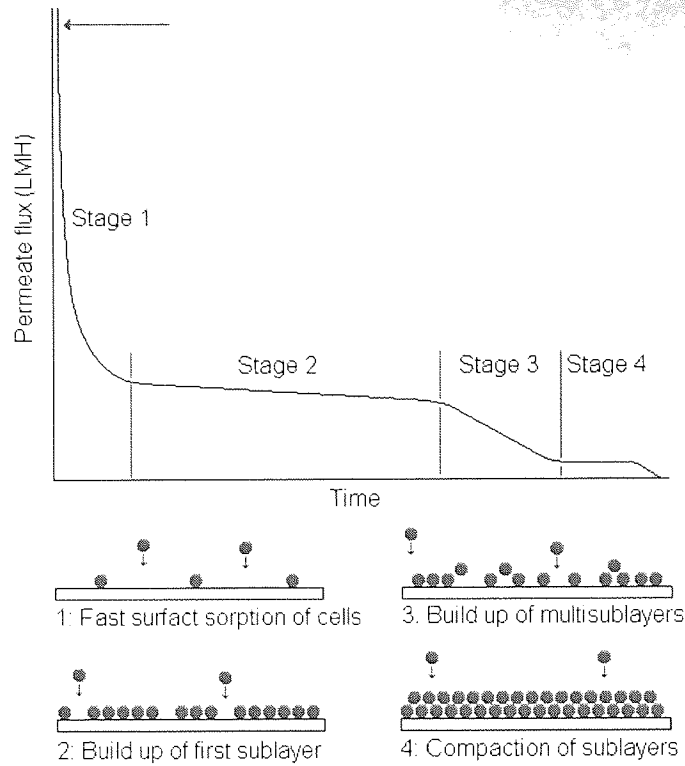
Figure 3-8: Schematic showing the four stages associated with the formation and consolidating a cell cake onto the surface of a filtration membrane. The flux-time plot details the effect that these stages impose on the permeation rates.

a.
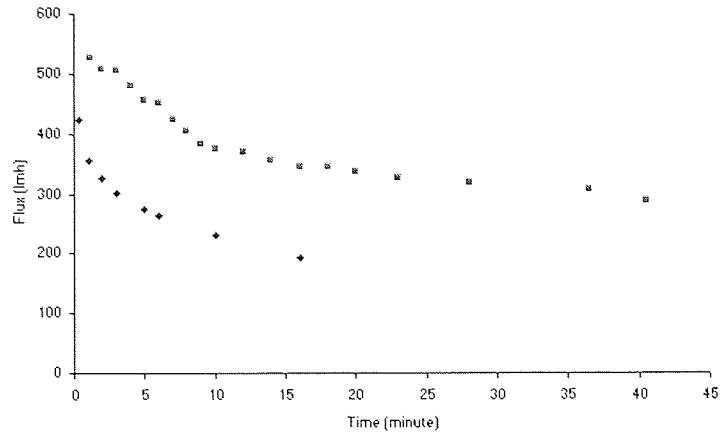
b.
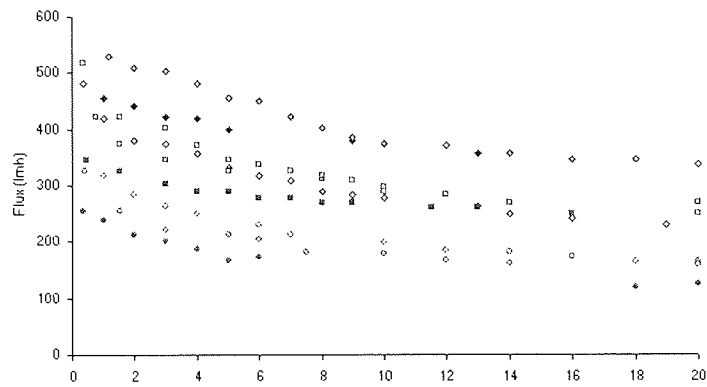
c.
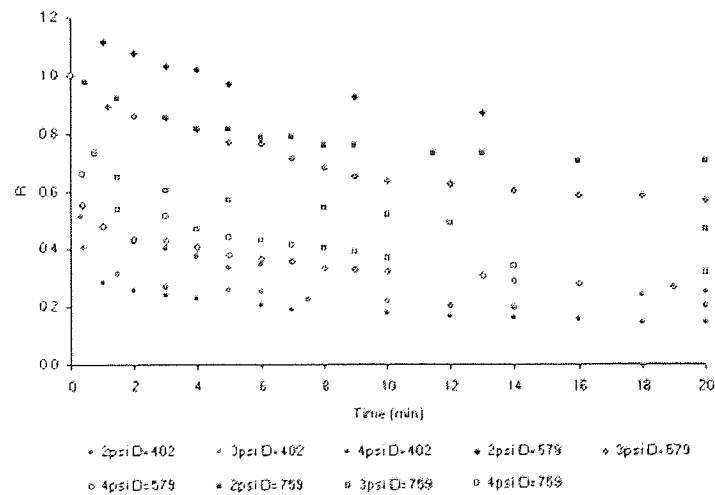
Figure 3-9: Flux-time plots of an OD 2.5 E.coli bacterial cell culture being processed at various Dean numbers (Dn) and transmembrane pressures (TMP) within an EFD cross-flow micro-filtration. (a.) Shows the effect that the previous and revised operating procedures impose of the flux-time plots (♦) Old method(▪) New method. (b.) Demonstrating the fouling rates associated with 408Dn, 579Dn aand 759Dn at the TMPs of 2, 3 and 4 psi.
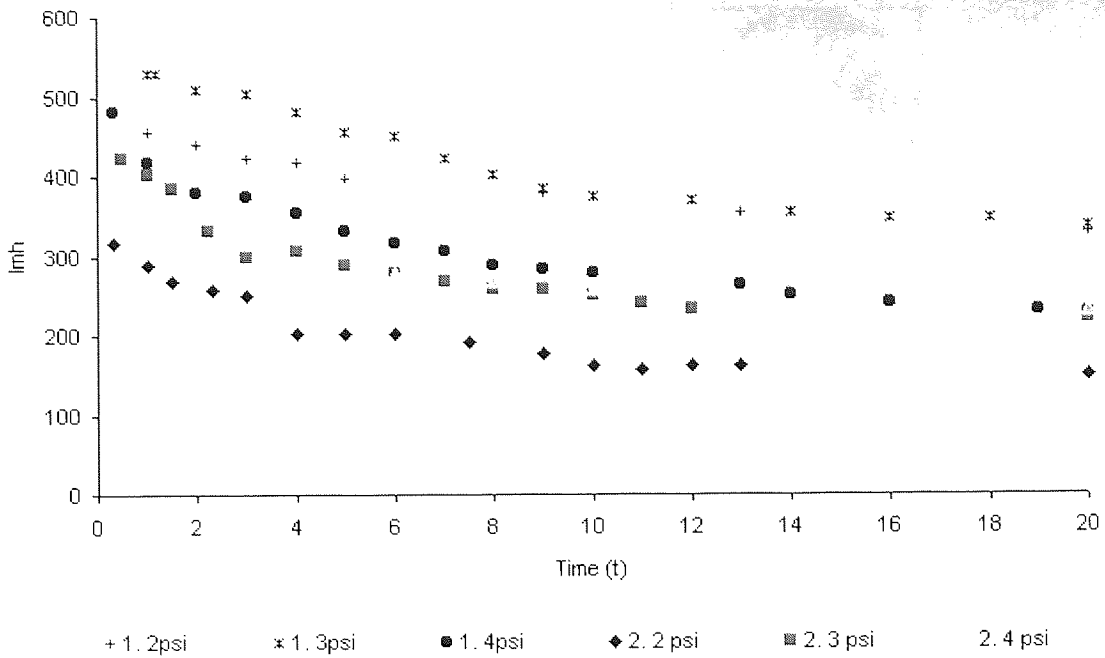
Figure 3-10: Flux-time plots of an OD16 E.coli bacterial cell culture being processed at 579 Dean number (Dn) and various transmembrane pressures (TMP) within an EFD cross-flow micro-filtration system. Demonstrating the fouling rates associated with 579 Dn at the TMP's of 2, 3 and 4 psi. (1) equates to OD 2.5 cell cultures and (2) OD 16 cell cultures.
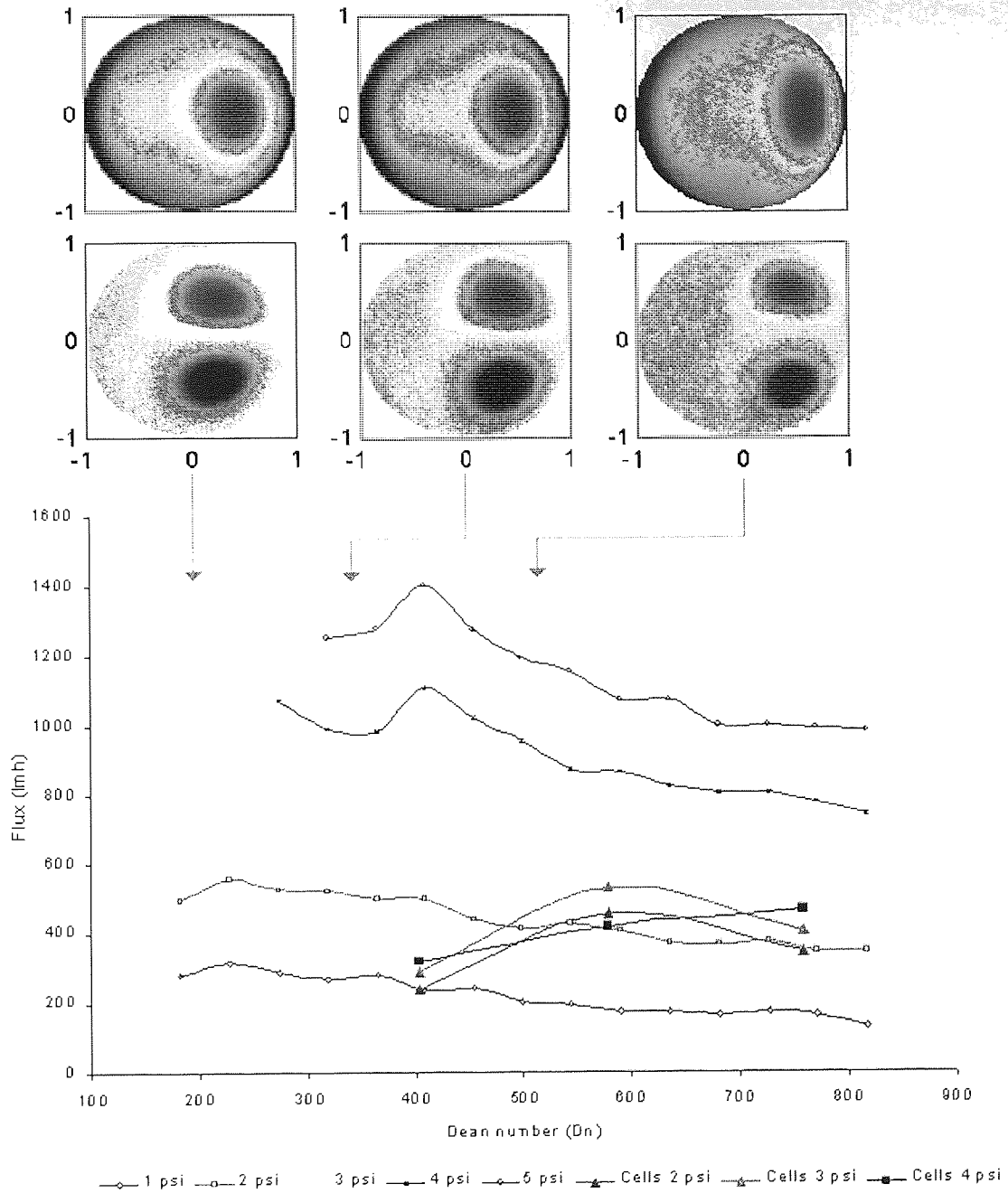
Figure 3-11: Impressions of the variations in the primary and secondary flow patterns as the Dean number (Dn) increases within a EFD cross-flow micro-filtration module. The suggested flow patterns are indicated from experimental, numerical (Liu et al., 1993), and series expansion methods (Kao, 1987).
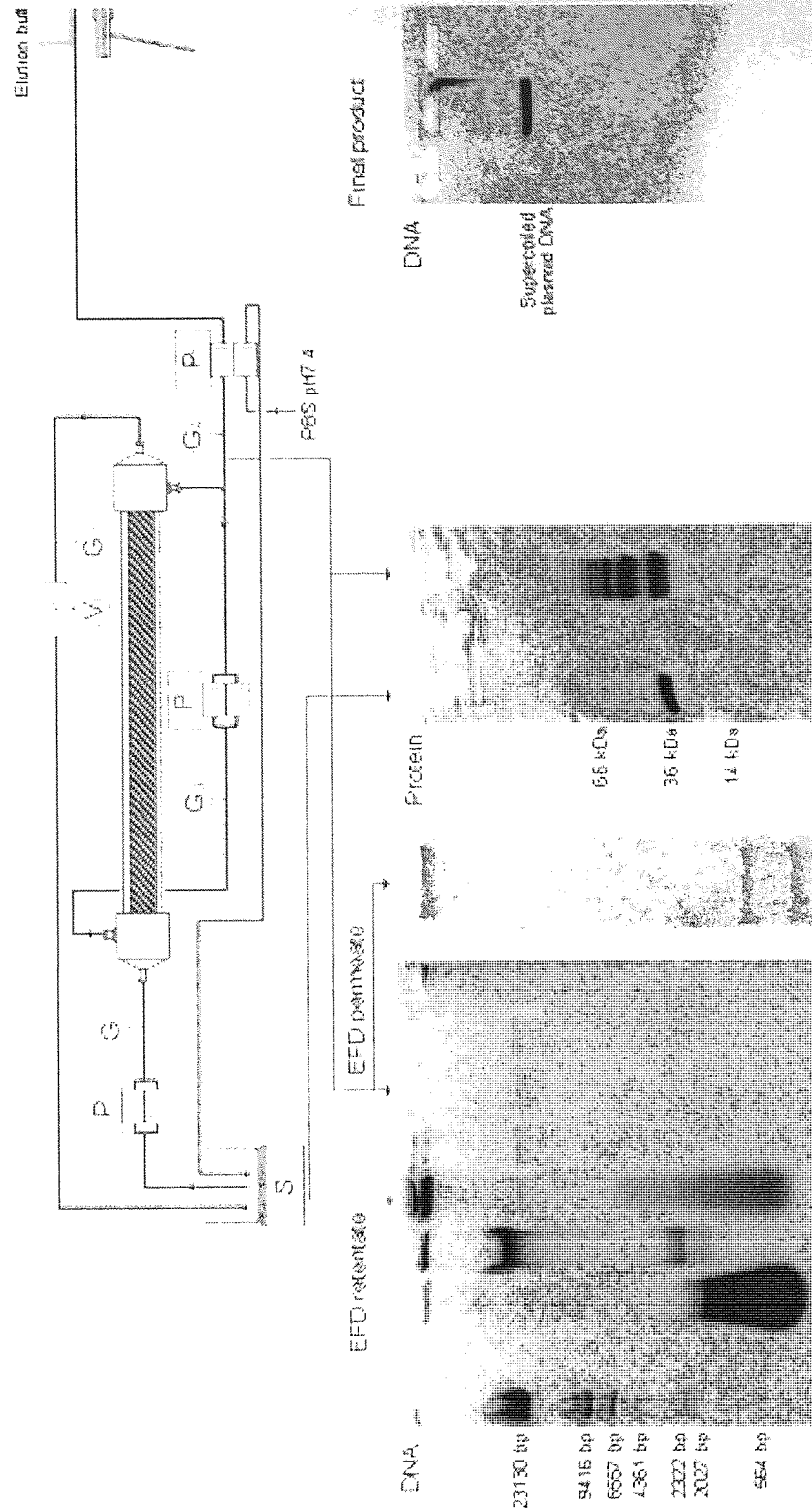
Figure 3-12: The purification of plasmid DNA using Dean-vortex micro-filtration technology and sequence-specific DNA affinity chromatography (SSC). Samples were taken from a single operation, processing a 2L E.coli DH5α culture transformed with the target plasmid pTS, and run on either 1% agarose gels stained with PicoGreen^{TM} or 12%TBE protein gels stained with Coomassie Blue. From the DNA (13.28 mg ~3 mg plasmid) and protein (7.2 mg) challenge passed though the EFD module, 0.94 mg of pTS was purified with no visible DNA or protein (<1.5 ng μl^{1}) contamination.
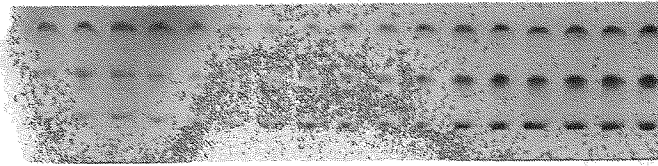
Figure 4-1: 1% Agarose electrophoresis gel of the plasmid pTS DNA for calibration purposes. The plasmid pTS (0-50 ng) was incubated (25°C, 1min) with PicoGreen™ (0.5µl) and loaded into the gel with sucrose loading buffer (5 µl). The fluorescent signal was identified and quantified using a TUNDRA™ digital imaging system, exciting the fluorescent probe at 495nm and detecting the emission at 535nm. The resulting calibration plot of DNA quantity and fluorsent intensity can be seen with Figure 4-2.
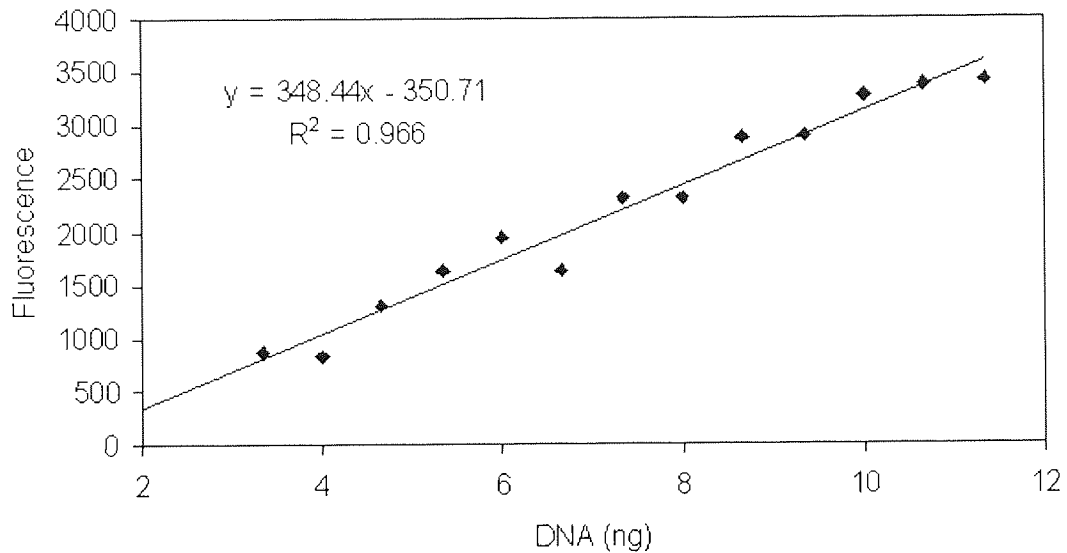
Figure 4-2: Calibration plot of the fluorescent signal emitted from PicoGreen™ when intercalated into the plasmid pTS DNA (Figure 5-1). Data line shows that the signal for the super-coiled plasmid (Lower band within Fig 4.1) where the upper band is linear pTS DNA and the middle band open-circular pTS DNA. The gel image was identified and quantified using a TUNDRA™ digital imaging device that counts the intensity units emitted per digital pixel within the DNA bands.
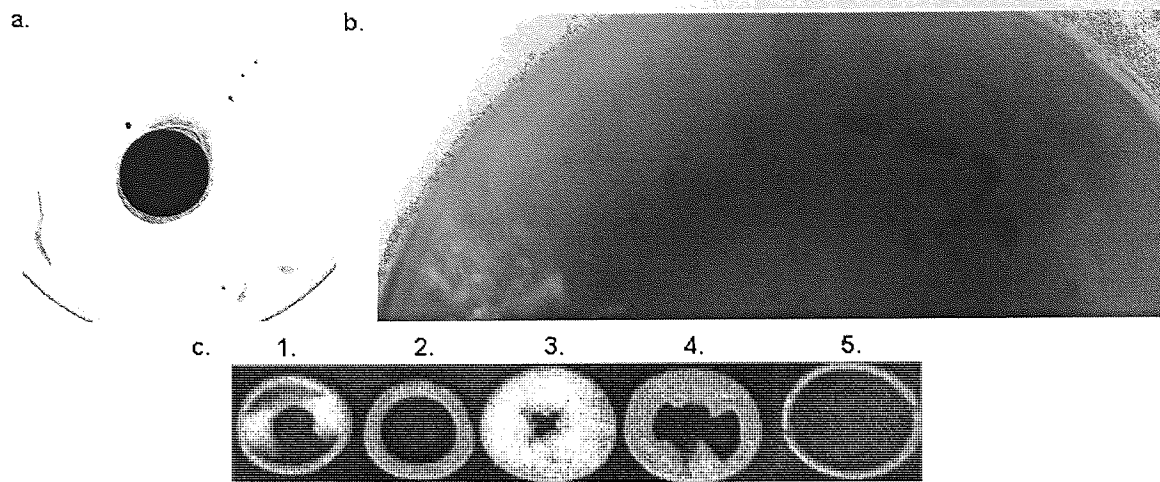
Figure 4-3: (a.) 13 mm Ultrabind™ and (b.) 150 mm Pall Gelman Ultrabind membranes were held in Millipore stainless steel housings and challenged with the fluorescent probe Cye3 at a concentration of 10 mg ml⁻¹ at flow-rate of 36 ml min⁻¹. (c.) Sartorius Sartobind Q membranes held in the manufactures pre-formed housing. Millipore 30mm polyethylene at 6.5 ml min⁻¹, 2. Millipore 25 mm SS316 at 6.0 ml min⁻¹, 3-5, Sartorius 30 mm at 6.0, 50, 430 ml min⁻¹. Data for (c.) was taken from Charlton, 1999. The images reveal the flow distribution across the membrane surfaces where no increases in the pressure drop was observed.

a.

b.

$$0.0000 \quad 2.1020 \quad 4.2040 \quad 6.3060 \quad 8.4080$$

c.

d.
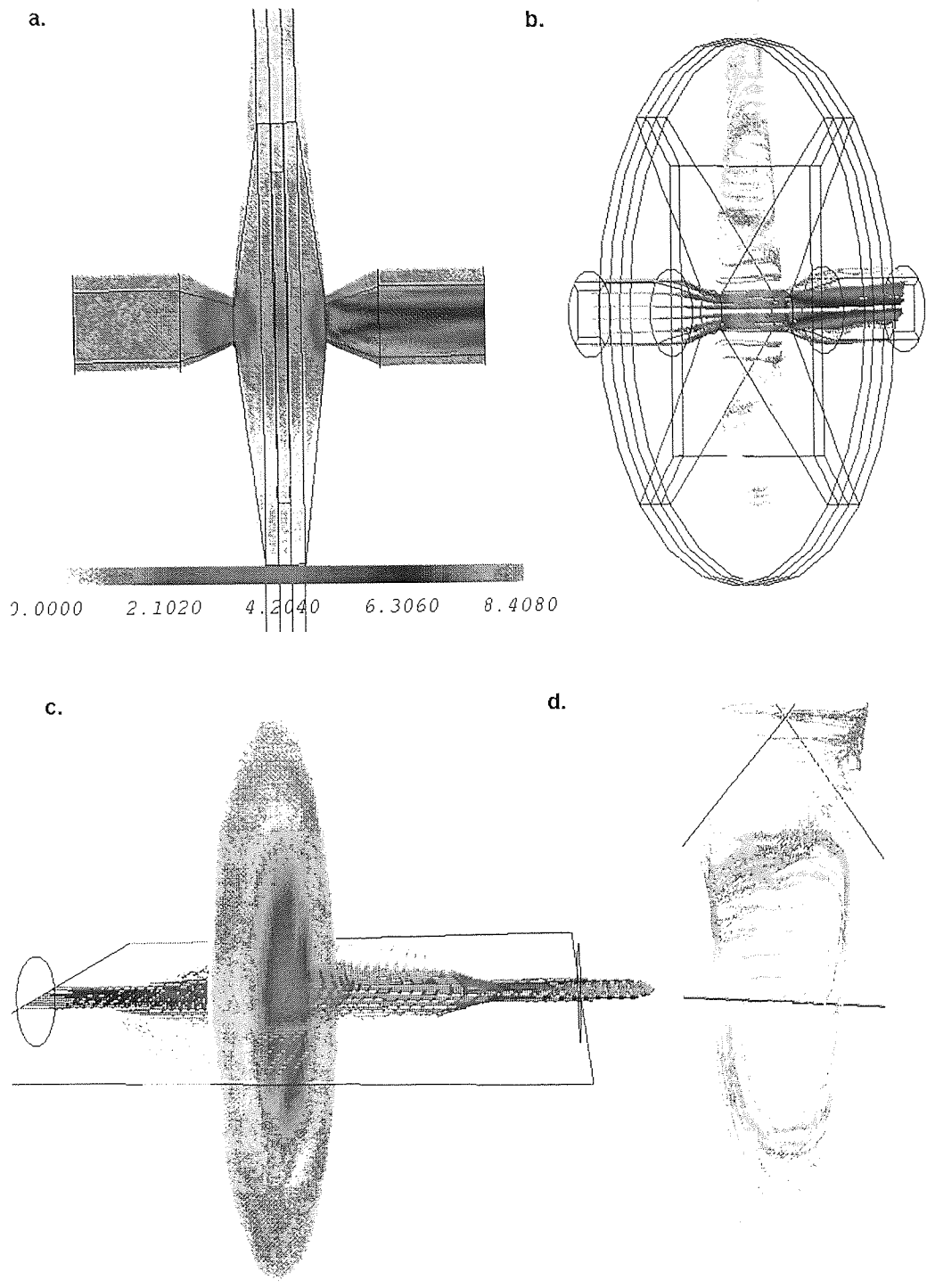
Figure 4-4: Showing the fluid distribution across the Sartobind Q15 membrane within the manufacturers pre-formed housing at 50ml min^{-1} as determined by CFX-4 computational fluid dynamic package.

0.000   1.743   3.486   5.229   6.973
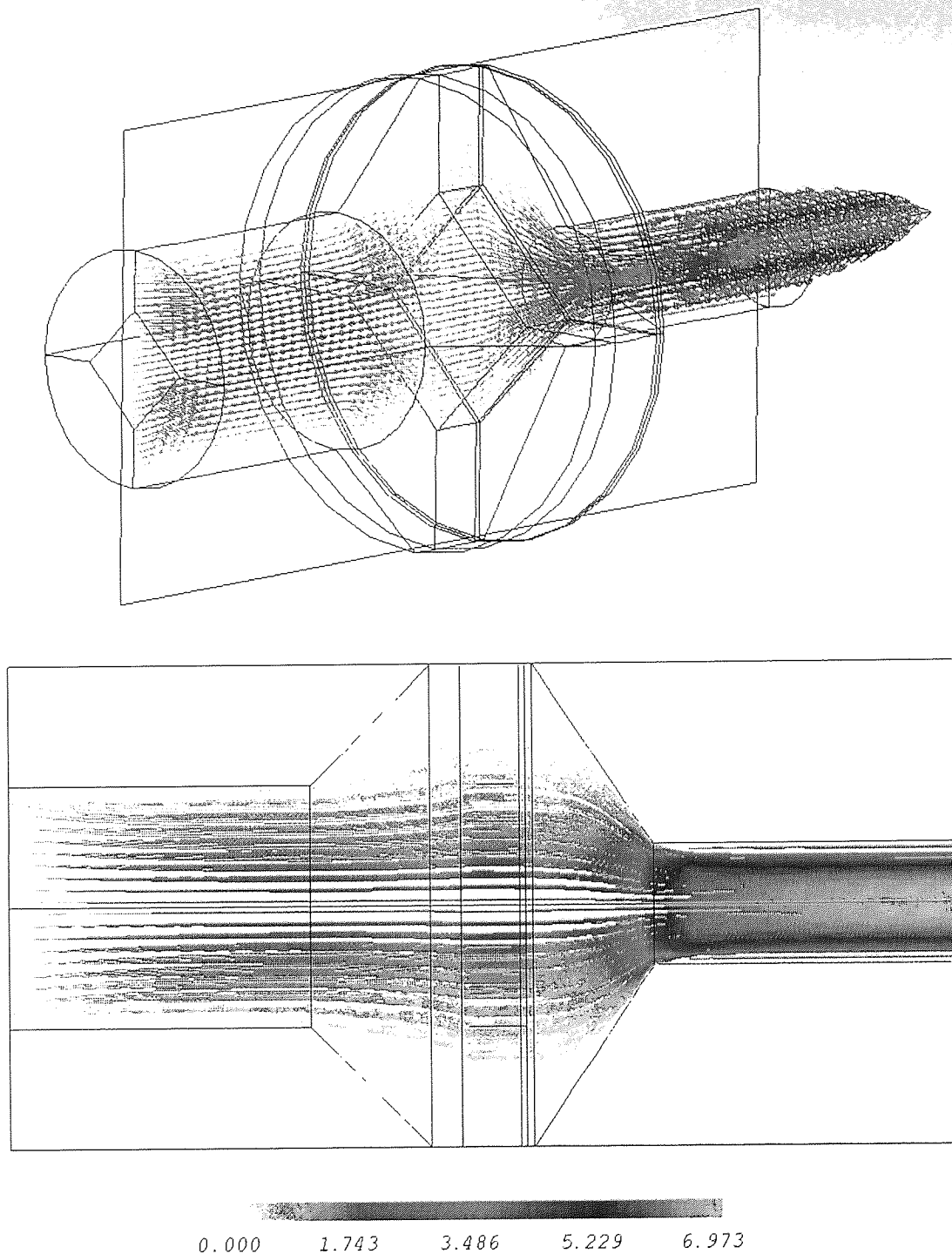
Figure 4-5: Showing the fluid distribution across the Pall Gelman Ultrabind™ US450 membrane within the Millipore 13 mm stainless steel housing at 50ml min^{-1} as determined by CFX-4 computational fluid dynamic package.

a.
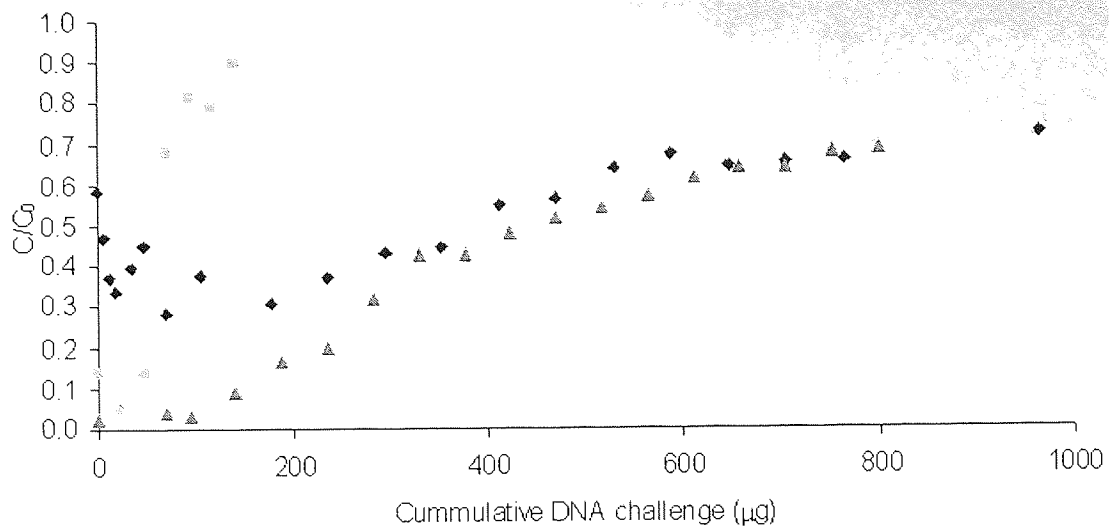
b.
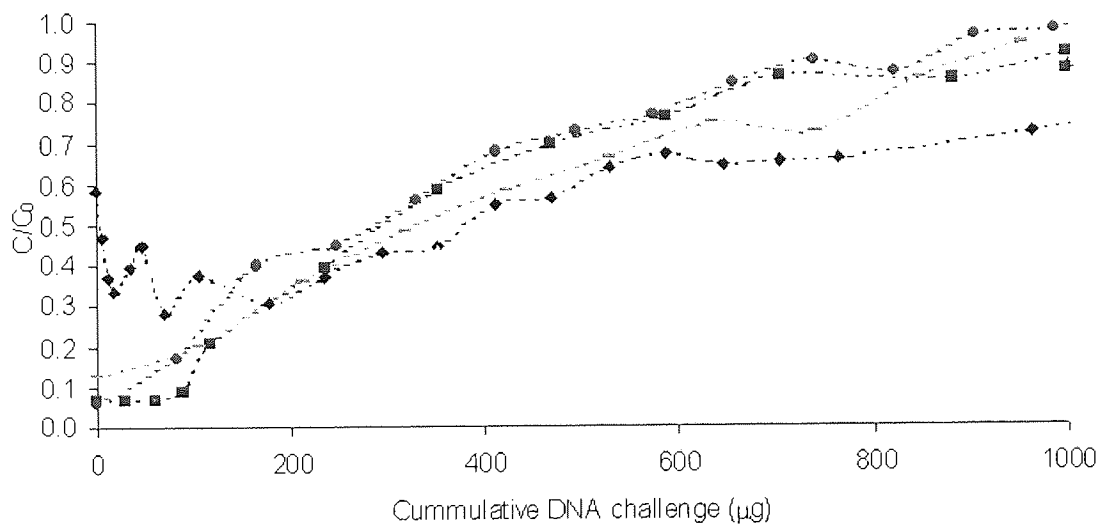
Figure 4-6: Breakthrough curves for Sartobind Q15 membrane when challenged with calf thymus DNA. Fractions were collected as assayed for DNA using UV adsorption at 260nm. Experimental conditions and symbols used: TE was employed as a buffer at pH7.4, the membrane diameter was 25mm and the concentration of DNA was approximately 1 μg ml^{-1}. (a.) Showing the erratic nature of the Sartorius pre-formed housing in replicating the breakthrough curves at 20 ml min^{-1}. (b.) The flow-rate of the challenge material was (-♦-) 10 ml min^{-1}, (   ) 30 ml min^{-1}, (-■) 50 ml min^{-1}, (-●-) 70 ml min^{-1} and (-—) 90 ml min^{-1}.
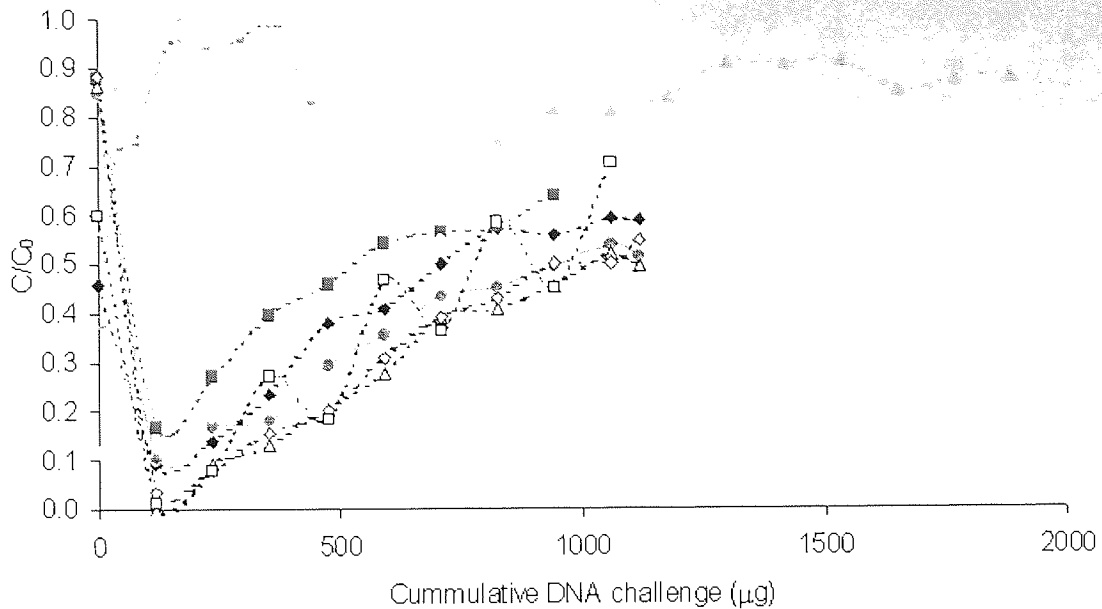
Figure 4-7: Breakthrough curves for Sartobind Q15 membrane when challenged with calf thymus DNA. Fractions were collected as assayed for DNA using UV adsorption at 260nm. Experimental conditions and symbols used: TE was employed as a buffer at pH7.4, the membrane diameter was 25mm and the concentration of DNA was approximately 1 μg ml^{-1}. The salt concentration in the challenge material was ( ) 0mM, (◆) 20mM, (■) 40mM, (●) 60mM, (△) 80mM, (◇) 100mM, (□) 140mM, ( ) 500mM, ( ) 7500mM and ( ) 7500mM.
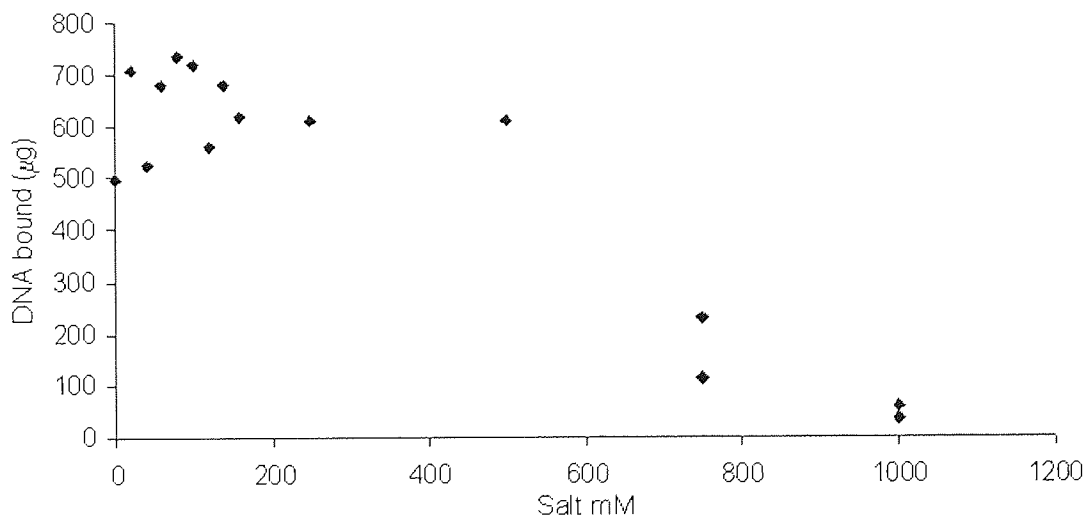

Figure 4-8: Equilibrium binding capacity for the Sartobind Q15 membrane when challenged with calf thymus DNA in buffers of various ionic strengths (i.e. salt concentration). The buffer TE pH7.4 was employed throughout, the flow-rate of the challenge material was 50 ml min^{-1}, the membrane diameter was 25mm where approximately 1000μg of ctDNA was challenged.

126
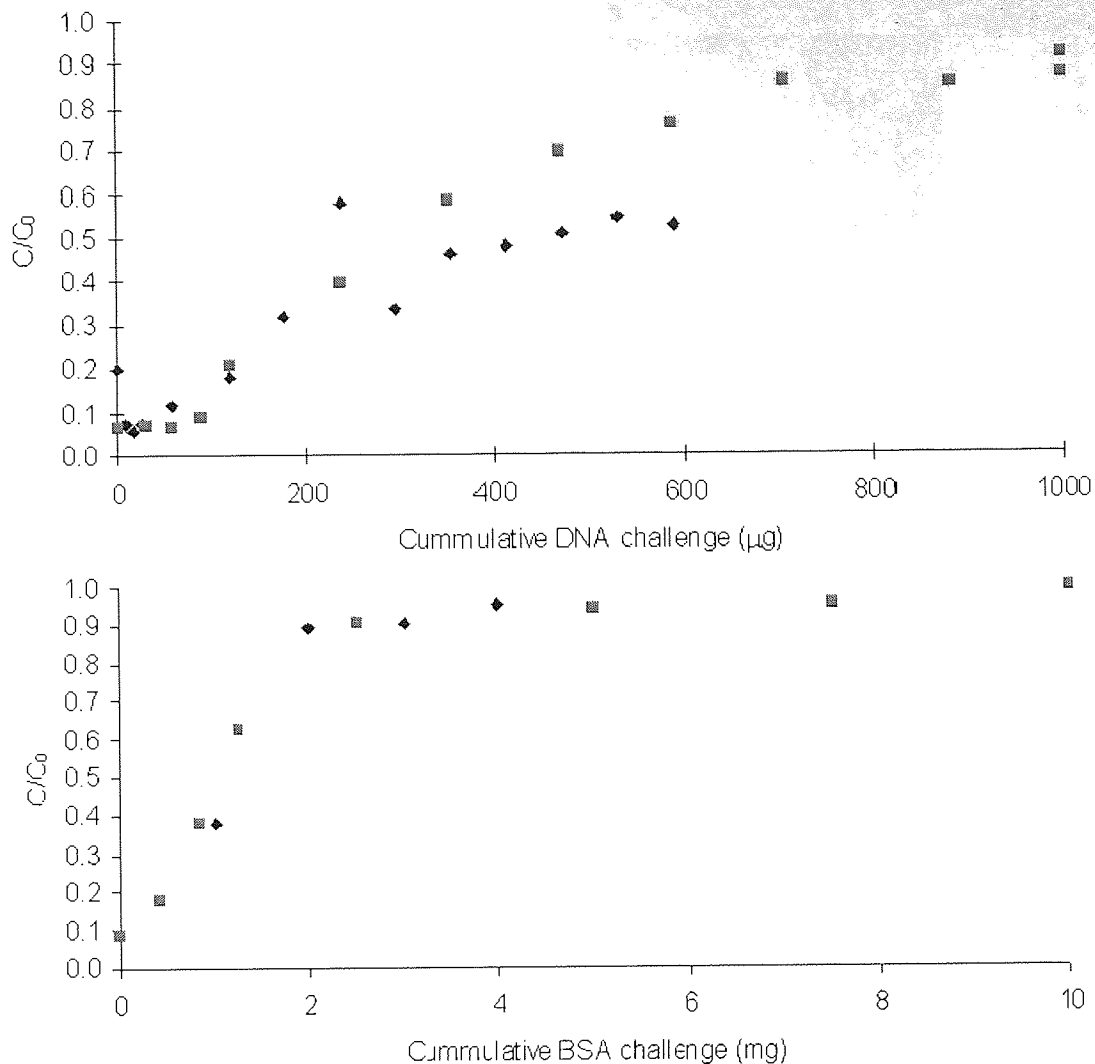
Figure 4-9: Breakthrough curves for Sartobind Q15 membrane when challenged with calf thymus DNA and bovine serum albumin. Fractions were collected and assayed for DNA (UV adsorption at 260 nm) and protein (Bradford reagent). Experimental conditions and symbols used: TE was employed as a buffer at pH 7.4, the flow-rate was 50 ml min^{-1}, the membrane diameter was 25 mm and the concentration of DNA and protein was approximately 1 μg ml^{-1} and 50 μg ml^{-1} respectively. Three consecutive challenges were made where ($\cdot$ ◆) was challenge 1 and ($\cdot$ ▦-) was challenge 2.
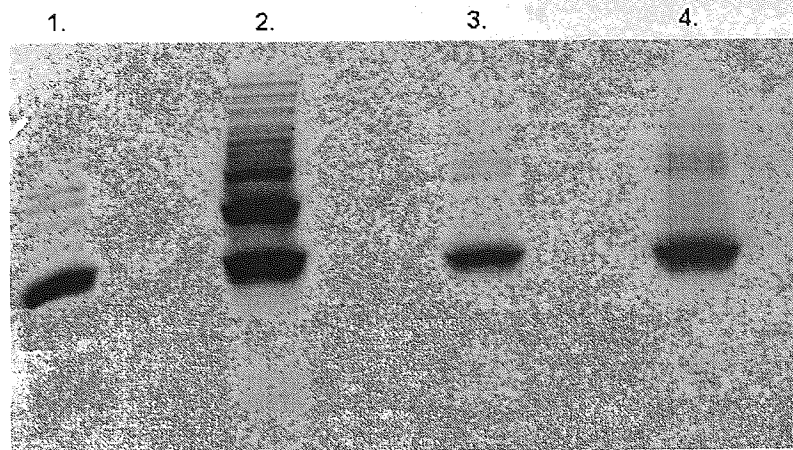
Figure 4-10: Samples were taken from the process stream where cellular protein released by freeze-thaw lysis was either (1.) passed through the EFD, (2.) retained by the EFD, (3.) eluted from the Sartorius Sartobind Q15 membrane or (4.) eluted from the Pall Gelman Ultrabind (111,000M$_w$ poly-L-lysine) membrane. The samples were incubated with SDS loading buffer at 95°C for 2 minutes and run through a 12% polyacrylamide denaturing electrophoresis gel. The proteins were made visible by incubating (60°C) with Coomassie blue.
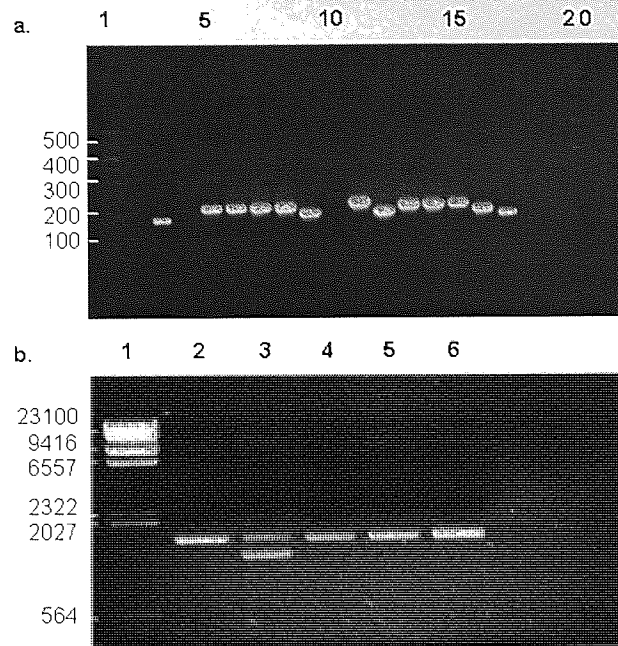
Figure 5-1: (a.) Agarose gel electrophoresis of PCR products obtained from pUC19 plasmids into which the 29bp oligonucleotide containing the 9bp recognition sequnce for the zinc-finger fusion-protein has been inserted into the pUC19 SmaI restriction site. The resulting amplifications for all the clones were examined on a 1.5% agarose electrophoresis gel. Lane 1 contains a 50-500bp DNA ladder, lane 3 contains the PCR product of contol pUC19 (170bp) and lanes 5-17, PCR products of the clones. (b.) Agarose gel electrophoresis of plasmids prepared from clones amplified in lanes 5, 7, 13 and 15 within Figure 5-1a. Lane 1 contains a λ HindIII DNA ladder. Plasmids were purified from E.coli by 'maxi-prep' (Promega) technology.
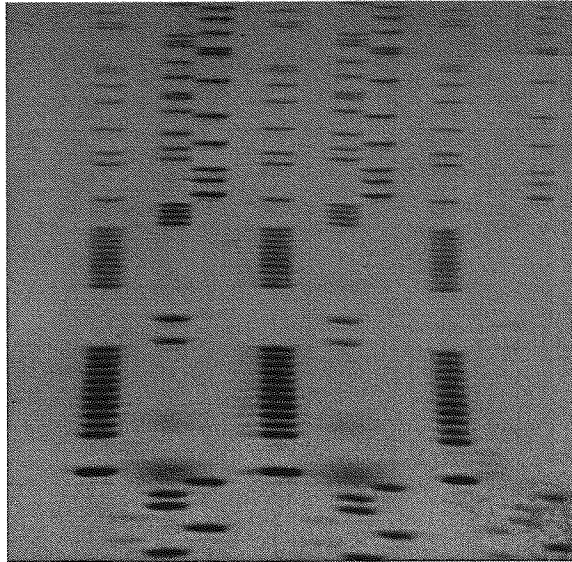
Figure 5-2: Autoradiograph showing the correct recognition sequence within the 29bp insert cloned into pUC19. The three sequnces correspond to lanes 4, 5 and 6 of Figure 5-1b. Sequnce 1: Lane 1=A, 2=C, 3=G and 4=T, corresponding to the correct insert 5'-AAA-AAA-AAA-AAG-CCG-CCC-CAA-AAA-AAA-AA-3'.
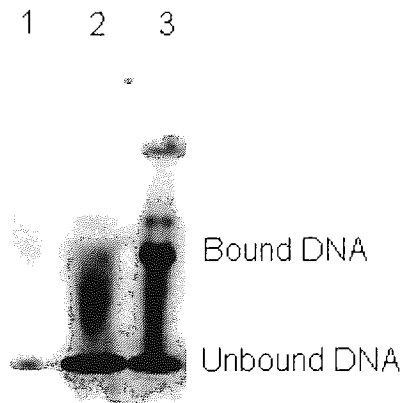

Figure 5-3: Gel-mobility assay demonstrating the sequence-specific protein-DNA interaction between GST-ZF and the target sequence located within a 29bp oligonucleotide end-labelled with the florescent probe Cye3 (Amersham). The oligonucleotide was electrophoresed past the fusion-protein within the 12% polyacrylamide non-denaturing gel at 80V and analysed by a TUNDRA™ digital imaging device. Identical molar quantities of fusion-protein and DNA were used where lane 2 shows pure DNA and lane 3 the mobility assay.
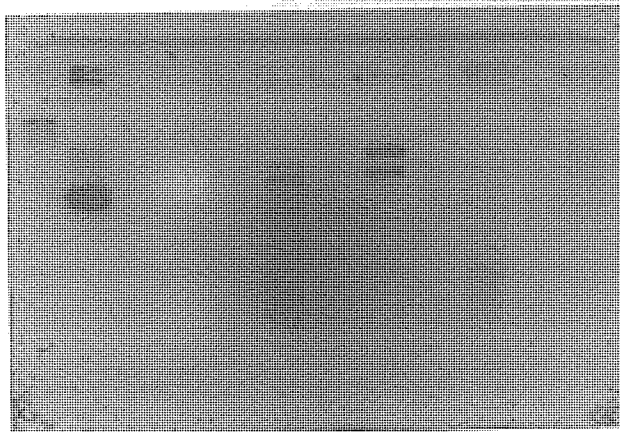
Figure 5-4: Agarose gel electrophoresis of plasmids, after complexation with the GST-ZF, eluted from the GSH-affinity matrix. Crude sources of pUC19 and pTS were prepared from 'freeze-thaw' cell lysis of transformed E.coli DH5α bacterial cells. The fusion-protein (137 fmol) and DNA was allowed to complex in TBS pH 7.4 and adsorbed onto the GSH-matrix (Sepharose 4B, Amersham). The mixture was washed copiously with the process buffers and eluted twice with reduced-glutathione (70 mM) elution buffer. The eluate was incubated with PicoGreen™ (0.5 μl, Molecular Probes) and analysed with a TUNDRA™ digital imaging device according to the developed electrophoretic assay format (Method 2.4.7, 1% agarose gel). Lane 1; λ Hind III marker, Lane 2; Calibration pTS (115.6 fmol), Lane 6; Crude pTS eluate (3.2 fmol), Lane 8; Pure pTS elution (9.95 fmol); Lane 10; Crude pUC19 elution (Trace), Lane 12; Pure pUC19 elution (Trace).
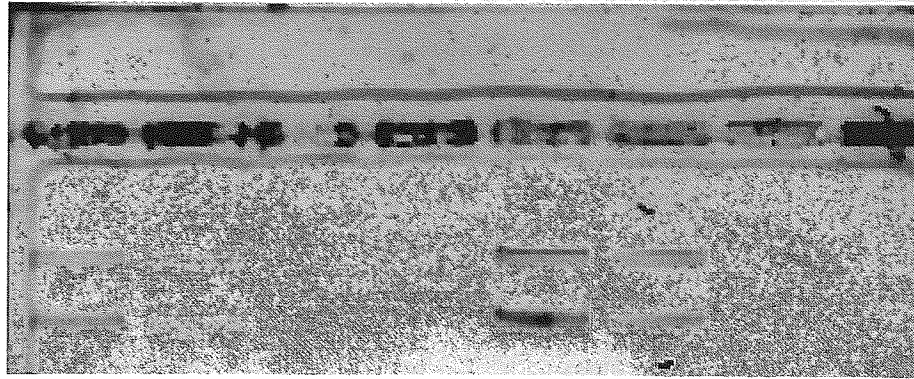
Figure 5-5: Agarose gel electrophoresis of plasmids eluted, after incubation with the GST-ZF, from the GSH affinity matrix. The fusion-protein (137 fmol) and the purified plasmids, pUC19 and pTS DNA (116 fmol), were allowed to complex in TBS pH7.4 and adsorbed onto the GSH-matrix (Sepharose 4B, Amersham). The mixture was washed copiously with the process buffers and eluted twice with reduced-glutathione (70mM) elution buffer. The eluate was incubated with PicoGreen™ (0.5 μl, Molecular Probes) and analysed with a TUNDRA™ digital imaging device according to the developed electrophoretic assay format (Method 2.4.7). Lanes 1-2; first and second elutions of pTS when containing 0.03% Tween[20], lanes 3-4; first and second elutions of pUC19 when containing 0.03% Tween[20], Lanes 5-6; first and second elutions of pTS when containing 0.05% Tween[20], Lanes 7-8; first and second elutions of pUC19 when containing 0.05% Tween[20].
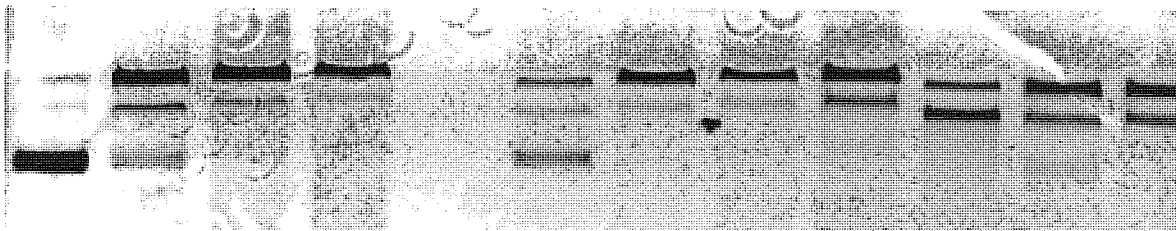

Figure 5-6: Agarose electrophoresis gel showing the band shift of the plasmid pTS after the introduction of high concentration GST-ZF and r-GSH. Using the developed assay to quantify the signal emitted by PicoGreen™, no loss was observed in comparison to the challenge DNA. Lane 1; containing pTS DNA (115.6 fmol), Lane 2; pTS DNA (115.6 fmol) and fusion protein (13 7 fmol), Lane 3; pTS DNA (115.6 fmol) and fusion protein (274 fmol), Lane 4; pTS DNA (115.6 fmol) and fusion protein (411 fmol), Lane 7; pTS DNA (115.6 fmol) and fusion protein (137 fmol) and rGSH (1 μmol), Lane 8; pTS DNA (115.6 fmol) and fusion protein (274 fmol) and rGSH (1 μmol), Lane 9; pTS DNA (115.6 fmol) and fusion protein (411 fmol) and rGSH (1 μmol), Lane 10-12; pTS DNA (115.6 fmol) and rGSH (1 μmol).
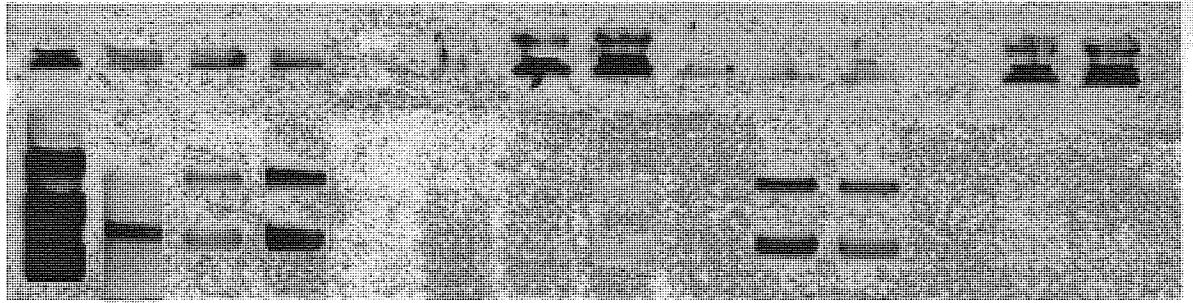
Figure 5-7: Agarose electrophoresis gel of the plasmids DNA eluted from the GSH-matrix aftercomplexation with the zinc finger fusion protein (GST-ZF). The GST-ZF (480 fmol), matrix and DNA (187.5 fmol) were allowed to complex within either TBS or PBS pH 7.4 process buffers containing either 0, 0.03 or 0.05% Tween[20]. When incubating the fusion protein with the DNA initially. Lane 1; Challenge pTS DNA (187.5 fmol), Lane 2,6; first and second elution of pTS DNA in PBS pH 7.4 containing no Tween[20], Lane 3,7; first and second elution of pTS DNA in TBS pH 7.4 containing 0.03% Tween[20], Lane 4,8; first and second elution of pTS DNA in TBS pH 7.4 containing 0.05% Tween[20]. When challenging the fusion-protein and matrix initially: Lane 9,12; first and second elution of pTS DNA in PBS pH 7.4 containing no Tween[20], Lanes 10,13; first and second elution of pTS DNA in TBS pH 7.4 containing 0.03% Tween[20], Lane 11,14; first and second elution of pTS DNA in TBS pH 7.4 containing 0.05% Tween[20].
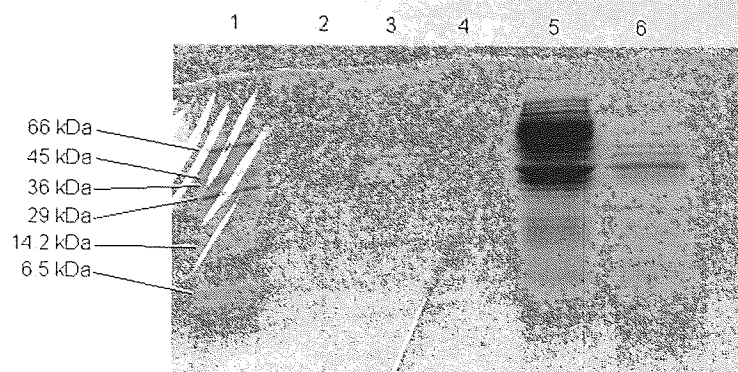
Figure 5.8: 12% SDS-PAGE electrophoresis gel. Samples were denatured at 95°C in SDS loading buffer and electrophoresed at 100V for 1hr. Lane 1; Molecular weight marker (Sigma UK), Lane 3; Purified fusion-protein, Lane 5; Cellular proteins present after E.coli DH5α lysis by freeze-thaw, Lane 6; Cellular proteins present after E.coli DH5α lysis by sonication.
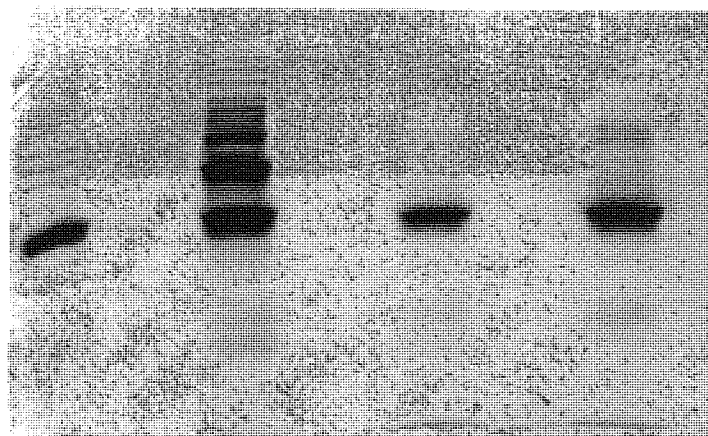

Figure 5-9: 12% SDS-PAGE electrophoresis gel run at 100V showing the cellular proteins from an E.coli DH5α cell culture that were retained and passed through an EFD (Millipore) filtration module after 6 cycles of Liquid N$_2$• 37°C cell lysis. Samples were denatured at 95°C for 3mins in SDS loading buffer. Lane 1; Cellular proteins retained by EFD, Lane 3; Cellular protein passed through EFD.
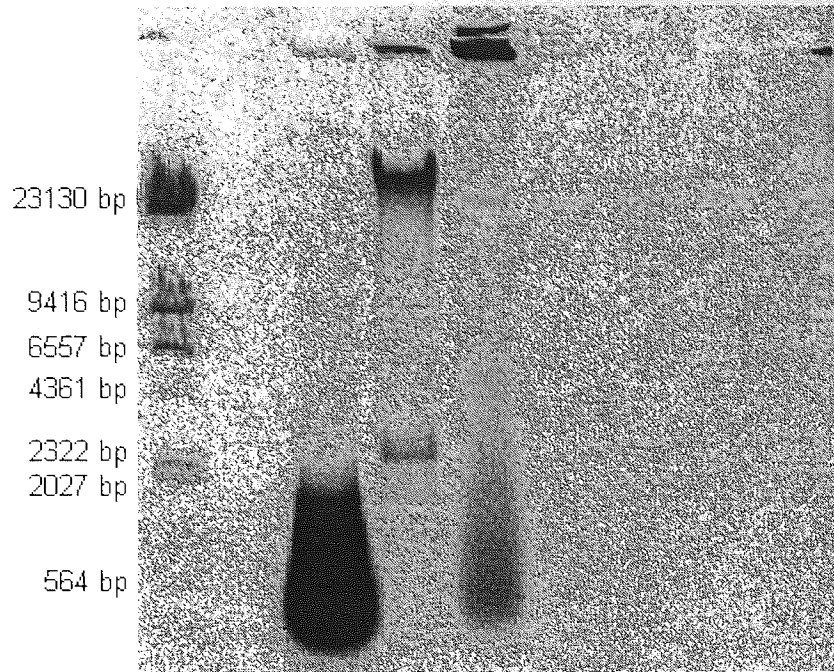
Figure 5-10: 0.3% Ultrapure agarose electrophoresis gel, run at 50 V, of the DNA retained by the EFD, passed through EFD, and challenged to the GSH-affinity membrane. Lane 1; λ Hind III marker, Lane 5; DNA retained by EFD, Lane 6-7; DNA passed through EFD, Lane 8; DNA unbound.

Figure 5-11: Agarose gel electrophoresis showing the DNA eluted from a GSH-membrane after concentration (Spin column, Promega) and incubation (60°C) with IPTG (1 M). The elution is compared to maxi-prepared pTS that only contains plasmid and no other DNA. The result is run on a 1% gel at 80V. No DNA is visible within the well. Lane 2; Pure pTS DNA (300 ng), Lane 4; Elution 1 pTS DNA, Lane 6; Elution 2 pTS DNA.

a.

γ-Glu   Cys   Gly

b.

γ-Glu   Cys   Gly
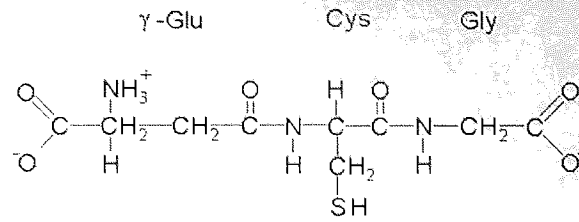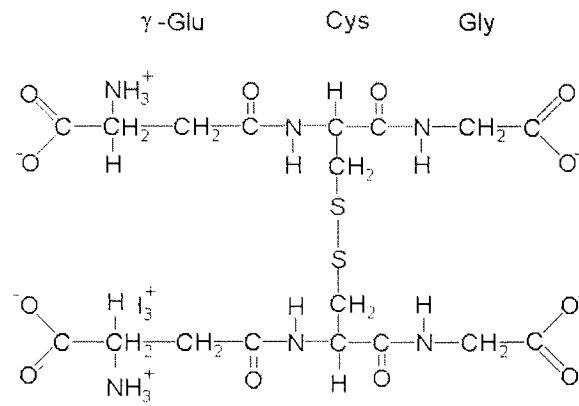
Figure 5-12: Molecular structure of the molecules (a.) reduced glutathione (rGSH) and (b.) glutathione (GSH) (Stryer; Biochemistry 1990).